Mugiya, Y., Kobayashi, N. and Motoya, S., Gonadal maturation in the abalone, *Haliotis discus hannai* at Taisei, Hokkaido. Bull. Fac. Fish. Hokkaido University, 31 (1980) 306–313.

Singhagraiwan, T. and Doi, M., Seed production and culture of a tropical abalone, *Haliotis asinina* Linne. The Eastern Marine Fisheries Development Center, Department of Fisheries, Ministry of Agriculture and Cooperatives, Thailand, 1993.

Sobhon, P., Apisawetakan, S., Chanpoo, M., Wanichanon, C., Linthong, V., Thongkukiatkul, A., Jarayabhand, P., Kruatrachue, M., Upatham, E.S. and Pumthong, T., Classification of germ cells, reproductive cycle and maturation of gonad in *Haliotis asinina* Linnaeus. Science Asia, 25 (1999) 3–21.

Stephenson, T.A., Notes on *Haliotis tuberculata*. J. Marin. Biol. Assoc. UK, 13 (1924) 480–495.

Takashima, F., Okuno, M., Nichimura, K. and Nomura, M., Gametogenesis and reproductive cycle in *Haliotis diversicolor diversicolor* Reeve. J. Tokyo Univ. Fish., 1 (1978) 1–8.

Tomita, K., The maturation of the ovaries of the abalone, *Haliotis discus hannai* Ino, in the Rebun Island, Hokkaido, Japan. Sci. Rep. Hokkaido Fish. Exp. Sta., 7 (1967) 1–7.

Webber, H.H. and Giese, A.C., Reproductive cycle and gametogenesis in the black abalone *Haliotis cracherodii* (gastropoda: prosobranchiata). Mar. Biol., 4 (1969) 152–159.

Young, J.S. and DeMartini, J.D., The reproductive cycle, gonadal histology and gametogenesis of the red abalone, *Haliotis rufescens* (Swainson). Calif. Fish and Game., 56 (1970) 298–309.

ELSEVIER

Parasitology International 50 (2001) 105–114

www.parasitology-online.com

Molecular cloning and characterization of cathepsin L encoding genes from *Fasciola gigantica*☆

Rudi Grams[a,*], Suksiri Vichasri-Grams[b], Prasert Sobhon[c], E. Suchart Upatham[b,d], Vithoon Viyanant[a,b]

[a] *Faculty of Allied Health Sciences, Thammasat University, Pathum Thani 12121, Thailand*
[b] *Department of Biology, Faculty of Science, Mahidol University, Bangkok, Thailand*
[c] *Department of Anatomy, Faculty of Science, Mahidol University, Bangkok, Thailand*
[d] *Faculty of Science, Burapha University, Chonburi, Thailand*

Received 14 March 2001; accepted 16 March 2001

Abstract

In this study cDNAs encoding cathepsin L-like proteins of *Fasciola gigantica* were cloned by the reverse transcription polymerase chain reaction method (RT-PCR) from total RNA of adult specimens. DNA sequence analyses revealed that six different cathepsin L cDNA fragments were isolated, which have DNA sequence identities of 87–99% towards the homologous genes from *F. hepatica*. Gene expression was studied at the RNA level by Northern and RNA in situ hybridizations. Northern analysis showed the cathepsin L genes to be strongly expressed in adult parasites as a group of 1050 nt sized RNAs. RNA in situ hybridization localized cathepsin L RNA to the cecal epithelial cells. Southern hybridization was used to determine the number of cathepsin L genes and indicated the presence of a family of closely related cathepsin L genes in the genome of *F. gigantica*. © 2001 Elsevier Science Ireland Ltd. All rights reserved.

Keywords: *Fasciola gigantica*; Cathepsin L; Molecular cloning; In situ hybridization; Southern analysis; Northern analysis

☆ *Note:* Nucleotide sequences data reported in this paper are available in the EMBL, GenBank and DDJB data bases under the accession numbers AF112566, and AF239264-AF239268.

* Corresponding author. Tel.: +66-2-9869055; fax: +66-25165379.
E-mail address: rgrams@alpha.tu.ac.th (R. Grams).

PII: S1383-5769(01)00068-X

1. Introduction

Fasciola gigantica is a common parasite of cattle and buffalo in Thailand. It causes severe disease in these animals and important economic losses to animal husbandry [1]. Cathepsin L cysteine proteinases are abundant proteins in *Fasciola* and form a major component of the material secreted by the parasite [2]. Besides their primary function as extracellular digestive enzymes they have been shown to prevent the adherence of eosinophils to newly excised juveniles by cleaving host immunoglobulin [3,4]. They can degrade extracellular matrix proteins such as fibronectin, laminin and native collagen which might help in parasite migration [5]. They have also been shown to cleave fibrinogen, thus producing a fibrin clot; an activity that might prevent bleeding from severed host blood vessels [6]. Partial protective immunity to *F. hepatica* infection has been shown in cattle when vaccinated with cathepsin L [7]. Furthermore, the use of cathepsin L for diagnosis of fascioliasis has been reported in several recent studies [8–11]. This molecular study was, therefore, conducted as a starting point for future work on diagnosis of and vaccination against fascioliasis in cattle in Thailand.

2. Materials and methods

2.1. Preparation of nucleic acids

Total RNA of adult *F. gigantica* was extracted in TRIZOL (Life Technologies) after homogenizing whole worms by an Ultra-Turrax (IKA). Genomic DNA was extracted from frozen and powdered adult *F. gigantica* in extraction buffer (0.1 M Tris-HCl, pH 8, 0.1 M NaCl, 20 mM EDTA). The proteins in the extract were digested by proteinase K [100 μg/ml] for 60 min at 50°C in extraction buffer/1% SDS and the DNA solution was deproteinized by extraction with phenol–chloroform. Coextracted RNA was degraded by RNase A [300 μg/ml] for 60 min at 37°C. Concentrations of nucleic acids were determined by spectrophotometry at 260 nm. Nucleic acids were stored at −20°C until usage.

2.2. RT-PCR, subcloning, sequencing and sequence analysis

One microgram of total RNA was reverse transcribed by Superscript II reverse transcriptase (Life Technologies) using the cathepsin L reverse primer (CatLR: 5′-TCA CGG AAA TCG TGC CAC C-3′) for 1 h at 42°C. The RT-product was used to amplify DNA fragments of the cathepsin L gene family by a standard PCR setup (30 cycles at 55°C, 72°C, 92°C, 1 min each step) based on *Taq* DNA polymerase (Life Technologies). Besides the reverse primer, three different cathepsin L forward primers were used to amplify the full length coding sequence (CatLF1: 5′-ATG CGA TTG TTC ATA TTA GC-3′, CatLF2: 5′-ATG AGA TTG GTA ATC CTA AC-3′, CatLF3: 5′-ATG CGG TGC TTC GTA TTA GC-3′) and one forward primer was used to amplify the sequence encoding the mature cathepsin L product (CatLF4: 5′-GTA CCC GAC AAA ATT GAC TG-3′). Sequences of the oligonucleotide primers were chosen from an alignment of the homologous DNA sequences from *F. hepatica* cathepsin L encoding genes present in the GenBank database. CatLF1 and CatLF4 correspond to nucleotides 31–50 and 352–371 of U62288, respectively, CatLF2 corresponds to nucleotides 8–27 of L33772, CatLF3 corresponds to nucleotides 17–36 of U62289, and CatLR corresponds to nucleotides 993–1011 of U62288 and is fully conserved in U62289 and L33771. Oligonucleotides were synthesized by NSTDA Bioservice Unit, Thailand and TIB MOLBIOL, Germany. The RT-PCR products were size-separated in agarose gels, cut and purified from the gel (Gel Extraction Kit, QIAGEN) and subcloned into either the T-Easy plasmid vector (Promega) or the T-extended *Eco*R V site of the pBluescript SK plasmid vector (Stratagene). Plasmid DNA was prepared using a plasmid miniprep kit (QIAGEN). For DNA sequencing the services of NSTDA Bioservice Unit, Thailand and MWG AG Biotech, Germany were used. Sequence analysis was done using MacMolly Lite (Softgene, Germany) in addition to SeqPup (D. Gilbert, http://iubio.bio.indiana.edu/soft/molbio/seqpup/), ClustalX [12] and MacBoxshade (M. Baron, ftp:/

/www.isrec.isb-sib.ch/pub/sib-isrec/boxshade/macboxshade/) for alignments and pretty prints therefrom. The cathepsin L DNA fragments were named alphabetically from CatL-A to CatL-F. The RT-PCR and cloning of products was later on repeated with RNA isolated from a single worm to confirm the results obtained by experiments on the RNA from several worms.

2.3. Nucleic acids hybridization experiments

For Southern analysis, 5 μg each of genomic DNA were digested with selected restriction enzymes (Life Technologies, Stratagene), *Eco*R V, *Hin*d III, *Pst* I, *Eco*R V/*Hin*d III, *Eco*R V/*Pst* I and *Hin*d III/*Pst* I, respectively and size-separated in a 0.7% agarose gel in TBE buffer. *Eco*R I/*Hin*d III digested lambda DNA was used as a size standard. For Northern analysis, 28 μg of total RNA was size-separated in a 1% agarose gel containing 6.5% formaldehyde in 1 × MOPS buffer. The RNA molecular weight marker I (Roche) was used to determine sizes of hybridizing RNAs. DNA and RNA were blotted to Nylon membranes (Schleicher & Schuell), fixed by baking at 80°C for 1 h and hybridized at 55°C (DNA) or 68°C (RNA) in 50% formamide, 5 × SSC, 2% blocking reagent, 0.1% *N*-lauroyl-sarcosine and 0.02% SDS for 15 h with a digoxigenin-labeled RNA antisense probe generated from the full length (981 bp) CatL-A clone (RNA DIG Labeling and Detection Kit, Roche). Enzymatic detection by alkaline phosphatase was done according to the manual. RNA in situ hybridization was done on paraffin cross-sections of adult *F. gigantica* using the cathepsin L probe mentioned above. Standard stringent hybridization conditions were used.

3. Results

3.1. Molecular cloning and sequence characterization

The RT-PCR resulted in the generation of a prominent 981 bp DNA fragment for all primer combinations which amplified the full length coding region, and in a 660-bp DNA fragment for the primer combination amplifying the region encoding the mature protein. The origin of the RT-PCR products from RNA was verified by a control PCR of genomic DNA that did not result in the amplification of such fragments when using the same primer combinations and reaction conditions, due to intron sequences in the genomic DNA (data not shown). DNA sequence analysis of selected subcloned PCR products revealed that they encoded six different forms of cathepsin L-like proteins with identities of the deduced amino acid sequences ranging from 75.3 to 99.1% (Table 1). Alignment of the amino acid sequences of cathepsin L proteins of *F. gigantica* and *F. hepatica* showed that these proteins are highly conserved between the two species (Fig. 1), [13–17]. Important residues found in S′, S2 and S3 substrate binding sites and the active site of human cathepsin L are conserved in all *Fasciola* cathepsin L sequences [18,19]. Cysteine residues forming disulfide bonds for proper folding of the protein are fully conserved. Also conserved are residues of the proregion that were found in human procathepsin L to be crucial for proper folding and/or contacts with residues of the mature protein [20]. The proregion inhibits enzyme activity [21,22] and is necessary for correct folding and stabilization of the enzyme [23]. Interestingly, residues thought to be important for lysosomal targeting of human cathepsin L are only partially conserved in *Fasciola* [24,25]. This is understandable because in *Fasciola* cathepsin L proteins are transferred in special vesicles and secreted into the gut lumen. For all but one (CatL-F) of the six cathepsin L proteins, a corresponding cathepsin L of *F. hepatica* exists that has a higher value of identity than any other of the analyzed *F. gigantica* proteins (Table 1). This indicates that gene duplication events and genetic modifications that led to the generation of this family of genes had taken place before *F. gigantica* and *F. hepatica* became two distinct species. Analysis of whether these are the 'true homologous' cathepsin L proteins or not has to await cloning and sequence analysis of all cathepsin L encoding genes from both species. Eventually, it will be necessary to determine substrate specificities for all members. Differences in the substrate

Table 1
Identity matrix of *Fasciola* cathepsin L amino acid sequences[a]

	CatL-A	CatL-B	CatL-C	CatL-D	CatL-E*	CatL-F*	L33771	L33772	S70380	U62288	U62289	Z22763*	Z22764*	Z22765	Z22766*	Z22767*
CatL-A																
CatL-B	98.2															
CatL-C	85.6	85.0														
CatL-D	78.5	79.1	79.8													
CatL-E*	98.2	99.1	83.6	76.7												
CatL-F*	79.9	80.4	84.9	75.3	79.9											
L33771	94.5	93.6	86.2	77.3	93.2	81.3										
L33772	85.3	85.0	89.9	78.8	85.4	83.6	86.8									
S70380	98.2	98.2	85.0	77.9	99.1	79.9	93.6	85.0								
U62288	93.6	92.9	85.9	77.3	92.2	80.4	96.3	84.7	92.9							
U62289	77.3	78.2	80.1	92.3	75.3	76.7	77.9	80.4	77.0	77.3						
Z22763*	73.3	72.1	77.0	70.3	72.1	73.9	72.1	73.9	72.7	70.9	69.7					
Z22764*	72.1	72.1	76.4	89.7	72.1	73.9	73.3	77.0	72.7	73.3	96.4	69.1				
Z22765	76.7	77.3	80.1	92.3	74.4	76.3	77.6	80.7	76.4	77.0	96.9	68.5	99.4			
Z22766*	83.0	83.0	90.3	76.4	83.0	82.4	86.1	93.3	83.6	83.0	78.8	77.0	78.2	78.2		
Z22767*	49.7	49.7	49.1	45.5	49.7	47.3	47.9	48.5	49.7	48.5	47.3	46.7	46.1	46.1	49.7	
Z22769*	84.9	84.2	81.8	73.3	84.2	75.2	87.9	82.4	84.9	88.5	74.6	70.9	73.5	73.5	83.6	47.3

[a] Values (expressed in %) are based on identical residues. * Only the partial sequence information available was used for calculations. L33771 [16]; L33772 (unpublished); S70380 [17]; U62288 [14]; U62289 [13]; Z22763-67, and Z22769 [15].

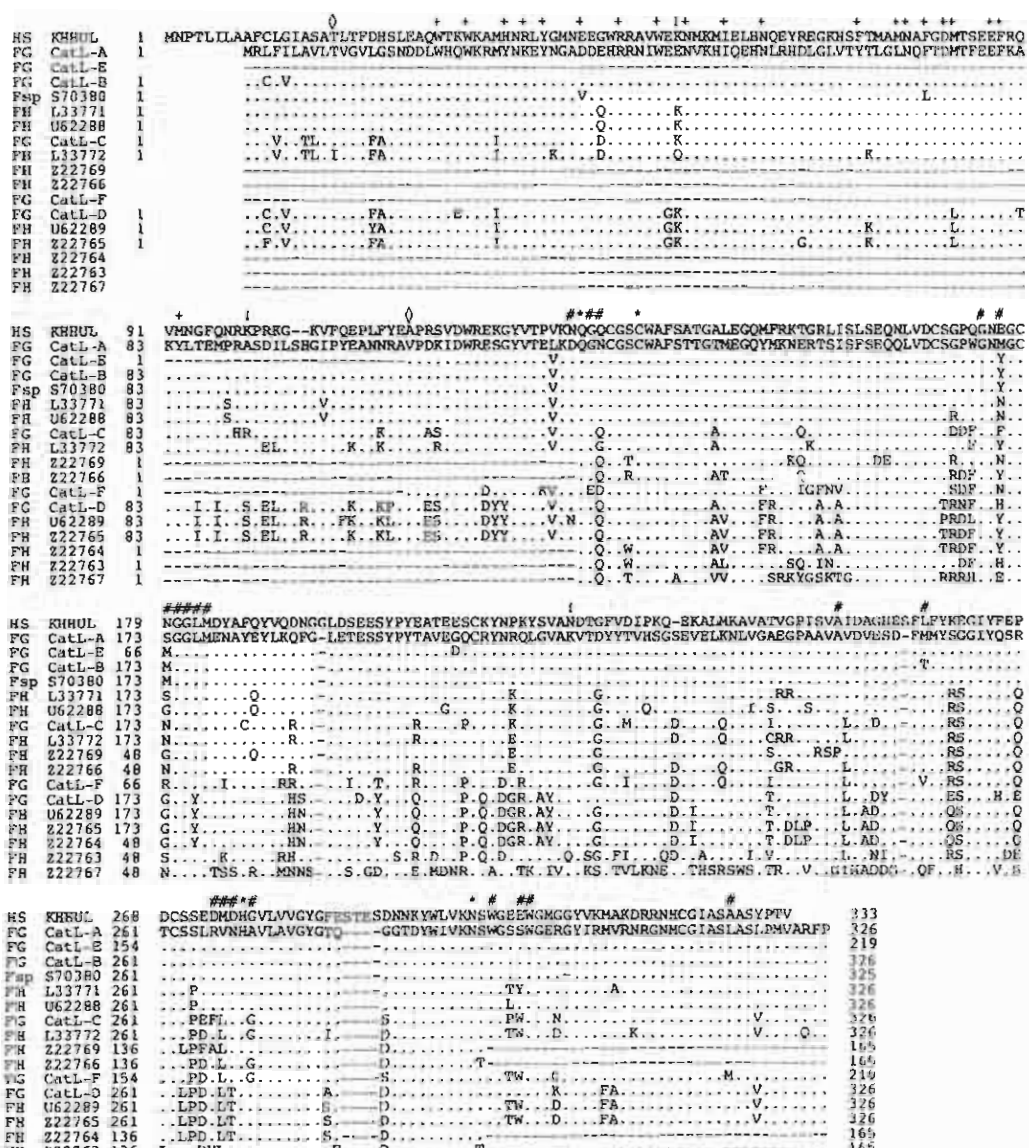

Fig. 1. Alignment of cathepsin L amino acid sequences. The six cathepsin L sequences (CatL-A–F) and 11 cathepsin L sequences of *Fasciola* published in GenBank were aligned with human cathepsin L. Full sequence information is given for human cathepsin L and CatL-A, differences towards CatL-A are shown for the other *Fasciola* sequences, only. Dashes indicate sequences that were not determined or internal gaps. Amino acids shown to participate in the formation of substrate binding sites (#), the active site (*), proper folding of the proregion (+) and in lysosomal targeting (!) in human cathepsin L. ◇ indicates the first amino acids of the proregion and the mature protein in human cathepsin L, respectively. L33771 [16]; L33772 (unpublished); S70380 [17]; U62288 [14]; U62289 [13]; Z22763-67, and Z22769 [15].

specificities were demonstrated for *F. hepatica* cathepsin L proteins [2]. It is expected that a more similar CatL-F homolog may exist in *F. hepatica*.

3.2. Southern analysis of CatL gene copy number

The number of cathepsin L genes in the parasite genome was determined by Southern hybridization using a DIG-labeled RNA antisense probe generated from CatL-A. This probe hybridized to all six cloned cathepsin L sequences due to the high values of identity among them (87–99% identity at the DNA level), even when using stringent hybridization conditions. Southern analysis of genomic DNA, resulted in a complex banding pattern with approximately 10 different hybridizing DNA fragments in each sample lane, ranging in size from 1.2 kb to more than 22 kb (Fig. 2). Hybridization conditions were stringent, and only restriction enzymes that do not cut the six cloned cathepsin L fragments were used for this analysis. This selection should help keep the number of hybridizing fragments as small as possible but non-analyzed intron sequences, which might contain these restriction sites, could still result in an overestimation of the number of cathepsin L gene copies in the genome of *F. gigantica*. The complete enzymatic digestion of the DNA was validated by hybridization with different species-specific probes (fatty acid binding protein and glutathione *S*-transferase gene fragments, data not shown). The number of hybridizing fragments did not vary between enzymes and enzyme combinations. We conclude that a cathepsin L gene family exists in *F. gigantica* comprising an estimated 10 closely related cathepsin L genes. More diverged members of this family were not detected due to the chosen hybridization conditions.

3.3. Gene expression analysis by Northern and in situ hybridization

For both Northern and in situ hybridization, the CatL-A antisense RNA probe described before was used. Northern analysis of total RNA revealed that transcription of active cathepsin L

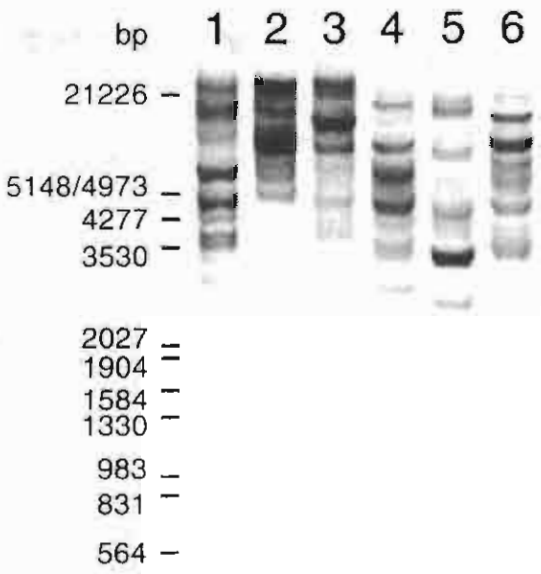

Fig. 2. Southern blot analysis of *F. gigantica* genomic DNA. Dashes to the left side indicate fragment positions of the molecular weight size marker, lambda DNA digested by *Eco*R I/*Hin*d III. Lanes 1–6: 5 μg DNA each were digested with *Eco*R V (1), *Hin*d III (2), *Pst* I (3), *Eco*R V/*Hin*d III (4), *Eco*R V/*Pst* I (5) and *Hin*d III/*Pst* I (6), respectively.

genes in the adult fluke results in a mixed mRNA population of approximately 1050 nucleotides length (Fig. 3). This size is somewhat smaller than reported for *F. hepatica* where transcripts of 1.2–1.3 kb could be detected, and this might be due to differences in the length of the poly(A) tail [15]. Hybridization signals could still be obtained from nanogram amounts of total RNA (data not shown). The abundance of cathepsin L proteins is therefore reflected at the RNA level and should group the gene family among the strongest expressed genes of *F. gigantica*. To detect only hybridization signals of gene-specific mRNAs it would be necessary to prepare short, gene-specific probes in every case. RNA in situ hybridization was done on paraffin cross-sections of adult specimens for an analysis of tissue-specific expression of cathepsin L genes. Strong hybridization signals were obtained in the cecal epithelial cells after short (1–5 min) incubation times, indicating again

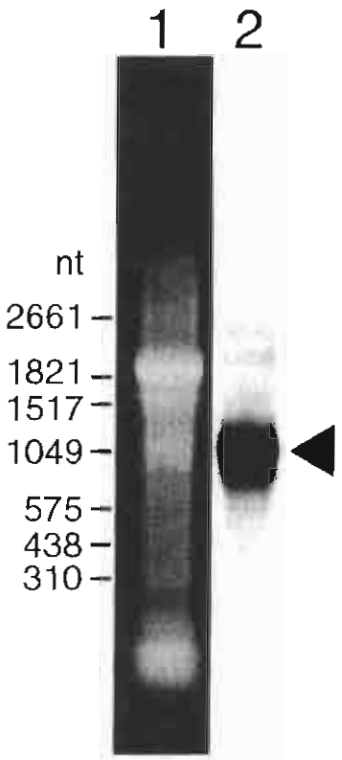

Fig. 3. Northern blot analysis of total RNA extracted from adult flukes. Dashes to the left side indicate fragment positions of the RNA molecular weight marker I (Roche). Lane 1: Agarose gel containing the size-separated total RNA before blotting. Lane 2: Northern hybridization with a CatL-A probe. Arrowhead: cathepsin L transcripts.

the abundance of these transcripts (Fig. 4). The detection of cathepsin mRNA in these cells correlates with results obtained by immunolocalization studies of cathepsin L proteinases in *Fasciola* [26,27].

4. Discussion

F. hepatica and *F. gigantica* are major trematode parasites of cattle and sheep. Although closely related, it is known that biological differences exist between the two species that make a thorough analysis not only worth considering but a necessity (reviewed in [28]). In this respect the present work was undertaken to provide basic information on the cathepsin L gene family in *F. gigantica*, and how it compares to that in *F. hepatica*. The data obtained will be of use for immunological studies of *F. gigantica* cathepsin L. Furthermore, it will be of interest to study gene-specific expression patterns during development to analyze whether selected cathepsin L genes might be especially useful for applied studies of diagnosis and immunological protection. As indicated by Roche et al. [14], not all cathepsin L proteins will be secreted into the gut lumen. Two different secreted forms of native cathepsin L could be purified from the excretion/secretion

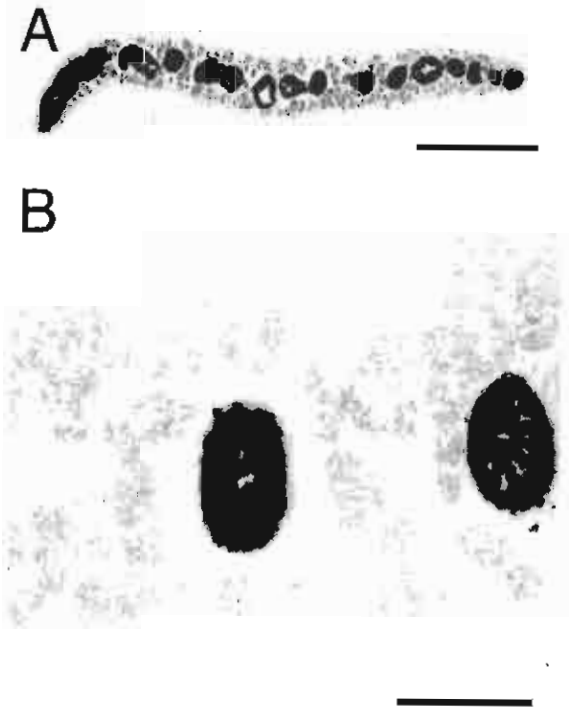

Fig. 4. Localization of cathepsin L mRNA by in situ hybridization on paraffin cross-sections of adult flukes. A DIG-labelled antisense RNA probe prepared from FgCatL-A was used. (A) Cross-section at 25% anterior worm length, bar = 1 mm. (B) Higher magnification of similar section, bar = 200 μm. Hybridization signals are restricted to the cecal epithelial cells.

(E/S) material of *F. hepatica* as revealed by N-terminal protein sequencing [2,26]. These cathepsin L proteins showed different in vitro activities towards synthetic substrates and varied slightly in their molecular weight. During later cloning of corresponding cDNAs, two cathepsin L clones were isolated and expressed in a yeast expression system [13,14]. The yeast-expressed *F. hepatica* proteins were secreted into the culture medium and showed the same substrate specificities of the native proteins that were observed before. Yet, the purified native proteins and the proteins encoded by the cDNA vary in their corresponding N-terminal amino acid sequences. Therefore, the E/S material seems to contain more than two different forms of cathepsin L that have similar substrate specificities. The two purified proteins bring the total number of cathepsin L proteins (genes) in *F. hepatica* to 13 and are not likely to be the last members of the family that are isolated. Our results show a comparable number of genes in *F. gigantica* with up to 10 closely related members. More divergent members were not detected due to the stringent hybridization conditions used. No analysis was done on the exact number of different clones obtained by RT-PCR, because we did not intend to clone each gene. It is arguable that some of the independently isolated cathepsin L sequences are alleles of the same gene. Among the *F. gigantica* sequences this might be the case for CatL-A, -B and -E, which are almost identical to *Fasciola* sp. S70380 [17]. The question as to whether the observed subtle differences are real existing sequence polymorphisms or were introduced by erroneous polymerase activities (e.g. endogenous RNA polymerase during transcription or reverse transcriptase and *Taq* DNA polymerase during RT-PCR) can only be answered by a comparative sequence analysis of RT-PCR products and genomic DNA from the same specimens. An independent RT-PCR experiment that was conducted with RNA isolated from a single worm to amplify the full coding sequence resulted in the cloning of cathepsin L genes, which have the same restriction fragment patterns as CatL-A, -C and -D when digested by *Eco*R I, *Hin*f I and *Hae* III.

Transcripts of the cloned cathepsin L genes are abundant in the adult fluke and are all approximately the same size (~1050 nucleotides). The size of the coding sequence (981 nt) indicates that beside a polyadenylated 3′-end only a few nucleotides will make up 5′- and 3′-untranslated regions of the processed mRNA. Therefore, space for regulative motifs, if any, contained in these regions of cathepsin L mRNAs will be limited. The transcripts can be readily identified in nanogram amounts of total RNA and are found by RNA in situ hybridization in the epithelial cells of the cecum. This finding corresponds to immunolocalization studies where cathepsin L was found to be concentrated in cytoplasmic vesicles of these cells, ready to be released into the cecal lumen. The huge amounts of transcripts, even when it is considered that they are expressed by several genes, indicate that besides a strong promotor, further transcription enhancing and tissue-specificity promoting elements will drive the expression of these genes. Analysis of how cathepsin L gene activity is regulated by such *cis*- and *trans*-acting elements should prove useful as common regulatory mechanisms can be expected among the members of the gene family. This might provide valuable information on how to disrupt gene activity of the whole gene family. Blocking gene expression should pose a major threat to the parasite, given the functions that cathepsin L proteins are assumed to have in immune evasion, tissue penetration, and nutrition [3,5,6]. In addition, isolation of the transcriptional enhancer sequences should be valuable for future studies involving gene transfer and expression studies in *Fasciola*. In summary, these results indicate that cathepsin L genes and encoded proteins are a promising target for further analysis with respect to the development of diagnosis and vaccination, as well as an example of molecular mechanisms of gene regulation in *Fasciola*.

Acknowledgements

We are grateful to Dr John Milne for critically reading the manuscript. This work was supported by grants from the National Center for Genetic Engineering and Biotechnology (NSTDA, BT-B-

06-2B-14-004) Thailand to V. Viyanant and the Thailand Research Fund (TRF, Senior Research Scholar Fellowship) to P. Sobhon.

References

[1] Srihakim S, Pholpark M. Problem of fascioliasis in animal husbandry in Thailand. Southeast Asian J. Trop. Med. Public Health 1991;22(Suppl):352–5.

[2] Dowd AJ, Smith AM, McGonigle S, Dalton JP. Purification and characterisation of a second cathepsin L proteinase secreted by the parasitic trematode *Fasciola hepatica*. Eur J Biochem 1994;223:91–8.

[3] Carmona C, Dowd AJ, Smith AM, Dalton JP. Cathepsin L proteinase secreted by *Fasciola hepatica* in vitro prevents antibody-mediated eosinophil attachment to newly excysted juveniles. Mol Biochem Parasitol 1993;62:9–17.

[4] Smith AM, Dowd AJ, Heffernan M, Robertson CD, Dalton JP. *Fasciola hepatica*: a secreted cathepsin L-like proteinase cleaves host immunoglobulin. Int J Parasitol 1993;23:977–83.

[5] Berasain P, Goñi F, McGonigle S et al. Proteinases secreted by *Fasciola hepatica* degrade extracellular matrix and basement membrane components. J Parasitol 1997;83:1–5.

[6] Dowd AJ, McGonigle S, Dalton JP. *Fasciola hepatica* cathepsin L proteinase cleaves fibrinogen and produces a novel type of fibrin clot. Eur J Biochem 1995; 232:241–6.

[7] Dalton JP, McGonigle S, Rolph TP, Andrews SJ. Induction of protective immunity in cattle against infection with *Fasciola hepatica* by vaccination with cathepsin L proteinases and with hemoglobin. Infect Immun 1996;64:5066–74.

[8] Cornelissen JBWJ, Gaasenbeek CPH, Boersma W, Borgsteede FHM, van Milligen FJ. Use of a pre-selected epitope of cathepsin-L1 in a highly specific peptide-based immunoassay for the diagnosis of *Fasciola hepatica* infections in cattle. Int J Parasitol 1999;29:685–96.

[9] O'Neill SM, Parkinson M, Dowd AJ, Strauss W, Angles R, Dalton JP. Short report: Immunodiagnosis of human fascioliasis using recombinant *Fasciola hepatica* cathepsin L1 cysteine proteinase. Am J Trop Med Hyg 1999;60:749–51.

[10] Strauss W, O'Neill SM, Parkinson M, Angles R, Dalton JP. Short report: Diagnosis of human fascioliasis: detection of anti-cathepsin L antibodies in blood samples collected on filter paper. Am J Trop Med Hyg 1999; 60:746–8.

[11] O'Neill SM, Parkinson M, Strauss W, Angles R, Dalton JP. Immunodiagnosis of *Fasciola hepatica* infection (fascioliasis) in a human population in the Bolivian Altiplano using purified cathepsin L cysteine proteinase. Am J Trop Med Hyg 1998;58:417–23.

[12] Thompson JD, Gibson TJ, Plewniak F, Jeanmougin F, Higgins DG. The CLUSTAL – X windows interface: flexible strategies for multiple sequence alignment aided by quality analysis tools. Nucleic Acids Res 1997; 25:4876–82.

[13] Dowd AJ, Tort J, Roche L, Ryan T, Dalton JP. Isolation of a cDNA encoding *Fasciola hepatica* cathepsin L2 and functional expression in *Saccharomyces cerevisiae*. Mol Biochem Parasitol 1997;88:163–74.

[14] Roche L, Dowd AJ, Tort J et al. Functional expression of *Fasciola hepatica* cathepsin L1 in *Saccharomyces cerevisiae*. Eur J Biochem 1997;245:373–80.

[15] Heussler VT, Dobbelaere DAE. Cloning of a protease gene family of *Fasciola hepatica* by the polymerase chain reaction. Mol Biochem Parasitol 1994;64:11–23.

[16] Wijffels GL, Panaccio M, Salvatore L, Wilson LR, Walker ID, Spithill TW. The secreted cathepsin L-like proteinases of the trematode, *Fasciola hepatica*, contain 3-hydroxyproline residues. Biochem J 1994;299:781–90.

[17] Yamasaki H, Aoki T. Cloning and sequence analysis of the major cysteine protease expressed in the trematode parasite *Fasciola* sp. Biochem Mol Biol Int 1993;31: 537–42.

[18] Fujishima A, Imai Y, Nomura T, Fujisawa Y, Yamamoto Y, Sugawara T. The crystal structure of human cathepsin L complexed with E-64. FEBS Lett 1997;407:47–50.

[19] Guncar G, Pungercic G, Klemencic I, Turk V, Turk D. Crystal structure of MHC class II-associated p41 Ii fragment bound to cathepsin L reveals the structural basis for differentiation between cathepsins L and S. EMBO J 1999;18:793–803.

[20] Coulombe R, Grochulski P, Sivaraman J, Ménard R, Mort JS, Cygler M. Structure of human procathepsin L reveals the molecular basis of inhibition by the prosegment. EMBO J 1996;15:5492–503.

[21] Carmona E, Dufour E, Plouffe C et al. Potency and selectivity of the cathepsin L propeptide as an inhibitor of cysteine proteases. Biochemistry 1996;35:8149–57.

[22] Roche L, Tort J, Dalton JP. The propeptide of *Fasciola hepatica* cathepsin L is a potent and selective inhibitor of the mature enzyme. Mol Biochem Parasitol 1999; 98:271–7.

[23] Tao K, Stearns NA, Dong J, Wu Q-long, Sahagian GG. The proregion of cathepsin L is required for proper folding, stability, and ER exit. Arch Biochem Biophys 1994;311:19–27.

[24] Cuozzo JW, Tao K, Cygler M, Mort JS, Sahagian GG. Lysine-based structure responsible for selective mannose phosphorylation of cathepsin D and cathepsin L defines a common structural motif for lysosomal enzyme targeting. J Biol Chem 1998;273:21067–76.

[25] Cuozzo JW, Tao K, Wu Q-long, Young W, Sahagian GG. Lysine-based structure in the proregion of procathepsin L is the recognition site for mannose phosphorylation. J Biol Chem 1995;270:15611–9.

[26] Smith AM, Dowd AJ, McGonigle S et al. Purification of a cathepsin L-like proteinase secreted by adult *Fasciola hepatica*. Mol Biochem Parasitol 1993;62:1–8.

[27] Yamasaki H, Kominami E, Aoki T. Immunocytochemical localization of a cysteine protease in adult worms of the liver fluke *Fasciola* sp. Parasitol Res 1992;78:574–80.

[28] Spithill TW, Smooker PM, Copeman DB. *Fasciola gigantica*: epidemiology, control, immunology and molecular biology. In: Dalton JP, editor. Fasciolosis. 1st ed. Oxon & New York: CABI Publishing, 1999:465–525.

ScienceAsia 27 (2001) : 1-14

Classification of Developing Oocytes, Ovarian Development and Seasonal Variation in *Rana tigerina*

Prapee Sretarugsa[a,*], Wattana Weerachatyanukul[a], Jittipan Chavadej[a], Maleeya Kruatrachue[b] and Prasert Sobhon[a]

[a] Department of Anatomy, Faculty of Science, Mahidol University, Rama VI Road, Bangkok 10400, Thailand.

[b] Department of Biology, Faculty of Science, Mahidol University, Rama VI Road, Bangkok 10400, Thailand.

[*] Corresponding author. E-mail: scpsr@mahidol.ac.th

Received 27 Oct 2000
Accepted 7 Nov 2000

ABSTRACT Developing oocytes in adult *Rana tigerina* can be divided into six stages based on size, color and histology. The stage I oocyte (50-350 μm) is characterized by translucent cytoplasm and a smooth nuclear membrane. The major portion of its cytoplasm contains a large quantity of free ribosomes. Cytoplasmic organelles confined to the peripheral part of oocyte include a few mitochondria, Golgi apparatus, primary and secondary lysosomes, and a few lipid droplets. The stage II oocyte (360-550 μm) contains alcian-blue positive cortical alveoli at the periphery and large central nucleoli in the nucleus. The stage III oocyte (560-900 μm) is characterized by the deposition of yolk platelets and formation of pigmented granules. The cortical alveoli are greatly increased in number as well as in size. Endocytotic activity on the surface of oocyte can be observed. The stage IV oocyte (910-1300 μm) is characterized by a large number of main yolk bodies, cortical alveoli and melanin granules. High endocytotic activities are observed. In the stage V oocyte (1310-1500 μm), most of the melanin granules migrate to the animal pole, while the cortical granules are concentrated underneath the oolemma. The stage VI or fully grown oocyte (1510-1700 μm) is characterized by a complete absence of melanin granules in the vegetal pole and by the cessation of endocytotic activity. Studying the development of ovaries in frogs at various ages reveals that definitive ovaries are formed in the one-month-old frog. Ovaries of two- to four-month-old frogs contain only stage I oocytes, while the ovaries of twelve-month-old frogs contain oocytes of all stages, which indicate the maturity of female frogs. Studying the seasonal variation of ovaries throughout the year reveals that there are no stage VI oocytes in ovaries collected from November to February, while these oocytes are present during the period from March to October.

KEYWORDS: *Rana tigerina*, developing oocytes, ultrastructure, ovarian development, seasonal variation.

INTRODUCTION

The classification of developing oocytes of anurans has been carried out by many researchers.[1-5] The most studied is *Xenopus laevis* whose oocytes have been classified into six stages based on their external appearance, color and size.[5] Similarly, in *Rana pipiens*, the same criteria have been used to classify developing oocytes.[2] In addition, oocytes can be classified by the uptake of vitellogenin or yolk protein into three stages: previtellogenesis, vitellogenesis and postvitellogenesis or mature oocytes.[1] There is currently little morphological data of the ovary and the classification of oocytes in *Rana tigerina*. Thus, one of the aims of the present study was to classify the developing oocytes in *R. tigerina* based on their morphological and histological features.

Detailed studies on the morphological changes in the oocyte cytoplasm, the oocyte-follicle cell relationships and the process of vitellogenesis have been carried out in *R. esculenta*,[6] *R. pipiens*,[7] *Triturus viridescens*[8] and *X. laevis*.[9,10] By comparison in *R. tigerina* there is still a lack of information on the ultrastructure of developing oocytes. Hence, another aim of the present study was to investigate the ultrastructure of developing oocytes of this species.

Reproductive cyclicity seems to be correlated with the climatic condition prevailing in the habitats. Slight annual variations in environmental conditions could disrupt breeding cycles. Annual variation in the precipitation seems to be the main factor in inducing periodicity in breeding activity. In habitats within equatorial regions with a constant warm and humid climate, amphibians may reproduce throughout the year, such as the frog *Rana erythraea* in Borneo,[11] and the toad *Bufo melanostictus* in Singapore and Jarkata.[12,13] In those regions with pronounced wet and dry seasons, the main breeding season

coincides with monsoon rains.[11] Even in the same species, a high variation in breeding period occurs, such as in the African toad *Bufo regularis*, whose breeding period coincides with the beginning of the rainy season from November to April in Tanzania[12] and in March in Kenya.[16] In Thailand where the climate is sharply split into wet and dry seasons, native frog species including *R. tigerina* are expected to be seasonal breeders. Therefore, another aim of this study was to study the histological changes of the ovarian cycle of *R. tigerina* during different months of the year. In addition, the development of ovaries in various ages of the female frogs and the reproductive maturity of this species were also investigated.

Materials and Methods

Experimental Animals

R. tigerina, the rural rice field frogs of Thailand, were cultured in the concrete tanks at the Faculty of Science, Mahidol University, Bangkok, Thailand. They were maintained in a natural environment with an approximate 12 hours light/dark cycle. The ambient temperature was 25-35°C, and the relative humidity ranged from 80 to 100%. Pelleted frog feeds were given daily in the afternoon. The water in the culture tanks was changed on alternate days.

Classification of ovarian follicles/ oocytes

Frogs were anesthetized by hypothermia and the ovaries were removed and transferred to 50% frog's Ringer solution.[17] Follicles with various sizes were randomly isolated from fragments of ovaries, and the diameters of follicles were measured with an eyepiece micrometer fitted in an Olympus stereomicroscope. The follicles/oocytes were classified into various stages based on their size and color.[5]

Histological study

Both ovarian fragments and isolated follicles were fixed either in Bouin's solution, or 10% buffered formalin for 3 hours. Then they were dehydrated through a graded series of ethanol, cleared in dioxane, and embedded in paraffin. Large-yolky oocytes were fixed for 6-8 hours in Bouin's solution or overnight in 10% buffered formalin. Then they were dehydrated in increasing concentrations of ethanol for 30 minutes each, and immersed in methyl benzoate for about 3 days before clearing for 1 hour with two changes of benzene. The tissues were infiltrated in a mixture of benzene and paraffin. Six-micron-thick sections were deparaffinized and stained with Harris's hematoxylin and eosin. Finally, they were examined under an Olympus MT-2 light microscope.

In addition, several staining techniques were employed for the detection of lipid, acid mucopolysaccharide, protein and glycoprotein in the oocytes. For the detection of lipid, small pieces of ovary were fixed in Ciaccio's solution and stained either with saturated oil red-O or Sudan III.[18] For the detection of acid mucopolysaccharide, small pieces of ovary were fixed in 2.5% glutaraldehyde and stained with 0.1% alcian blue, concomitantly with 0.1% Kernechtrot nuclear fast red.[18] For the detection of protein and glycoprotein, the ovarian tissue was fixed either in Bouin's solution or in buffered formalin. Sections were stained with Lee-Brown's modified Mallory trichrome dye.[18]

Ultrastructural study

For transmission electron microscopy (TEM), all stages of oocytes were prefixed for 18-24 hours in 2.5% glutaraldehyde in 0.05M cacodylate buffer pH 7.4 at 4°C and washed in the same buffer. Thereafter, they were postfixed in 1% osmium tetroxide in the same buffer at 4°C for 1 hour and stained *en bloc* with 0.5% aqueous uranyl acetate. Then they were dehydrated through increasing concentrations of ethanol and embedded in Araldite resin. In case of large-yolky oocytes, a low viscosity Spurr's resin[19] was used instead of Araldite. Ultrathin sections were cut and stained with uranyl acetate, followed by Reynold's lead citrate.[20] Finally they were examined under a Hitachi H-300 transmission electron microscope at 75 kV.

Development and seasonal variation of ovarian follicles

Four to six developing frogs from one month to 14 months old were collected at each month for this study. Ovarian follicles of various sizes were isolated, classified, and counted under a stereomicroscope as previously described. For each frog at least 300-500 follicles from right and left ovaries were counted to establish the percentage of various stages of oocytes at each month. In addition, pieces of ovaries from frogs collected at each month were also prepared and examined by conventional light microscopy as previously described.

For the study on the seasonal variation of the ovary, adult frogs aged more than 12 months were used. The ovaries from 4-6 frogs were obtained every month during the year. Various stages of oocytes were classified and counted under a stereomicroscope as previously described.

Results

Stages of oocytes/follicles

The multilobed ovary of an adult frog contains developing oocytes which can be classified into six stages based on size, color and histology.

Stage I oocyte: previtellogenic stage

Under the stereomicroscope, the stage I oocyte exhibits a translucent cytoplasm with a diameter ranging from 50-350 μm (Fig 1A). The nucleus is clearly visible through the cytoplasm and occupies a large portion of the oocyte. At light microscopic level, the cytoplasm of the previtellogenic stage I oocyte appears heavily basophilic. In addition, it also acquires a smooth nuclear membrane and nucleoli of various sizes (Fig 1B). In the late stage I oocyte, the cytoplasm stains paler when compared to the early stage.

Stage II oocyte: previtellogenic stage

This stage develops an opaque ring around its concentric nucleus. Its size ranges from 351-550 μm (Fig 1A). Towards the end of this stage, the cytoplasm is almost completely opaque so that the nucleus becomes inconspicuous under a stereomicroscope. Hence, the translucent stage I oocyte can be easily separated from the dark opaque stage II oocyte. Histologically, the presence of a few rows of peripheral vacuoles (cortical alveoli) seems to be the most predominant characteristics of stage II oocyte (Fig 1B). In addition, numerous nucleoli which vary in size can be observed in each cell.

Stage III oocyte: vitellogenic stage

The opacity is complete in the stage III oocyte as it appears intensely white. The diameter of stage III oocyte is 560-900 μm (Fig 1A). Histologically, the number of vacuoles gradually increases, and they become dispersed towards the central area (Fig 1C). Yolk platelets are formed and rapidly replace the central vacuoles. The vitelline envelope also becomes conspicuous under the follicle cells. Pigmented granules first appear in this stage and are located at the periphery of the oocyte. The nucleus of the stage III oocyte possesses a convoluted nuclear membrane and numerous nucleoli.

Stage IV oocyte: vitellogenic stage

The distinct morphological feature of the stage IV oocyte is the pigmentation of the surface as light-brown to brown. The oocyte is 910-1300 μm in diameter (Fig 1A). Yolk platelets completely replace the central vacuoles, while the remaining vacuoles are located around the periphery of oocyte (Fig 1C). The nucleus is surrounded by a highly convoluted nuclear membrane and contains a large number of nucleoli.

Stage V and VI oocytes: vitellogenic and fully grown stages

Distinct polarity occurs in the last two stages, ie, stage V (1310-1500 μm) and stage VI (1510-1700 μm) (Fig 1A). This is manifested by the difference in pigmentation underneath the oolemma of the animal pole in contrast to the vegetal pole which contains large-yolk platelets instead; the nucleus also shifts to the animal pole (Fig 1D). The vacuoles are decreased in number while the yolk accumulation increases. The animal pole in the stage VI oocyte has only one row of vacuoles on the periphery, whereas two or three rows of vacuoles are present in the vegetal pole (Fig 1E, F).

Cytochemical studies of the oocytes are shown in Table 1. These revealed that there is no lipid component present in the vacuoles. Most of the bright red and brown lipid droplets are intermingled among yolk platelets and vacuoles. The distribution of lipid droplets at the periphery is more concentrated than that in the inner region of the late stage oocytes. Vacuoles, positively stained with 0.1% alcian blue, are developed in the stage II oocyte, and they become scattered throughout the cytoplasm in the stage III oocyte, and then accumulate at the periphery of stage IV to VI oocytes. Mallory trichrome dye stained the vitelline envelope in the stage II oocyte and revealed it as a thin layer. The thickness of the vitelline envelope gradually increases in stage III and IV oocytes and then reaches its maximal thickness in the stage V oocyte. In addition, yolk platelets also stained positive with this dye and appeared first in the stage III oocyte as bright red clusters on the cell periphery.

Table 1. Histochemistry of staging oocytes.

Structure	Stain		
	Oil Red-O/ Sudan III	Alcian blue	Mallory trichrome
Lipid droplet	+	-	-
Vacuole	-	+	-
Yolk platelet	-	-	+
Vitelline envelope	-	-	+

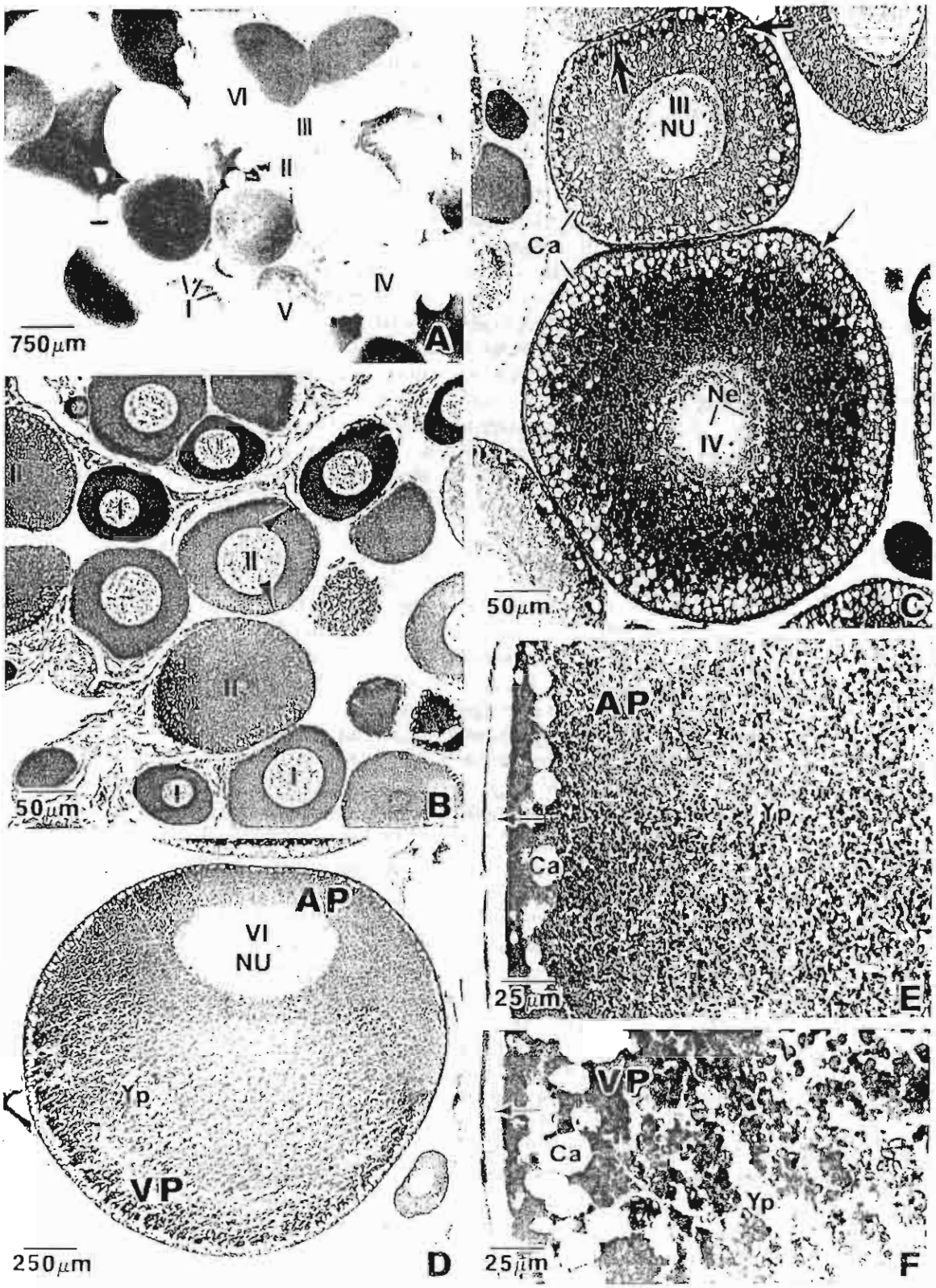

Fig 1. Stereomicrographs of ovarian fragments displaying randomly arranged follicles at stages I-VI (A). B,F: Light micrographs of ovarian fragments showing histology of stage I,II, III,IV and VI oocytes. Arrowhead, cortical alveolus (Ca); thick arrows, pigmented granules; thin arrows, vitelline coat; Nu, nucleus; Ne, nucleolus; AP, animal pole; VP, vegetal pole; Yp, yolk platelets.

Ultrastructure of developing oocytes

All stages of oocytes are covered with three cellular layers (Fig 2A). The outermost layer is a simple squamous surface epithelium. Beneath this is a layer of fibroblasts which secrete ground substance and make collagen fibers. The innermost layer is made up of follicle cells which project their cytoplasmic processes into the perivitelline space. These cells are joined together with desmosomes. In addition, the oocyte coat consists of a non-cellular layer, the vitelline envelope, whose fibers are arranged in three directions interposed between microvilli extending from the oocyte surface (Fig 2B).

The stage I oocyte contains a large quantity of free ribosomes and clusters of lysosomes. Mitochondria are loosely distributed throughout the cytoplasm (Fig 2C, C1). Within the perivitelline space, there are short cytoplasmic projections both from follicular cells called follicular processes, and from the oocyte surface called microvilli. The nucleus is surrounded by a wavy nuclear membrane and contains euchromatin and various sized electron-dense nucleoli (Fig 2D).

The stage II oocyte is characterized by the presence of vacuoles or cortical alveoli on the periphery (Fig 2E). Some cortical alveoli are coalesced and some are closely associated with lysosomes. The Golgi complex is well developed. In this stage, the vitelline envelope begins to form as isolated bundles of fine filaments within the perivitelline space. Both the microvilli of the oocyte and the cytoplasmic processes of the follicle cell become longer. The number of elongated to spherical shaped mitochondria is increased, and these are distributed around the nucleus (Fig 2F).

As previously mentioned, two major distinct features of the stage III oocyte are the deposition of yolk platelets and the formation of pigmented granules. Cortical alveoli become larger in size (Fig 3A). Groups of mitochondria are observed among the yolk platelets of vitellogenic oocytes, and endocytotic activity on the surface of the oocyte is initiated (Fig 3A1). Newly synthesized yolk platelets exhibit bipartite characteristics: the central paler compact body which is arranged into a crystalline lattice, and the peripheral electron-dense portion (Fig 3A2). Although pigmentation begins in this stage, most oocytes still contain only a few membrane-bound melanin granules called premelanosomes. The stage IV oocyte is characterized by coloration of the surface which is due to the presence of membrane-bound melanin granules (Fig 3B). Abundant endocytotic vesicles could be observed under the oolemma. A large number of endosomes appear close to lysosomes and some are fused with these lysosomes which contain electron-dense material (Fig 3C). More electron-dense main yolk bodies were observed in addition to the newly formed yolk platelets. Groups of mitochondria and lipid droplets are intermingled among yolk platelets (Fig 3D). Later, there is an increase in the number of yolk platelets in the perinuclear cytoplasm, while microvilli are increased in length and number. A highly folded nuclear membrane results in a sacculated nuclear outline (Fig3E).

In the stage V oocyte, most pigmented granules migrate toward the animal pole (Fig 4A), leaving only a few of them at the vegetal pole and perinuclear zone (Fig 4B). During this stage, the cortical alveoli with their translucent content are conspicuous underneath the oolemma. Some endocytotic activity could still be observed (Fig 4C). Although the general ultrastructures of the stage VI oocyte are quite similar to the stage V oocyte, the pigmented granules are completely absent from the vegetal pole, but endocytotic activity could be rarely observed (Fig 4D).

Development of ovarian follicle/ovary

A definitive ovary can also be observed in the one-month-old frog. It appears as a small oval organ and consists of a large number of primodial germ cells which undergo intense mitotic division. Most of the central region is occupied by mesenchymal cells referred to as the primary germinal cavity. This later develops into the secondary germinal cavity (Fig 5A, B). The presence of some stage I oocytes among the oogonia, primodial germ cells and stromal cells was observed. Lobulation of the ovary appears in the second month of development which results in multilobed ovaries. The number of stage I oocytes increases in the ovary of two-month-old frogs (Fig 5D). No oogonia were observed in the ovary of the four-month-old frog (Fig 5E). Stage II, III and IV oocytes become evident in the fifth, seventh and eleventh month of development, respectively (Fig 5F, G, H) while the last two stages (V and VI) appear when the frogs reach the age of 12 months.

The histograms in Figure 6 illustrate the percentages of various stages of oocytes during development, corresponding to the histological appearances as previously described. There are only stage I oocytes in the ovaries of frogs between one and four months of age. In the fifth, seventh and eleventh month, the proportions of stage II, III and IV oocytes are 1.5, 0.7, and 10.1%, respectively. The

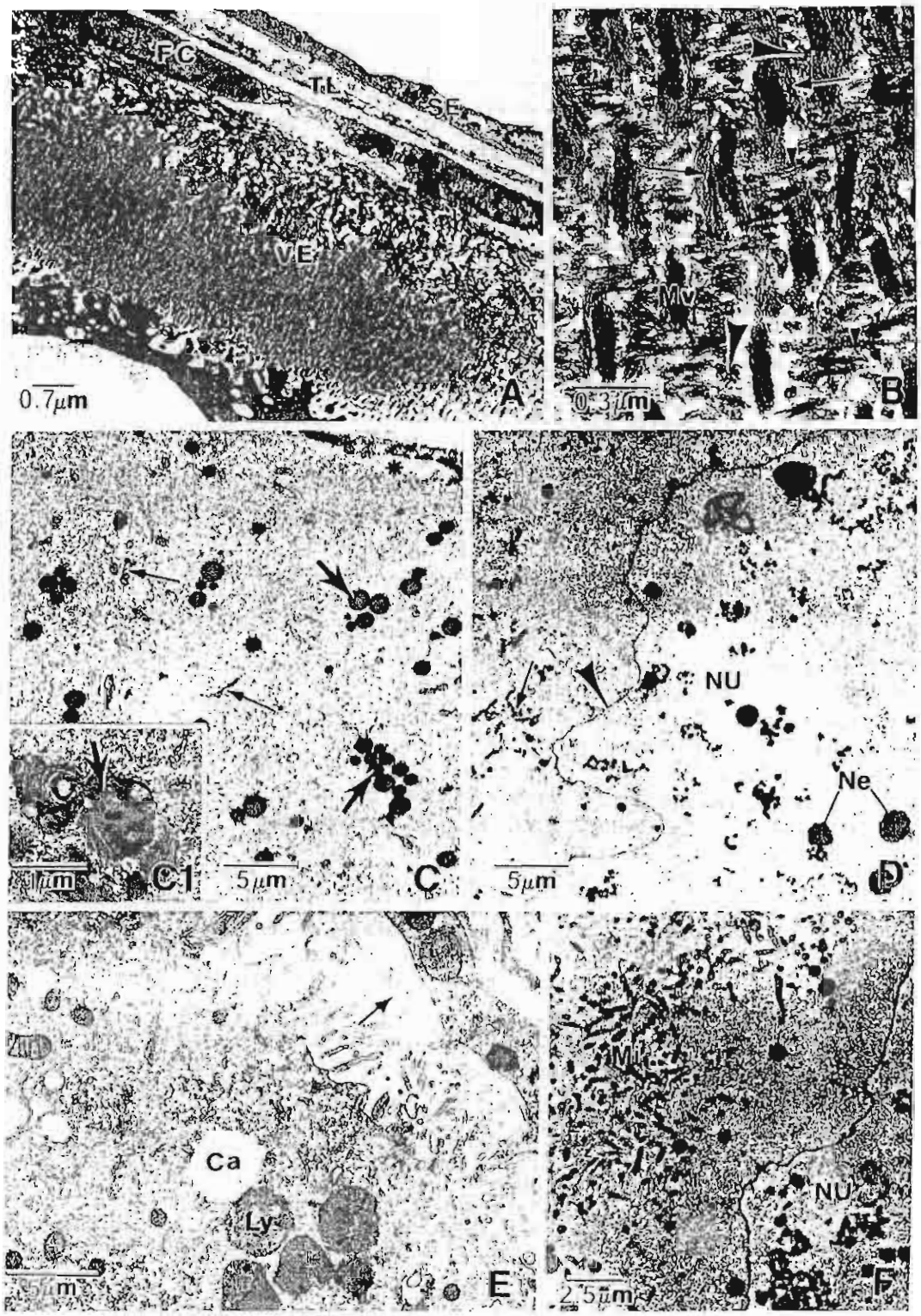

Fig 2. A. Electron micrographs illustrating the organization of the oocyte coat. SE, surface epithelium; TL, theca layer; FC, follicle cells; VE, vitelline envelope. B. High magnification of vitelline envelope displaying the intermingling of fibers arranged parallel (arrows), across (arrowheads) and perpendicular (smaller arrows) to the microvilli (Mv). C, C1, D. Stage I oocyte showing the distribution of mitochondria (arrows) and aggregation of lysosomes (large arrows). NU, nucleus; arrowhead, nuclear membrane; asterisk, perivitelline space. E, F. Stage II oocytes demonstrating the presence of cortical alveoli (Ca) associated with lysosomes (Ly), a bundle of fine filaments (arrow) and the groups of mitochondria (Mi). NU, nucleus.

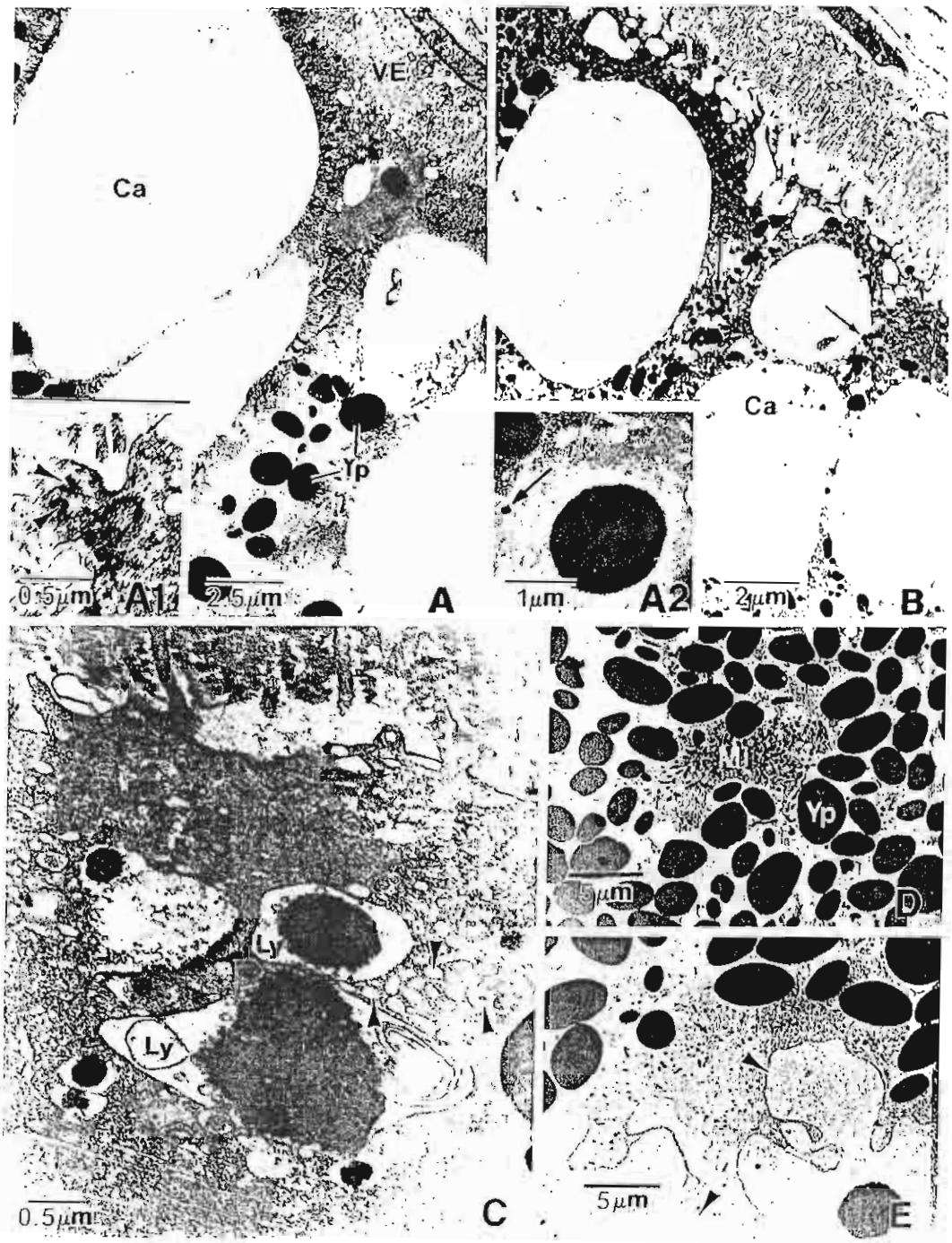

Fig 3. A. Electron micrographs of stage III oocytes showing the presence of yolk platelets (Yp), coated pits and vesicles (arrowheads) (A1) and pigmented granules (arrow) (A2). A2. Yolk platelet shows a bipartite structure. VE, vitelline envelope. B-D. Stage IV oocytes displaying a large number of yolk platelets, pigmented granules (arrows), endosomes (arrowheads) close to the lysosomes (Ly) containing electron-dense material, and the mitochondrial cluster. E. Nuclear membrane of stage IV oocyte showing numerous folds (arrow heads).

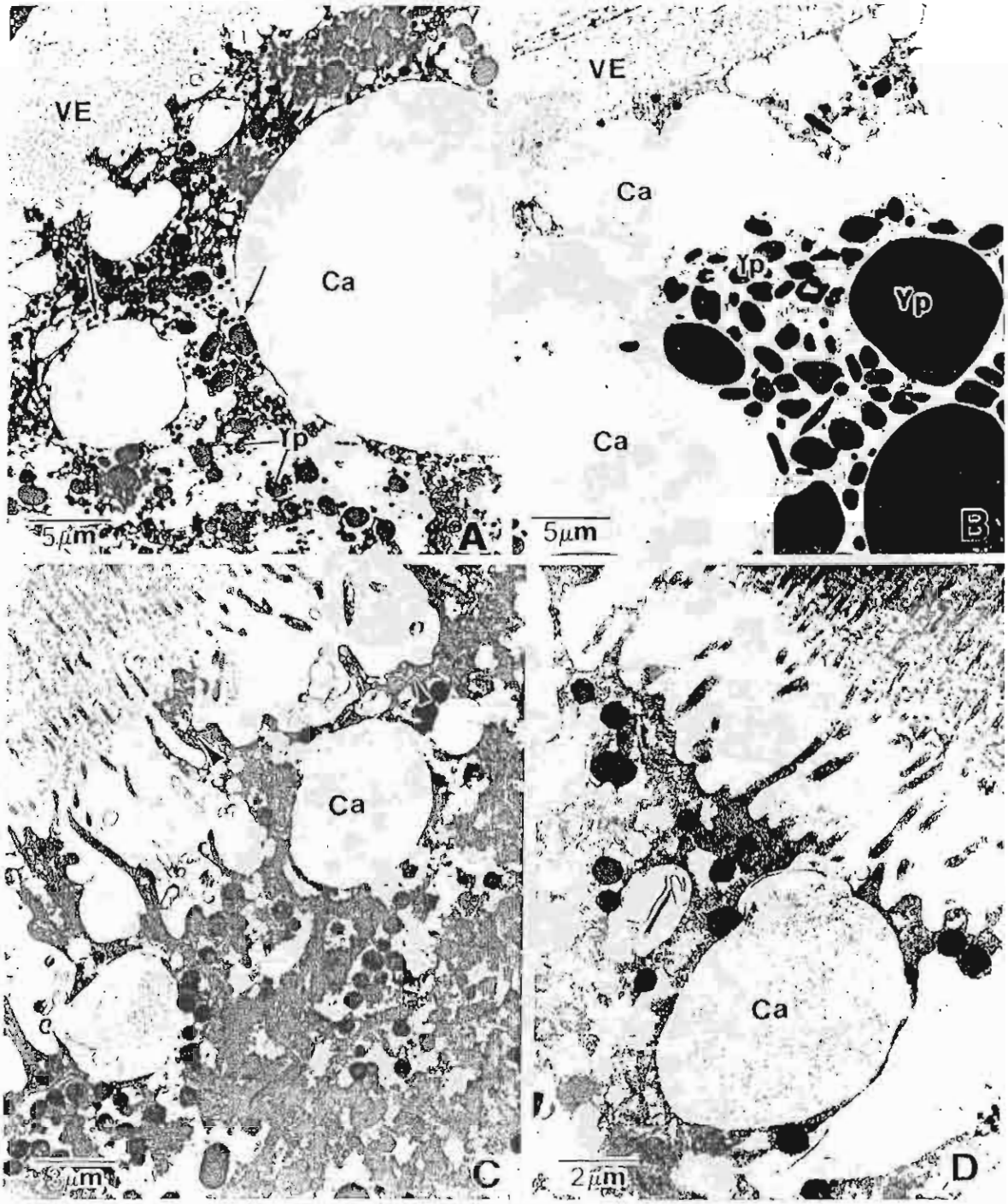

Fig 4. Electron micrographs of stage V oocytes displaying the presence of pigmented granules (arrows) and cortical alveoli (Ca) at the animal pole (A) whereas a few pigmented granules and 2-3 layers of cortical alveoli appear at the vegetal pole (B). Yp, yolk platelets; VE, vitelline envelope. Some endocytotic vesicles (arrowheads) are present in the stage V oocytes (C) while they are rare or absent in the stage VI oocytes (D).

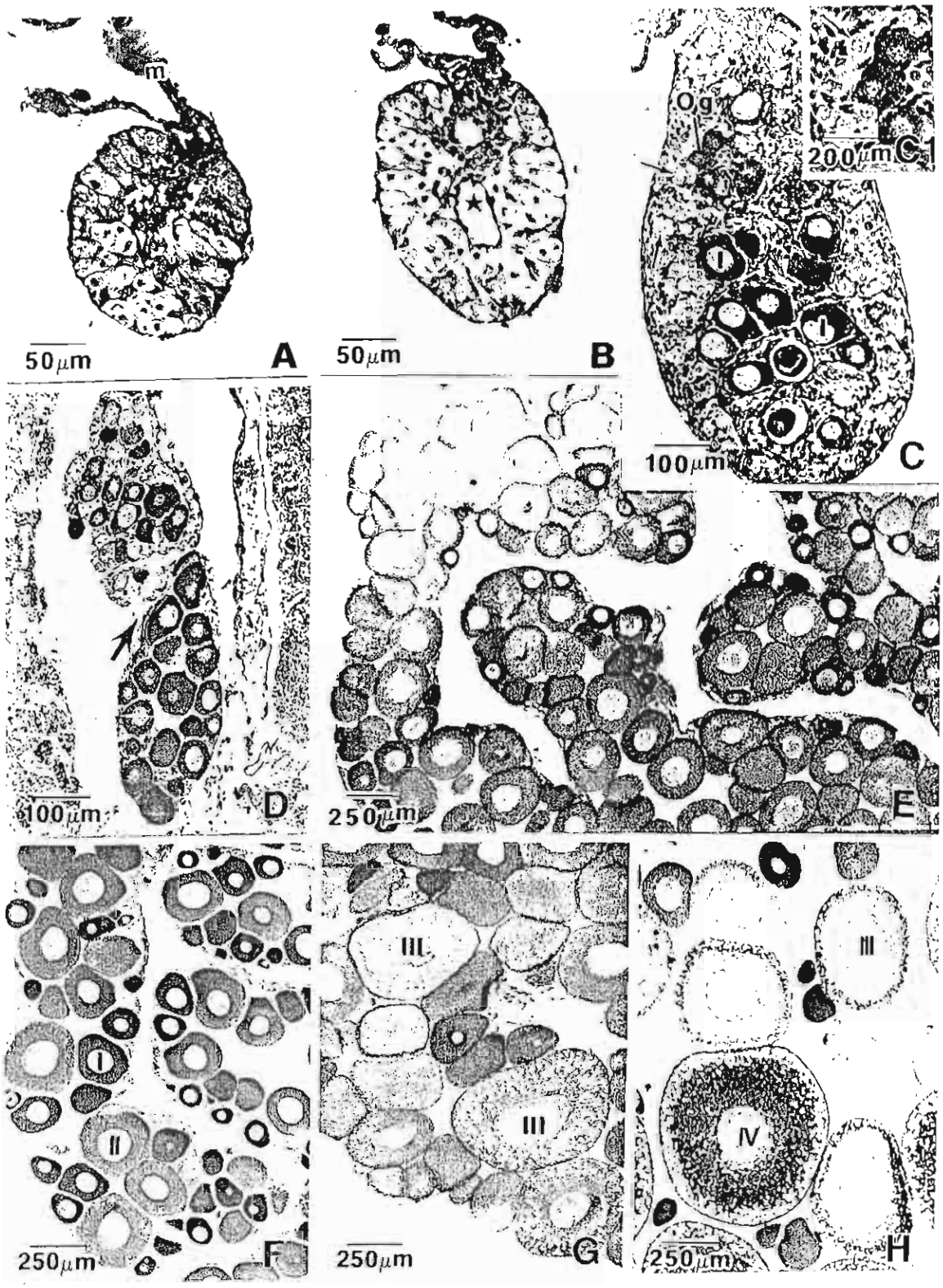

Fig 5. A-C Sections of one-month-old ovaries showing the primary (empty star) and secondary germinal cavities (dark star) and the mitotic division of primordial germ cells (PGC) (A,B). Oogonia (Og), PGC (arrows) and diplotene stage I oocytes (I) are present (C). Higher magnification of oogonia and PGC are illustrated in C1. D: Two-month-old ovaries displaying the stage I oocytes intermingled with PGC and oogonia. E: Four-month-old ovary consisting of only stage I oocytes. F,G,H: Ovaries aged five, seven and eleven months displaying stage II, III and IV oocytes, respectively.

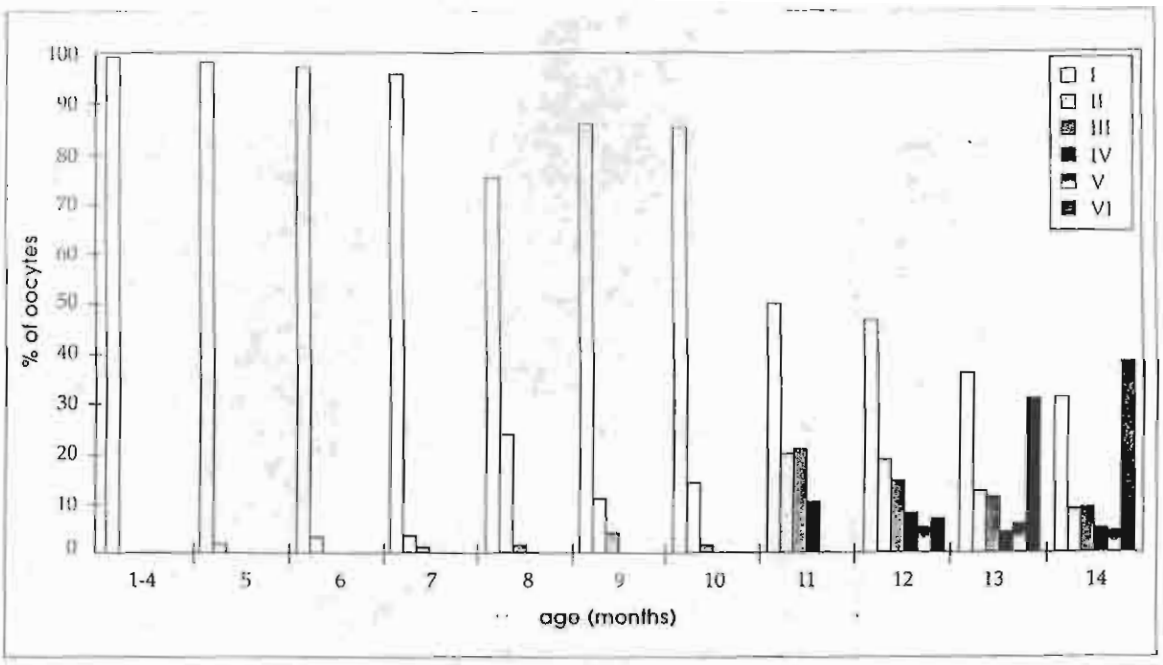

Fig 6. The appearance of ovarian follicles of *R. tigerina* aged one to fourteen months as expressed by mean percentage of all stage oocytes (observed during 1993-1995).

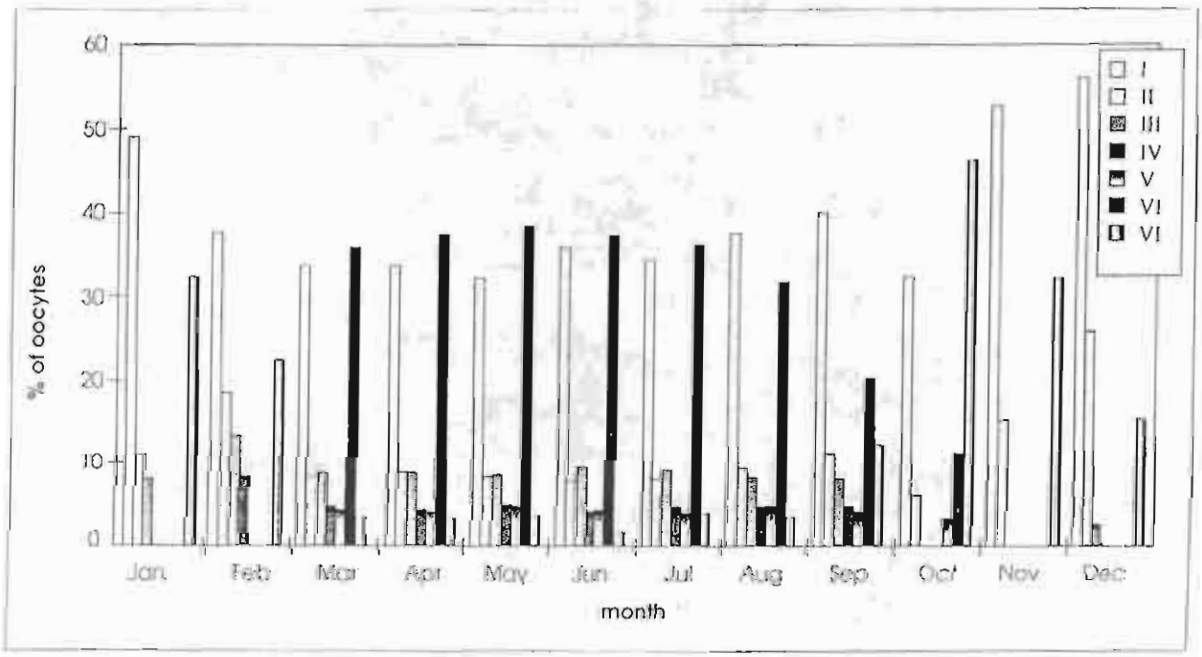

Fig 7. Annual changes of ovarian follicles of *R. tigerina* as expressed by mean percentage of all stage oocytes (observed during 1993-1995).

ovaries of twelve-month-old frogs contain stage V and VI oocytes. The proportions of stage VI oocytes are remarkably increased when the frogs are thirteen (30.4%) and fourteen (37.5%) months old.

Seasonal variation of the ovary

The histograms in Figure 7 reveal that during November and February most of the oocytes were in stage I (>40%) whereas some were in stages II and III. It was observed that stage I and II oocytes (previtellogenic oocytes) appeared all year round. Stage VI oocytes were present only from March to October, where percentages of these oocytes were 35.5, 37.2, 38.1, 37.1, and 36.1 in March, April, May, June, and July, respectively. In August and September, the percentage of stage VI oocytes was 20% and decreased to 11.2% in October. Degenerated oocytes appeared throughout the year and were increased in number during October to February.

Disscussion

Oogenesis in ovaries of *Rana* species has been studied by many investigators. The criteria for dividing oocytes into many stages are mainly based on the size, the amount and the distribution of yolk and pigment,[2,3,6] and the morphology of chromosomes.[21] In the present study, we used several criteria for characterizing the developing oocytes of *R. tigerina*. These included the size, color, as well as the internal morphology, in conformity with the classification of oocytes in the other *Rana* species and *X. laevis* as previously described.[1-5]

The outer coat of oocytes of *R. tigerina* is composed of surface epithelium, a connective tissue layer and a follicular cell layer as well as a layer of vitelline fibers arranged in three directions (called the vitelline envelope or coat). This feature is common in most species of anurans. The formation of the vitelline envelope in *R. tigerina* can be first detected as isolated bundles of fine filaments in the stage II oocyte similar to those found in oocytes of *X. laevis*[5]. However, TEM studies employing IgG-conjugated colloidal gold revealed that vitelline envelope antigens were distributed throughout the whole cytoplasm and began to deposit around the surface of the stage I oocyte.[22] This study indicated that the cytoplasm of the stage I oocyte already contained components reactive with anti-vitelline coat antibodies[12], thus suggesting that the oocyte may play a major role in synthesizing its own vitelline envelope.

In *X. laevis*,[10] the microvilli extending from the oocyte surface gradually increase in number and length particularly in stage III and IV oocytes. These changes of microvilli are similar to those observed in the oocyte of *R. tigerina* in the present study. In addition, the present study revealed that the full thickness of vitelline envelope was observed in the stage V oocyte. The increased number and length of microvilli might be needed to increase the surface area of oocytes during development. Since amphibian oocytes must store nutrient materials in the form of yolk platelets, they need a relatively large surface area for the uptake of the nutritive substances which are necessary for the yolk formation. Corresponding to this demand, during stage III and IV oocytes of *R. tigerina*, there are extensive pinocytotic activities, which may reflect the mechanism whereby materials enter the cytoplasm through the endocytotic pathway as reported in *X. laevis*.[10] Dumont[23] (1978) has suggested that this mechanism is involved in the uptake of vitellogenin that binds to the specific receptors on the oocyte surface at preformed membrane sites known as coated pits which then give rise to coated vesicles. The evidence supporting the uptake of vitellogenin *in vitro* was demonstrated by the injection of 1% vital dye trypan blue into the dorsal lymph sac of female anurans.[24-27] These studies showed that the uptake of trypan blue began in stage III oocytes and reached the maximal level in stage IV oocytes, then the activity declined in the last two stages. These results are similar to those reported by Wallace[28] (1970) using an *in vitro* study, and are also compatible with the increased pinocytotic vesicles in state III oocytes, and their decrease in stage V and VI oocytes as observed in the present study.

It has been reported that vitellogenin or yolk protein is the precursor of yolk platelets during vitellogenesis.[29] The term vitellogenesis means the process of synthesizing yolk platelets and includes vitellogenin formation from the liver.[30] Follett and Redshaw[30] (1967) used serum lipophosphoprotein (SLPP) to substitute for vitellogenin. SLPP is transported *via* blood circulation to the ovaries, where it is taken up by the oocytes under the influence of gonadotrophic hormones.[11] After transport into the oocytes, SLPP is dissociated into two components, phosvitin and lipovitellin, and these are finally reconstituted to form yolk platelets. The present study has demonstrated that the yolk formation begins in stage III, as in *X. laevis*.[5] Perhaps this occurs through the increased receptor-mediated endocytosis as discussed earlier, since a large number of endosomes and electron-dense lysosomes could be observed in stage IV oocytes.

Mitochondrial clusters observed in vitellogenic oocytes in this study are commonly observed in many anurans.[32] This might be due to the need for a large energy supply for the synthesis of new macromolecules and for the assembly of various structures in the oocytes. The increase of mitochondria numbers during vitellogenesis may be due to their rapid proliferation, as it has been suggested that out of the total of 16-17 rounds of mitochondrial DNA replication during oogenesis, 12 rounds take place before the onset of vitellogenesis.[33]

The present study also revealed the abundance of free ribosomes in the cytoplasm of all stages of oocytes especially around the nucleus, while only a little rough endoplasmic reticulum was observed. This is thought to be a basic characteristic of anuran oocytes,[33] since free ribosomes are the site where various proteins are synthesized for usage within the cell. During vitellogenesis, mRNA molecules are actively synthesized but they are mainly stored in an inactive form. When the synthesis of the large mRNA population stops, the production of rRNA begins and continues during the whole oogenesis. Whether these changes in RNA synthetic patterns are directly due to the uptake of vitellogenin or to the appearance of yolk platelets is still unknown.[33] During development of oocytes of *R. tigerina*, the nuclear envelope changes from having a smooth contour in the earlier stages to being more highly folded in later stages. This change may be in response to the need for a large surface area for the transport of the various classes of RNA to the cytoplasm, and the reverse transport of proteins into the nucleus across the nuclear membrane via nuclear pores.[33]

Our cytochemical study using alcian blue staining agrees with TEM results that the vacuoles first appear in the stage II oocyte, and their number is increased in stage III and IV oocytes. However, they are reduced to one or two layers at the periphery of the fully grown oocyte. These vacuoles are similar to the cortical alveoli of teleost oocytes as reported by Selman *et al.*[34,35] They appear empty in routine histological sections due to the extraction of their content during the tissue preparation. Alcian-blue staining of these vacuoles indicates the presence of mucopolysaccharide content. In *X. laevis*, it was found that N-acetyl-β-D-glucosaminidase activity was associated with similar cortical granules.[36] An autoradiographic study also demonstrated the incorporation of [^{3}H] glucose into the content of cortical alveoli of teleost oocytes.[37] Moreover, we found that they disappear in the fertilized egg (unpublished data).

Histological observations of developing ovaries in this study revealed that the structures of the one-month-old ovary are quite variable because each frog with the same age has a different growth rate, and this affects the ovarian development. All oogonia had differentiated into stage I oocytes by the time the frogs reached four months. These stage I oocytes cease development at the diplotene stage of first meiosis.[33] Stage VI oocytes which occur in 12-month-old frogs may represent the age which female frogs reach maturity. This is in contrast to *Bufo bufo* in Europe, which reach maturity after the age of 3-4 years.[37,38] This finding implies that the growth rate of anurans living in the tropics is much faster than those living in a cold climate.

One of the most remarkable characteristics of amphibians is the change of ovarian cyclicity in correlation with the variation in environmental or seasonal conditions,[39,40] especially the seasonal climatic cycle of temperature and precipitation. In tropical countries, where there is pronounced wet and dry seasons, the breeding and non-breeding periods are clearly separated. In India (in Dharwad), the main breeding season of frogs coincides with the peak of monsoon rain during June to August.[41] The climate in Thailand is similar, and the breeding season of *R. tigerina* coincides with the period of monsoon rain that generally extends from May to September. The appearance of stage I and II or previtellogenic oocytes throughout the year as in other anurans,[42] suggests that there is always a reserved pool of oocytes. The decline in their number is associated with the recruitment of oocytes from this pool to final vitellogenic oocytes as occurs in *R. tigerina* between April-June.[43] This study revealed that the degenerated oocytes also appear all year round and increase during October to February, which correlates with the decline of stage VI oocytes. This suggests that atresia during that period is due to the degeneration of the stage VI oocytes, which could be due to the lower level of gonadotropins.[44,45]

In the present study, it was found that the mature-stage VI oocytes are observed only during March to October. The presence of stage VI oocytes slightly precedes the onset of rainy season, but their termination is close to the end of the season. Thus, this period is referred to as the breeding season while the period during November to February is referred to as the non-breeding season. Moreover, the presence of stage VI oocytes during March to October is correlated with the large amount of spermatozoa in the testis in male frogs[46] and abundance of basophils which produce gonadotropins in the pars distalis of *R. tigerina*.[47]

Acknowledgements

This work was supported by National Science and Technology Development Agency (NSTDA) (Grant # 01-35-006) and Thailand Research Fund (Senior Research Scholar Fellowship to Prasert Sobhon). Dr. Bob Cowan helped in the preparation of the manuscript.

References

1. Wittek M (1952) La vitellogenase chez les amphibiens. *Arch Biol* 63, 134-98.
2. Kemp N (1953) Synthesis of yolk in oocytes of *Rana pipiens* after induced ovulation. *J Morph* 92, 487-511.
3. Grant P (1953) Phosphate metabolism during oogenesis in *Rana temporaria*. *J Exp Zool* 124, 513-43.
4. Balinski BL and Devis BJ (1963) Origin and differentiation of cytoplasmic structures in the oocytes of *Xenopus laevis*. *Acta Embryol Morphol Exp* 6, 53-108.
5. Dumont JN (1972) Oogenesis in *Xenopus laevis* (Daudin). I. Stages of oocytes development in laboratory maintained animals. *J Morph* 136, 153-79.
6. Wartenberg H and Gusek W (1960) Elektronenoptische untersuchungen uber die feinstruktur des ovarialeies and des follikelepithels von amphibien. *Exp Cell Res* 19, 199-209.
7. Ward RT (1962) The origin of protein and fatty yolk in *Rana pipiens* II. Electron microscopical and cytochemical observations of young and mature oocytes. *J Cell Biol* 14, 309-41.
8. Hope J, Humphries AA Jr and Bourne GH (1963) Ultrastructural studies on developing oocytes of the salamander *Triturus viridescens*. I. The relationship between follicle cells and developing oocytes. *J Ultrastructure Res* 9, 302-324.
9. Wallace RA (1985) Vitellogenesis and oocyte growth in non-mammalian vertebrates. *Dev Biol* 1, 469-502.
10. Wallace RA and Selman K (1990) Ultrastructural aspects of oogenesis and oocyte growth in fish and amphibians. *J Electron Microsc* 16, 175-201.
11. Inger RF and Greenberg B (1956) Morphology and seasonal development of sex characters in two sympatric African toads. *J Morph* 99, 549-74.
12. Berry PY (1964) The breeding pattern of seven species of Singapore Anura. *J Anim Ecol* 33, 227-43.
13. Church G (1960) Annual and lunar periodicity in the sexual cycle of the Japanese toad, *Bufo malanostictus* Scheider. *Zoologica* 45, 181-8.
14. Jorgensen CB, Shakoonala K and Vijayakumars S (1986) Body size reproduction and growth in a tropical toad, *Bufo melanostictus*, with a comparison of ovarian cycles in tropical and temperate zone anurans. *Oikos* 46, 379-89.
15. Chapman BM and Chapman RF (1985) A field study of population of leopard toads (*Bufo regularis regularis*). *J Anim Ecol* 28, 267-86.
16. Keith RA (1968) A new species of *Bufo* from Africa, with comment on the toads of the *Bufo regularis* complex. *Amer Mus Novit* 2345, 1-22.
17. Wallace RA, Jare DW, Dumont JN and Seca MW (1973) Protein incorporation by isolated amphibian oocytes. III. Optimum incubation conditions. *J Exp Zool* 184, 321-34.
18. Lillie RD and Fullmer HM (1976) Histopathologic Technic and Practical Histochemistry 4th ed, McGraw-Hill Book Company, New York, 942 pp.
19. Spurr AR (1960) A low-viscosity epoxy resin embedding medium for electron microscopy. *J Ultrastructure Res* 26, 31-43.
20. Reynolds ES (1963) The use of lead citrate at high pH as an electron opaque stain in electron microscopy. *J Cell Biol* 17, 208-12.
21. Duryee WR (1950) Chromosome physiology in relation to nuclear structure. *Ann NY Acad Sci* 50, 920-53.
22. Yamaguchi S, Hedrick JL and Katagiri C (1989) The synthesis of localization of envelope glycoprotein in oocytes of *Xenopus laevis* using immunocyto chemical methods. *Develop Gr* 31, 85-94.
23. Dumont JN (1978) Oogenesis in *Xenopus laevis* (Daudin) VI. The route of injected tracer transport in the follicle and developing oocyte. *J Exp Zool* 204, 193-217.
24. Ramamurty PS (1964) On the contribution of follicle epithelium to the deposition of yolk in the oocyte of *Panorpa communis*. *Exp Cell Res* 33, 601-4.
25. Teller WH and Anderson LM (1968) Functional transformation accompanying the initiation of a terminal growth phase in the *Cecropia* month oocyte. *Dev Biol* 17, 512-35.
26. Dumont JN and Wallace WA (1968) The synthesis transport and uptake of yolk proteins in *Xenopus laevis*. *J Cell Biol* 39, 37 (Abstr).
27. Wallace RA and Dumont JN (1968) The induced synthesis and transport of yolk protein and their accumulation by the oocyte in *Xenopus laevis*. *J Cell Physiol* 72(suppl 1), 73-89.
28. Wallace RA (1970) Studies on amphibian yolk IX. *Xenopus vitellogenin*. *Biochim Biophys Acta* 215, 176-83.
29. Pan ML, Bell WJ and Belfer WH (1969) Vitellogenic blood protein synthesis by insect fat body. *Science* 465, 393-4.
30. Follett BK and Redshaw MR (1967) The effect of oestrogens and follicle stimulating hormone on the metabolism of lipid and proteins in *Xenopus laevis* Daudin. *J Endocrinol* 35, 5-6.
31. Follett BK (1967) The effect of oestrogen and gonadotrophin on lipid and protein metabolism in *Xenopus laevis*. *J Endocrinol* 40, 439-56.
32. Ward RT and Ward E (1968) The origin and growth of cortical granules in the oocytes of *Rana pipiens*. *J Microsc* 7, 1021-30.
33. Brachet J and Alexandre H (1986) Introduction to Nuclear Embryology 2nd ed, pp 39-65. Springer-Verlag, Berlin-Heidelberg.
34. Selman K, Wallace R A and Barr V (1986) Oogenesis in *Fundulus heteroclitus* IV. Yolk-vesicle formation. *J Exp Zool* 239, 277-88.
35. Selman K, Wallace RA and Barr V (1988) Oogenesis in *Fundulus heteroclitus* V. The relationship of yolk vesicle and cortical alveoli. *J Exp Zool* 246, 42-56.
36. Greve LC, Prody GA and Hedrick JL (1985) N-Acetyl-B-D-glucosaminidase activity in the cortical granules of *Xenopus laevis* eggs. *Gamete Res* 12, 305-12.
37. Hemelaar A (1985) An improved method to estimate the number of year rings resorbed in phalanges of *Bufo bufo* and its application to populations from different latitudes and altitudes. *Amphib-reptilia* 6, 323-42.
38. Hemelaar A (1988) Age, growth and other population characteristics of *Bufo bufo* from different latitudes and altitudes. *J Herpetol* 22, 369-388.
39. Bragg A and Wesse AO (1950) Growth rates and age at sexual maturity of *Bufo cognatus* under natural conditions in central Oklahoma Amphibia and Reptilia, pp 47-58. In researches on the amphibia of Oklahoma, Illus. Univ. Oklahoma Press: Norman, 154 pp.
40. Kanamadi RD and Saidapur SK (1982) Pattern of ovarian activity in the Indian toad *Bufo melanostictus* (Schn). *Proc Indian Natl Sci Acad* B48, 307-16.
41. Jorgensen CB, Larsen LO and Loltz B (1979) Annual cycles of fat bodies and gonads in the toad *Bufo bufo bufo* (L), compared with cycles in other temperate zone anurans. *Biol Skr* 22, 1-37.
42. Sklavounou PK and Tsombounis G (1980) Annual ovarian cycle in the frog, *Rana ridibunda*, in northern Greece. *J Herpetol* 24, 185-91.

43. Hoque B and Saidapur SK (1994) Dynamics of oogenesis in the tropical anuran *Rana tigrina* (Amphibia : Ranidae) with special reference to vitellogenic cycles in wild-caught and captive frogs. *J Biosci* 19, 339-52.
44. Hoque B and Saidapur SK (1995) Pattern of oocyte growth and recruitment in unilaterally ovariectomized adult *Rana tigrina* in different reproductive phase, and in juvenile frogs. *Indian J Exp Biol* 33, 646-51.
45. Pramoda S and Saidapur SK (1984) Annual changes in the somatic weight, hypophyseal gonadotrophs, ovary, oviduct and abdominal fat bodies in the Indian bullfrog *Rana tigerina*. *Proc Indian Natl Sci Acad* B50, 387-98.
46. Sretarugsa P, Nakiem V, Sobhon P, Chavadej J, Kruatrachue M and Upatham ES (1997) Structure of testis of *Rana tigerina* and its changes during development and seasonal variation. *J Sci Soc Thailand* 23, 75-86.
47. Sretarugsa P, Munkhetvit P, Cherdwongchareonsuk D, Sobhon P, Chavadej J, Kruatrachue M and Kikuyama S (1996) Characterization and localization of immunoreactive growth hormone and prolactin cells in pars distalis of bullfrog *Rana catesbeiana*. *Thai J Physiol Sc* 9,18-34.

Journal of Shellfish Research, Vol. 20, No. 2, 000–000, 2001.

CHARACTERIZATION OF TRABECULAR CELLS IN THE GONAD OF *HALIOTIS ASININA* LINNAEUS

S. APISAWETAKAN,[1]* M. CHANPOO,[1] C. WANICHANON,[1] V. LINTHONG,[1] M. KRUATRACHUE,[2] E. S. UPATHAM,[2,3] T. PUMTHONG,[4] AND P. SOBHON[1]

Departments of [1]Anatomy and [2]Biology, Faculty of Science, Mahidol University, Rama VI Road, Bangkok 10400, Thailand; [3]Department of Medical Science, Faculty of Science, Burapha University, Chonburi 20131, Thailand; [4]The Coastal Aquaculture Development Center, Department of Fisheries, Ministry of Agriculture and Cooperatives, Klong Wan, Prachaubkirikhun 77000, Thailand

ABSTRACT Trabeculae are the connective tissue sheets that extend perpendicularly from the outer capsules of both testis and ovary to make contact at their innermost ends with the inner capsules separating the gonad from hepatopancreas. Thus they divide the gonad into small compartments, and each trabecula forms the axis for individual spermatogenic or oogenic units, from which maturing germ cells are generated. When studied by light and electron microscopes, each trabecula is composed of central capillaries surrounded by muscle cells, collagen fibers, fibroblasts, and granulated cells which contain large rugby-shaped electron dense granules about 270 × 550 nm in size. The granulated cells branch extensively, and their processes become closely associated with bundles of nerve fibers that contain two types of granules, i.e., electron-dense and electron-lucent spherical-shaped granules with diameter about 165 nm and 150 nm, respectively. Thus, bundles of nerve and branches of granulated cells provide profuse innervation of the capsules and trabeculae. The granulated cells may be endocrine cells of the gonad which produce certain gonadotrophic factors yet to be identified.

KEY WORDS: *Haliotis asinina*, gonad, capsules, trabeculae, connective tissue cells, endocrine cells

INTRODUCTION

Studies on endocrinology of reproduction in mollusks present a number of interesting challenges because of a great variability of existing patterns. Most detailed studies of the modes of reproduction and corresponding endocrine controls have been carried out in *Aplysia* spp. (subclass Opisthobranchiata) and *Lymnaea* spp. (subclass Pulmonata) (Joose 1979, Joose 1988). In Prosobranchiata, including *Haliotis* spp., little is known about the reproductive hormones and their cellular origins. In mollusks studied so far, neurosecretory cells that are the putative sources of reproductive hormones, such as egg-laying hormone, are mostly localized in cerebral, pleuropedal and visceral ganglia (Bern & Hagadorn 1965, Dorsett 1986, Hahn 1994). The gonad represents another site where hormones controlling reproduction may be produced, as seen in the cases of Leydig cells and Copora luteal cells that lie in the connective tissue scaffold of vertebrates' gonad.

Our previous observations indicated a close association between cells in the connective tissue scaffold of the gonad of *H. asinina* and gamete cells during their development in various phases of the reproductive cycle (Sobhon et al. 1999). There are several types of cells present in the connective tissue of the gonad, including highly granulated cells with structural characteristics resembling those of endocrine cells (Apisawetakan et al. 1997, Sobhon et al. 1999). These observations together with the report by Chanpoo et al. (2000) strongly imply that reproductive hormones, such as egg-laying hormone, may also be produced intramurally within the connective tissue of the gonad by certain granulated cells. Moreover, there could be other cell types that are involved in the development of germ cells in the gonad that could evolve from the connective tissue compartment. Therefore, in the present study we have characterized various types of cells in the connective tissue scaffold of the gonad and attempted to define their possible functions.

*Corresponding author. E-mail address:

MATERIALS AND METHODS

Collection of H. Asinina Specimens

Adult *H. asinina*, reared in the land-based culture system, were provided by the Coastal Aquaculture Development Center, Prachaubkirikhun province, Thailand. They were cultured in concrete tanks that were well flushed with mechanically circulated water and air delivery system to maintain a stable environment. Seawater was pumped directly from the nearby bay and passed through subsand filter before use (Singhagraiwan & Doi 1993). The animals were fed with diet of macroalgae (usually *Gracilaria* spp. and *Laminaria* spp.) and supplemented with artificial food.

Specimen Preparation

Gonads were cut into small pieces, fixed in Bouin's fluid, and prepared for light microscopic examination by paraffin method. For semithin sections and TEM studies, specimens were fixed in a solution of 3% glutaraldehyde in 0.1 M sodium cacodylate buffer pH 7.8 at 4°C for overnight, postfixed in 1% osmium tetroxide in 0.1 M sodium cacodylate buffer at 4°C for two hours, then dehydrated in graded series of ethanol, cleared in propylene oxide, infiltrated and embedded in Araldite 502 resin, which was finally polymerized at 30°C, 45°C and 60°C for 24, 48 and 48 hours, respectively. The specimens were then semithin-sectioned at one-micron thickness in a Porter Blum MT-2 ultramicrotome, stained with Methylene Blue or PAS, and observed in an Olympus Vanox light microscope. Ultrathin sections were cut and stained with lead citrate-uranyl acetate and viewed under a Hitachi TEM H-300 at 75 kV.

RESULTS

Connective Tissue Scaffold of the Gonad

The connective tissue frameworks that support the gonad in *H. asinina* consist of the outer capsules surrounding the ovary and testis, and the inner capsules that separate hepatopancreas from the surrounding gonadal tissues. Flat connective tissue sheets, called

trabeculae, extend perpendicularly from the outer gonadal capsules through the interior of the gonads to touch the inner capsules. As a result, the gonads are partitioned into small incomplete compart-
F1 ments (Fig. 1A and B). Each trabecula acts as the axis on which early and growing germ cells are closely attached (Fig. 1C and D), thus giving rise to a discrete gametogenic unit representing, perhaps, clone of germ cells which may arise from a single group of
F2 gonial cells. In each trabecula, muscle cells (Fig. 2A and D) lying alongside the central capillaries and fibroblasts together with collagen fibrils form the trabecular core. Granulated cells, which may be endocrine cells, are distributed in rows along both sides of each trabecula, separated from the gonadal compartment by thick basal laminae (Fig. 4A–C).

The Gonadal Capsules

The connective tissue of the trabeculae blends imperceptibly with those of the outer and inner capsules. The outer gonadal capsule is 40–50 μm thick and consists of 10 layers of cells (Fig. 2A and B). It is covered externally by a single layer of cuboidal or columnar epithelium, which consists of 2 types of cells. Type 1 are the principal cells which are tightly adhered to each other (Fig. 3A

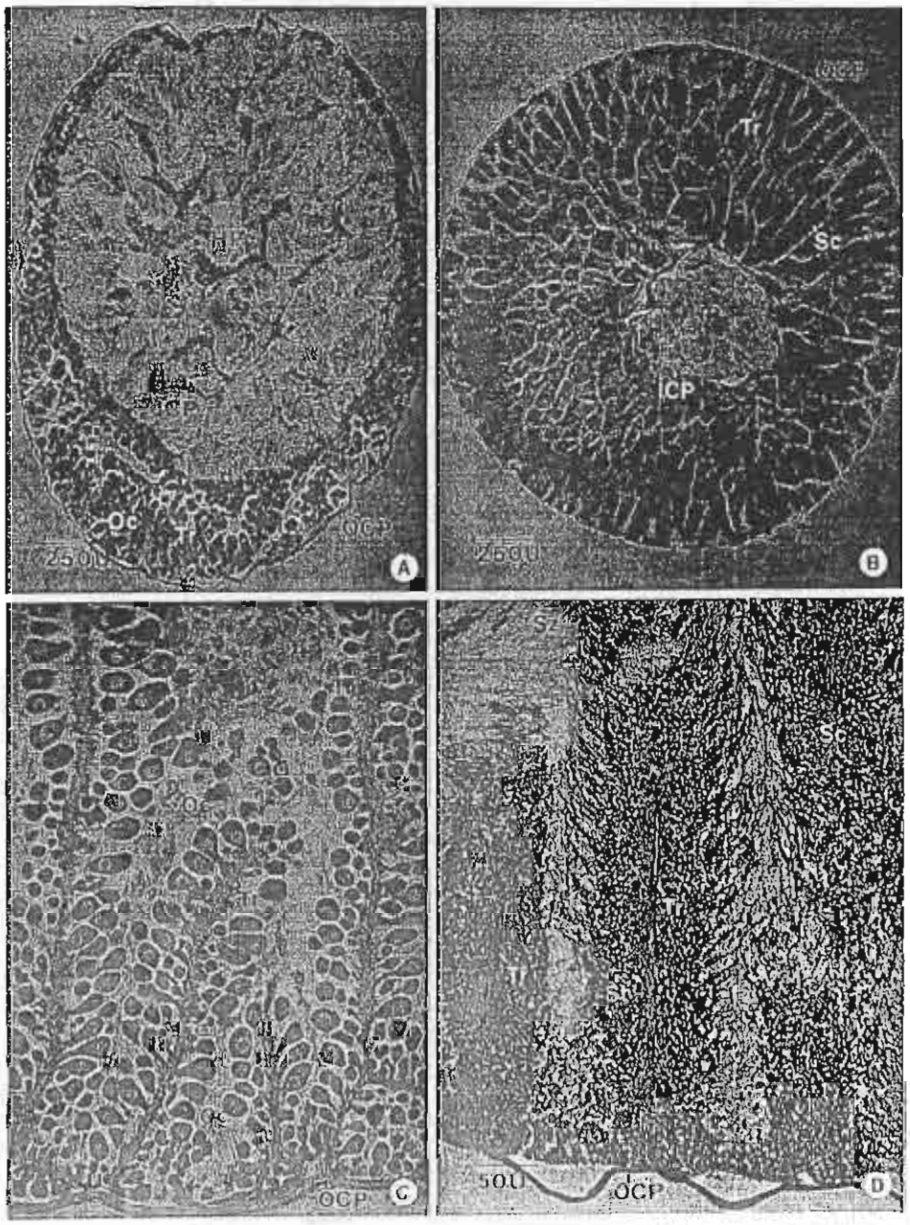

Figure 1. (A, B) Paraffin sections of ovary (A) and testis (B) around hepatopancreas (HP). Both organs are surrounded by outer and inner capsules (OCP, ICP), and trabeculae (Tr) form partitions between gonadal compartments. (C, D) Paraffin sections, showing oogenetic units of growing oocytes (Oc), and spermatogenic units of spermatocytes (Sc), spermatids (St) and spermatozoa (Sz) around each trabecula (Tr).

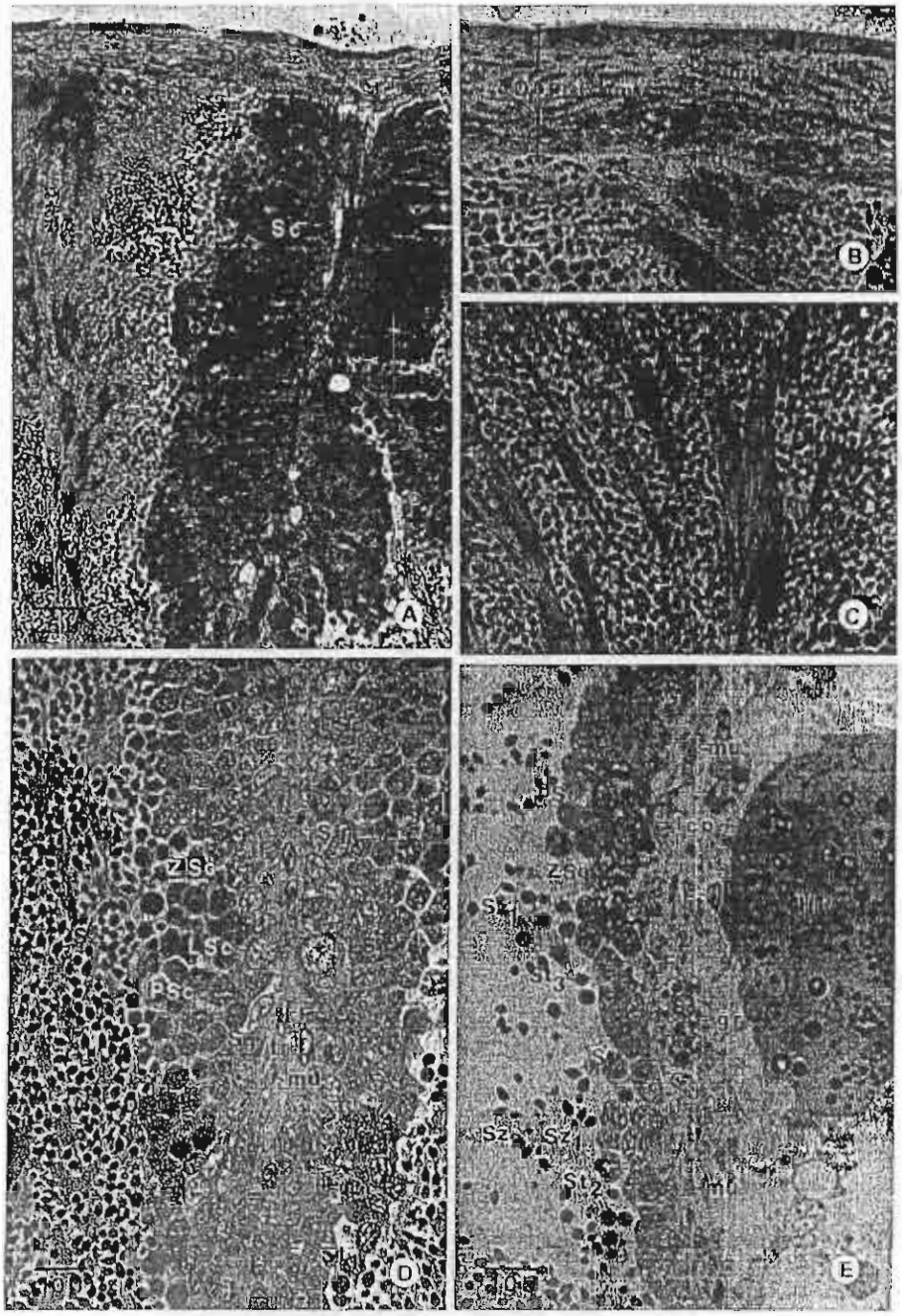

Figure 2. (A–C) Semithin sections of the testis stained with PAS, showing the outer capsule (OCP), and a spermatogenic unit around each trabecula (tr) (in A, B) and the accumulation of mature spermatozoa in gonadal lumen (in C). In B, note that the outer capsule consists of cuboidal epithelium (epl) with alternate layers of muscle cells (mu) and collagen bundles. Granulated cells and their processes (gr) are presented in large number. (D, E) Semithin sections of the testis stained with methylene blue, showing cellular components of trabeculae (in D) and the inner capsules (in E-ICP), and various stages of spermatogonia, spermatocytes, spermatids and spermatozoa surrounding the trabecula (Sg, LSc, PSc, ZSc, SSc, St, Sz) (granulated cells = gr; fibroblast = F; muscle cells = mu).

[F] and B). The nuclei of these cells are elongated and have a thin rim of heterochromatin along the inner facet of the nuclear envelopes, and prominent nucleoli. There are large connecting blocks of heterochromatin scattered throughout the inner part of the nuclei. The cytoplasm is filled up with rough endoplasmic reticulum, and the apical cytoplasm contains a few dense irregular bodies that appear like lysosomes. The outer surface of the cells bears numerous microvilli. Type 2 are the goblet-like cells, whose apical cytoplasm is filled with moderately dense spherical granules, each about 600–650 nm in diameter (Fig. 3A and C). The nuclei of these cells are

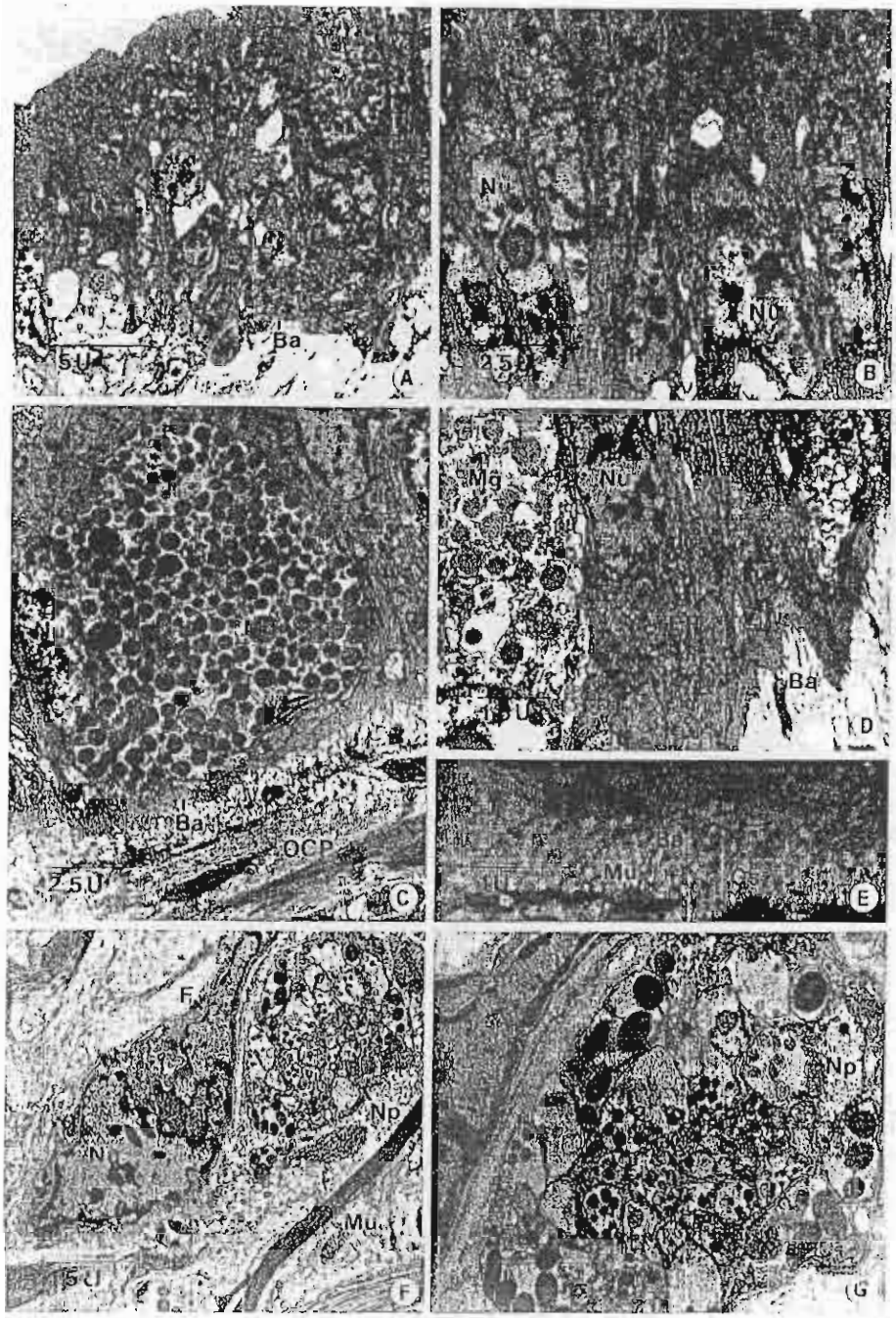

Figure 3. TEM micrographs of epithelium covering surface of the outer capsule. (A–D) Principal cells (Pc) and mucous cells (Mc): the former are columnar or cuboidal-shaped cells tightly adhered together. Their cytoplasm contain numerous rough endoplasmic reticulum (rER) and lysosome-liked granules (Ly). Mucous cells contain abundant mucin granules (Mg) that fill up the apical cytoplasm. (E) The thick basal lamina (Ba) supporting surface epithelium, and layers of ground substance (Gs) and muscle cells (Mu). (F, G) Fibroblasts (F), and nerve bundles (Np) that innervate the outer capsule. In G, nerve processes containing dense and light spherical granules, about 165 and 150 nm in diameter (2, 3), are surrounded by processes of granulated containing large rugby shaped granules about 270 × 550 nm in size (1).

eccentrically located toward the bottom, and they appear fairly similar to those of the first cell type. Both types of cells rest on a very thick basal lamina about 550 nm in width (Fig. 3A and D) which contains a meshwork of very fine filaments (Fig. 3E). Internal to the basal lamina are alternate layers of spindle-shaped muscle cells and the extracellular matrix which appears homogeneous and electron-lucent (Fig. 2B and Fig. 3E–3F). Among this extracellular matrix are fibroblasts, collagen fibrils, and small

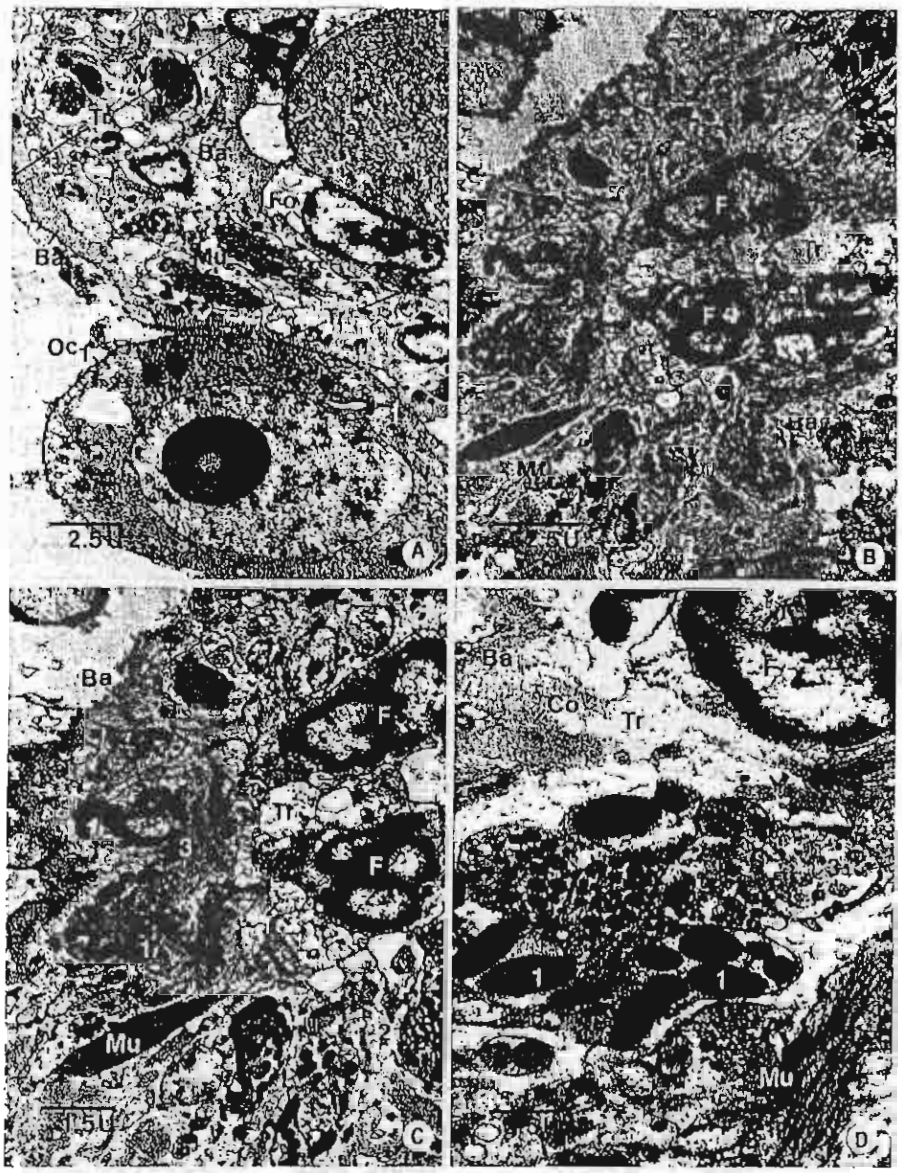

Figure 4. (A–D) TEM micrographs of a trabecula (Tr) in an ovary, which is separated from the gonadal compartment containing oocyte (Oc_1) by a thick undulating basal lamina (Ba). Within the core of each trabecula, there are collagen fibrils (Co), fibroblasts (F), muscle cells (Mu) and numerous processes of granulated cells (1) in close association with nerve processes (2, 3).

nerve bundles (Fig. 3F and G). The latter consist of nerve processes of various sizes, some of which contain electron-dense spherical granules (about 165 nm in diameter), while others contain more electron-lucent granules (about 150 nm in diameter). The peripheral part of each bundle is usually surrounded by branches of granulated cells that contain large rugby-shaped granules (about 270 × 550 nm in size). Most of the nerve bundles are situated close to the inner facet of the capsule, which is lined by a single squamous epithelium resting on another thick layer of basal lamina, that separates the capsule proper from the gonadal compartment (Fig. 2B). The inner capsule consists of a thin layer of loosely arranged connective tissues and muscle cells. It is separated from the gonadal compartment and hepatopancreatic tissue by basal laminae (Fig. 2E). The cellular constituents are composed of muscle cells, fibroblasts, and granulated cells which appear to be more abundant than in other areas of the connective tissue scaffold (Fig. 2E).

Trabecular Compartment

Each trabecula could be considered as a circumscribed compartment. As described earlier, this compartment is the continuation of the outer capsule, hence their main cellular compositions are muscle cells and fibroblasts embedded in the extracellular matrix and collagen fibrils. This compartment is partitioned off from adjacent gonadal compartments by thick convoluted basal laminae similar to those observed lining the outer and inner capsules (Fig. 4A–C). In addition, there are rows of granulated cells or their [F4]

branches disposed at a regular interval along the trabecular sides of the basal laminae (Fig. 4A–C).

Muscle Cells

These cells are intermediate in characteristics between skeletal and smooth muscle cells of vertebrates. They have short thick filaments, each of which is surrounded by 12 to 15 long thin filaments. The thin filaments are attached to the dense bodies which are scattered throughout the cytoplasm, with some adhering to the plasma membrane (Fig. 5A–D).

Fibroblasts

These cells are similar in characteristics with their counterparts in vertebrates' connective tissues, and they are embedded within the collagen fibrils which they synthesize (Fig. 3F and Fig. 4B and C).

Granulated Cells

These cells have oval nuclei with thin rims of heterochromatin along the nuclear envelopes, and patches of heterochromatin in the center (Fig. 2E and 6A). They also have long processes that become closely associated with bundles of axons, which may come from neurons outside the gonads. As a result, there appear to be three types of granules within and around each bundle of axons and branches of granulated cells (Fig. 3F–G and Fig. 6C–F) similar to those found in the capsules. Isolated cytoplasmic branch of granulated cells containing groups of large granules are also frequently observed lying in rows near muscle cells (Fig. 5A and E), and under the undulating basal laminae that separate the trabeculae from the germ cell compartments (Fig. 4B–C and 6B). At many sites muscle cells appear in close apposition to solitary branches of granulated cells (Fig. 5E).

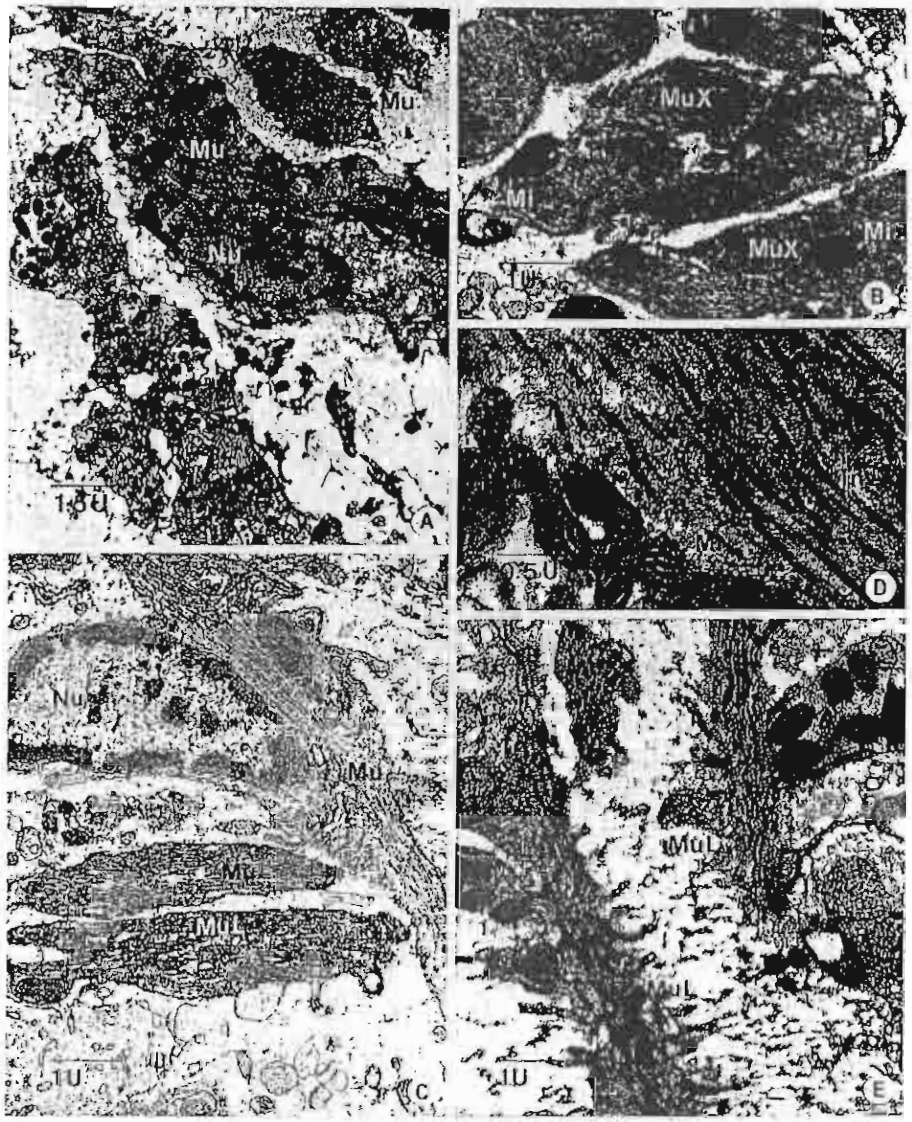

Figure 5. TEM micrographs of muscle cells, showing close association with the processes of granulated cells (I-in A, E). Cross (in B) and long sections (in C, D) of muscle cells, exhibit dense thick filaments (Te) each of which is surrounded by numerous thin filaments (Tn). A large number of mitochondria (Mi) are also present in muscle cells.

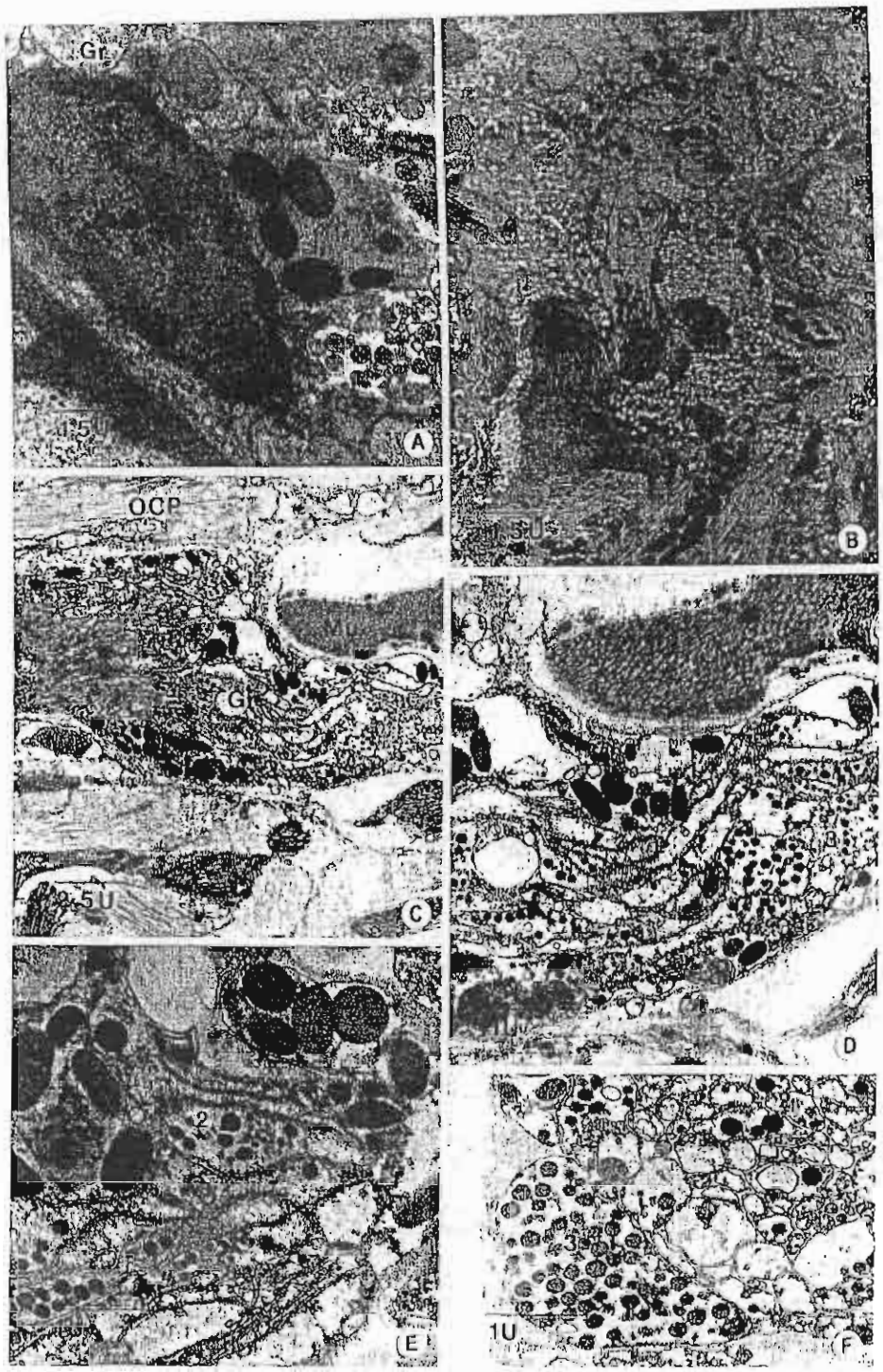

Figure 6. (A, B) TEM micrographs of a granulated cell (in A). The cell has an oval nucleus with patches of heterochromatin along the nuclear envelope and in the center. The cytoplasm contains large rugby-shaped granules about 270 × 550 nm in size, with electron-dense matrix (1). In B, branches of granulated cells (1) are dispersed at interval along the basal lamina (Ba). (C–F) The nerve bundles in trabeculae consisting of two types of axons that contain dense (2) and light (3) spherical granules (about 165 and 150 nm in diameter). Processes of granulated cells (1) are closely associated with the periphery of each nerve bundle (in D, E).

DISCUSSION

The general histology of the gonad and classification of various types of germ cells in many species of abalone, such as, *H. tuberculata* (Stephenson 1924, Croft 1929), *H. discus hannai* (Tomita 1967, 1968), *H. cracherodii* (Webber & Giese 1969), *H. rufescens* (Young & DeMartini 1970, Martin et al. 1983), *H. diversicolor diversicolor* (Takashima et al. 1978), *H. asinina* (Apisawetakan et al. 1997, Sobhon et al. 1999) have been reported. However, most studies neglect the cellular compositions and detailed structure of the connective tissue scaffold of the gonad, apart from mentioning casually that the gonadal capsules and trabeculae are made of fibro-muscular tissues.

In our detailed studies using both light and electron microscopy, we found that the cellular compositions of connective tissue scaffold are more complex than previously thought. Within these connective tissue frameworks, which may be termed trabecular-capsular compartment, there are many types of cells that may be involved in the physiology of the gonad, including the production of reproductive hormone, and the release of mature gametes. These cells are muscle cells, fibroblasts and granulated cells.

The most striking feature is the presence of a large number of granulated cells, with large-endocrine like granules, in the trabeculae and capsules of the gonads. It is remarkable that these types of cells and their branches form an extensive network within the connective tissue scaffold of the gonad. Immunolocalization studies of abalone egg-laying hormone (aELH) performed by our group demonstrated that these cells could be one of the primary producers and/or storage sites of aELH (Chanpoo et al. 2000). Even more remarkable is that there are numerous nerve processes, which consist primarily of axons containing neurochemical vesicles, coming into close contact with branches of granulated cells. These bundles of nerve and granulated cell processes are mostly observed within the gonadal capsules. Judging from this appearance, gonads of *H. asinina* are highly innervated organs. In contrast to vertebrates, it is possible that the nervous system still play a more direct role in controlling the physiology of the gonad.

The muscle cells show typical features as present in most invertebrate species, and these characteristics are intermediate between skeletal and smooth muscle cells of vertebrates (Bennett & Threadgold 1973, Stitt et al. 1992). The thick filaments are short bundles consisting primarily of paramyosin protein (Ishii & Sano 1980) and each is surrounded by up to 12 to 15 thin filaments. This indicates that the muscle cells may be able to generate contractile force greater than that of vertebrate smooth muscle. It was found that branches of granulated cells, the putative egg-laying hormone producer, are lying close and frequently tightly adhered to the muscle cells. Immunolocalization study by our group demonstrated that aELH also bind to muscle cells in the capsules and cores of trabeculae (Chanpoo et al. 2000). It is, therefore, possible that aELH, upon being released from the granulated cells, may stimulate the contraction of muscles in trabeculae and capsules of the gonad, and results in the release of mature gamete cells from the abalone at the time of spawning.

Fibroblasts and collagen fibrils appear to be similar in most respects to their counterparts in vertebrates' connective tissues. Thus, their functions could be primarily supportive.

ACKNOWLEDGMENT

This investigation was supported by the Thailand Research Fund (Senior Research Scholar Fellowship to P. Sobhon).

LITERATURE CITED

Apisawetakan, S., A. Thongkukiatkul, C. Wanichanon, V. Linthong, M. Kruatrachue, E. S. Upatham, T. Pumthong & P. Sobhon. 1997. The gametogenic processes in a tropical abalone, *Haliotis asinina* Linnaeus. *J. Sci. Soc. Thailand* 23:225–240.

Bennett, C. E. & L. T. Threadgold. 1973. Electron microscope studies of *Fasciola hepatica*. XIII. Fine structure of newly excysted juvenile. *Exp. Parasitol.* 34:85–99.

Bern, H. A. & I. R. Hagadorn. 1965 Neurosecretion. In: T. H. Bullock & G. A. Horridge, editors. Structure and function in the nervous system of invertebrate. San Francisco: Freeman. pp. 353–429.

Chanpoo, M., S. Apisawetakan, A. Thongkukiatkul, C. Wanichanon, V. Linthong, M. Kruatrachue, E. S. Upatham, T. Pumthong & P. Sobhon. 2000. Localization of egg-laying hormone (ELH) in the gonads of a tropical abalone, *Haliotis asinina* Linnaeus. *J. Shellfish Res.* ~~submitted~~ in press.

Croft, D. R. 1929. *Haliotis*. *Liverpool Mar. Biol. Comm. Mem.* 29:1–174.

Dorsett, D. A. 1986. Brains to cells: The neuroanatomy of selected gastropod species. In: A. O. D. Willows, editor. The mollusca. Vol. 9. New York: Academic Press. pp. 101–87.

Hahn, K. O. 1994. The neurosecretory staining in the cerebral ganglia of the Japanese abalone (ezoawabi), *Haliotis discus hannai*, and its relationship to reproduction. *Gen. Comp. Endocrinol.* 93:295–303.

Ishii, A. I. & M. Sano. 1980. Isolation and identification of paramyosin from liver fluke muscle layer. *Com. Biochem. Physiol.* 65B:537–541.

Joose, J. 1979. Evolutionary aspects of the endocrine system and of the hormonal control of reproduction of molluscs. In: E. J. W. Barrington, editor. Hormones and evolution. Vol. 1. New York: Academic Press. pp. 119–57.

Joose, J. 1988 The hormones of molluscs. In: H. Laufer & R. G. H. Downer, editors. Endocrinology of selected invertebrate types. New York: A. R. Liss. pp. 89–140.

Martin, G. G., K. Romero & C. Miller-Walker. 1983. Fine structure of the ovary in the red abalone *Haliotis rufescens* (Mollusca: Gastropoda). *Zoomorphol* 103:89–102.

Singhagraiwan, T. & M. Doi. 1993. Seed production and culture of a tropical abalone, *Haliotis asinina* Linnaeus. Thailand: The Eastern Marine Fisheries Development Center, Department of Fisheries, Ministry of Agriculture and Cooperatives. 33 pp.

Sobhon, P., S. Apisawetakan, M. Chanpoo, C. Wanichanon, V. Linthong, A. Thongkukiatkul, P. Jarayabhand, M. Kruatrachue, E. S. Upatham & T. Pumthong. 1999. Classification of germ cells, reproductive cycle and maturation of the gonad in *Haliotis asinina* Linnaeus. *ScienceAsia* 25:3–21.

Stephenson, T. A. 1924. Notes on *Haliotis tuberculata*. *J. Mar. Biol. Assoc. UK.* 13: 480–495.

Stitt, A. W., I. Fairweather, A. G. Trudgett, C. F. Johnston & S. M. L. Anderson. 1992. Localisation of actin in the liver fluke, *Fasiola hepatica*. *Parasitol. Res.* 78:96–102.

Takashima, F., M. Okuno, K. Nichimura & M. Nomura. 1978. Gametogenesis and reproductive cycle in *Haliotis diversicolor diversicolor* Reeve. *J. Tokyo Univ. Fish.* 1:1–8.

Tomita, K. 1967. The maturation of the ovaries of the abalone, *Haliotis discus hannai* Ino, in Rebun Island, Hokkaido, Japan. *Sci. Rep. Hokkaido Fish. Exp. Sta.* 7:1–7.

Tomita, K. 1968. The testis maturation of the abalone, *Haliotis discus hannai* Ino, in Rebun Island, Hokkaido, Japan. *Sci. Rep. Hokkaido Fish. Exp. Sta* 9:56–61.

Webber, H. H. & A. C. Giese. 1969. Reproductive cycle and gametogenesis in the black abalone *Haliotis cracherodii* (Gastropoda: Prosobranchiata). *Mar. Biol.* 4:152–159.

Young, J. S. & L. D. DeMartini. 1970. The reproductive cycle, gonadal histology and gametogenesis of the red abalone, *Haliotis rufescens* (Swainson). *Calif. Fish Game* 56:298–309.

line 1-7/line

Journal of Shellfish Research, Vol. 20, No. 2, 000–000, 2001.

LOCALIZATION OF EGG-LAYING HORMONE IN THE GONADS OF A TROPICAL ABALONE, *HALIOTIS ASININA* LINNAEUS

M. CHANPOO,[1,*] S. APISAWETAKAN,[1] A. THONGKUKIATKUL,[3] C. WANICHANON,[1] V. LINTHONG,[1] M. KRUATRACHUE,[2] E. S. UPATHAM,[2,4] T. PUMTHONG,[5] P. J. HANNA,[6] AND P. SOBHON[1]

Departments of [1]Anatomy and [2]Biology, Faculty of Science, Mahidol University, Bangkok 10400, Thailand; Departments of [3]Biology and [4]Medical Science, Faculty of Science, Burapha University, Chonburi 20131, Thailand; [5]The Coastal Aquaculture Development Center, Department of Fisheries, Ministry of Agriculture and Cooperatives, Klong Wan, Prachuabkhirikhun 77000, Thailand; [6]School of Biological and Chemical Sciences, Faculty of Science and Technology, Deakin University, Geelong, Australia

ABSTRACT Connective tissue frameworks of the gonad of *H.asinina* consist of the outer gonadal capsule, flat sheets of connective tissue, called trabeculae, that extend from the former toward the inner capsules separating the gonad from the hepatopancreas. Trabeculae, thus, partition the gonad into compartments; and each trabecula acts as the axis on which growing germ cells are attached and proliferate. Each trabecula contains small capillaries in the center, surrounded by muscle cells, collagen fibers intermingled with fibroblasts, and a substantial number of granulated cells that branch extensively. Localization of abalone egg-laying hormone (aELH) was performed by immunoperoxidase technique using polyvalent antibody against recombinant aELH as a probe. Anti-aELH exhibited strong bindings, which implied the presence of aELH, to muscle cells and granulated cells within trabeculae and capsules of both male and female gonads. The cytoplasm of immature oocytes (stages 1, 2, 3) were moderately stained, while that of mature oocytes (stages 4, 5) were only weakly stained. In contrast, male germ cells were not stained.

KEY WORDS: *Haliotis asinina*, gonad, capsules, trabeculae, connective tissue, egg-laying hormone

INTRODUCTION

Donkey's ear abalone, *Haliotis asinina*, is a commercially important abalone species in Thailand because of their maximum proportion of flesh, good taste and relative abundance in Thai coastal water (Singhagraiwan & Doi 1993). The high demand for this abalone has increased pressure on natural stocks, which needed to be maintained if the population is to remain sustainable. So far, most studies have been on practical aspects of finding the optimal aquaculture system while knowledge concerning the reproductive biology of this abalone has received little attention.

A number of gastropod species has been studied with respect to the effects of the egg-laying hormones on their reproductive activities. In *Aplysia californica*, an opisthobranch, egg laying was caused by the injection of the extract from bag cells of abdominal ganglion (Arch 1976, Kupfermann 1967). Administration of the extract from caudo-dorsal cells (CDC) of cerebral ganglia in *Lymnaea stagnalis*, a pulmonate, also caused egg laying (Geraerts & Bohlken 1976). In prosobranchs, injections of crude homogenates of pleuropedal and visceral ganglia could induce spawning in *H. discus hannai* (Yahata 1973). The peptide that activated egg laying in *Aplysia* spp. had been characterized and called egg-laying hormone (ELH) (Chiu et al. 1979), whereas it was called caudo-dorsal cell hormone (CDCH) in *L.stagnalis* (Ebberink et al. 1985), and abalone egg-laying hormone (aELH) in *H. rubra* (Wang & Hanna 1998). These egg-laying hormones may be related, judging from their amino acid numbers and compositions. ELH has 36 amino acids and molecular weight about 4.3 kD (Chiu et al. 1979), in comparison to CDCH, which has molecular weight about 4.5 kD (Ebberink et al. 1985), and aELH about 4.3 kD (Wang & Hanna 1998). Genes encoding ELH, CDCH and aELH have been cloned (Schaller et al. 1983, Vreugdenhil et al. 1988, Wang & Hanna 1998). The nucleotide sequence encoding aELH of *H.rubra* was found to have a 95.4% homology with that of CDCH in *L.stagnalis*, but only 51.9% homology with that of ELH in *A.californica*. Only one amino acid difference was found between aELH of *H.rubra* and CDCH of *L.stagnalis*, while there were 19 amino acid differences between aELH of *H.rubra* and ELH of *A.californica* (Wang & Hanna 1998).

It has been suggested that ELH acts directly on muscle of the capsules and trabeculae of the gonads to initiate egg laying and sperm release in the manner analogous to the action of oxytocin on myoepithelial cells of vertebrates (Coggeshall 1972). In abalone, it remains to be studied where this hormone is synthesized, and how it is distributed in the reproductive organs. In the present study, we have investigated the distribution of this hormone in the gonads of both male and female *H. asinina* by using mouse polyclonal antibody to recombinant aELH of *H. rubra* for immunohistochemical detections.

MATERIALS AND METHODS

Experimental Animals

Sexually-mature male and female *H.asinina* age more than two years old were obtained from The Coastal Aquaculture Development Center, Prachuabkirikhun Province, Thailand, during the months June to July and August to September which are the periods when the gonads enter the proliferate and maturing-spawning phases. These abalone were reared in a land-based aquaculture system by being kept in concrete tanks, which were well flushed with sand-filtered sea water, and aerated with mechanical air delivery system. They were given appropriate algal food, usually *Gracilaria* and *Laminaria* spp., *ad libitum*, and supplemented with artificial food, and kept under normal daylight cycle.

Samples were taken from the gonads of at least five animals of either sex at both periods of collection. The tissues were prepared

*Corresponding author. E-mail address:

for histological examinations by paraffin-embedded and epoxy plastic-embedded (semi-thin) methods as used for transmission electron microscopy and for detecting the distribution of aELH by immunoperoxidase method.

Paraffin and Semi-Thin Methods

For histological studies, gonadal tissues were cut into small pieces, fixed in Bouin's fixative, dehydrated and embedded in paraffin, then sectioned at 5 μm thick and stained with hematoxylin-eosin or PAS-hematoxylin. For semi-thin sections, gonadal tissues were fixed in 2.5% glutaraldehyde in 0.1 M phosphate buffer, dehydrated in ethanol, cleared in propylene oxide, and then embedded in Araldite 502 plastics. Semi-thin sections at 1–2 μm were cut with the ultramicrotome and stained with methylene blue or PAS.

Immunoperoxidase Method

Frozen sections of gonadal tissues were fixed with acetone at −10°C for 10 minutes. After blocking endogenous peroxidase by immersing in 3% H_2O_2 for 15 minutes the sections were washed with 0.05 M Tris buffer saline (TBS), pH 7.6. The sections were overlaid, in moist chamber, with 0.1% glycine in 0.05 M TBS, and 4% BSA in 0.05 M TBS, for 30 minutes each, to block non-specific bindings. Then the sections were covered for one hour with primary antibody consisting of mouse polyclonal antibody against recombinant *H.rubra* egg-laying hormone (Wang & Hanna 1998), with dilution 1:10,000. The control sections were incubated with 0.05 M TBS in place of primary antibody. After that the sections were incubated with secondary antibody, which is biotinylated rabbit anti-mouse IgG (Zymed Co., California, USA), with dilution 1:100, for 30 minutes. The sections were then washed in TBS, covered with the combination of Z-avidin and biotinylated peroxidase (Zymed Co.) in the same buffer, with dilution 1:100, for 30 minutes. Finally, the sections were immersed in the substrate solution containing 5 ml of 0.03% (w/v) 3,3' diaminobenzidine (DAB) plus 17 μl H_2O_2, for 15 minutes. Finally, the sections were washed several times with distilled water, and some were counter-stained with hematoxylin before being mounted in buffered glycerol, and observed in an Olympus Vanox microscope.

RESULTS

Connective Tissue Frameworks

Connective tissue scaffolds of the gonads in either sex consist of the outer capsule which is made of several alternate layers of muscle and collagen bundles, lined on the outside by a single layer of cuboidal epithelium (Fig. 1A, B, F). On the inside the connective tissue of the capsule extend inwards to form sheets, called trabeculae, that have straight hemolymph capillaries running in their cores. Surrounding the capillaries are muscle cells, collagen fibrils, fibroblasts, and granulated cells (Fig. 1A, B, E, F). The interior ends of trabeculae are connected with the inner capsule made of thin loose connective tissue layer that separates gonad from hepatopancreas. Thus, trabeculae divide the gonads into small compartments, and each trabecula forms the axis on which germ cells are attached and proliferate. Early stage cells, such as spermatogonia and oogonia are seen closely bound to the connective tissue of trabeculae. Middle stage germ cells, such as spermatocytes and oocytes, are more detached and appear further away from trabeculae. Mature cells including spermatozoa and stage 5 oocytes, which are the majority of cells found in the gonads in mature phase, are completely detached from the trabeculae and fill up the lumen of the compartments (Fig. 1A, B). Of special interest is the presence of granulated cells, whose soma are large and have ovoid shape about 10×18 μm in size. Each cell has a small spherical nucleus that contains mostly euchromatin. The cytoplasm contains numerous dense spherical granules about 0.3–0.6 μm in size (Fig. 1C, D, E). In PAS stained sections, the granules exhibit PAS positive substance (Fig. 1C, D). The granulated cells may give off extensive branches since in many locations only cytoplasmic processes containing dense granules were observed (Fig. 1E, F). Generally, granulated cells are present in all areas of the connective tissue scaffolds; however, they tend to have a higher number in the outer and inner capsules of the gonads.

Immunoperoxidase Staining

By using immunoperoxidase method, the presence of brownish staining suggested that there are strong and specific bindings of anti-aELH in the trabeculae and the capsules of the gonads in both sexes. The brownish stain is distinct on the overall content of trabeculae and capsules which delimit gonadal compartments of both the ovary and testis of the mature phase abalone (Fig. 3A–D, Fig. 4A, B), in contrast to the control sections which are completely unstained (Fig. 2A). Within each trabecula, there are more intensely stained spots or streaks, which at high magnification, appear to be muscle cells and granulated cells that contain large brownish granules in the cytoplasm (Fig. 3B, D, Fig. 4B, C, D). The latter cells are similar in appearance and general distribution with the granulated cells observed in paraffin and semithin sections, which exhibit better cellular morphology. The positively stained granulated cells were observed in both the outer and inner capsules and the trabeculae. However, there appear to be a higher concentration of these positive cells in the inner capsule that separates gonads from hepatopancreas (Fig. 2B, C, Fig. 4A, B), in both proliferate (Fig. 2B–D) and mature phases (Fig. 4A–D) of the gonadal cycle. Connective tissue in the trabeculae and in the capsules are moderately stained, but they appear more intense in mature than the proliferate phase of the gonadal cycle (Fig. 2B, 3A). In the ovary, the cytoplasm of early oocytes (stages 1, 2, 3) which are the majority of cells in proliferate phase are moderately stained (Fig. 2A, B), while the cytoplasm of mature oocytes (stages 4, 5) which is the majority of cells in mature phase is only weakly stained (Fig. 3A, B, C). In contrast, there is no staining of either early male germ cells or spermatozoa in the testis (Fig. 4A, B, C).

DISCUSSION

The expression of the egg-laying peptide gene in the bag cells of abdominal ganglion, atrial gland, and pleural ganglion of *A. californica* has been detected by *in situ* hybridization, using radiolabeled cDNA probes to ELH mRNA (McAllister et al. 1983). Some work had also been done to locate the ELH receptor within the ovotestis of *A. californica*. ELH binding-protein from ovotestis was purified by ELH affinity column chromatography, and antibodies were produced for localizing this protein in *A. californica* gonad (Choate et al. 1993). It was revealed that the cytoplasm of oocytes is the only site of immunoreactivity, which was never detected in spermatocytes and spermatozoa. In *L. stagnalis*, *in situ* hybridization experiments with cDNA probes revealed a high level of CDCH mRNA expression in caudodorsal cells in the cerebral ganglia, and the observed expression pattern correlated with im-

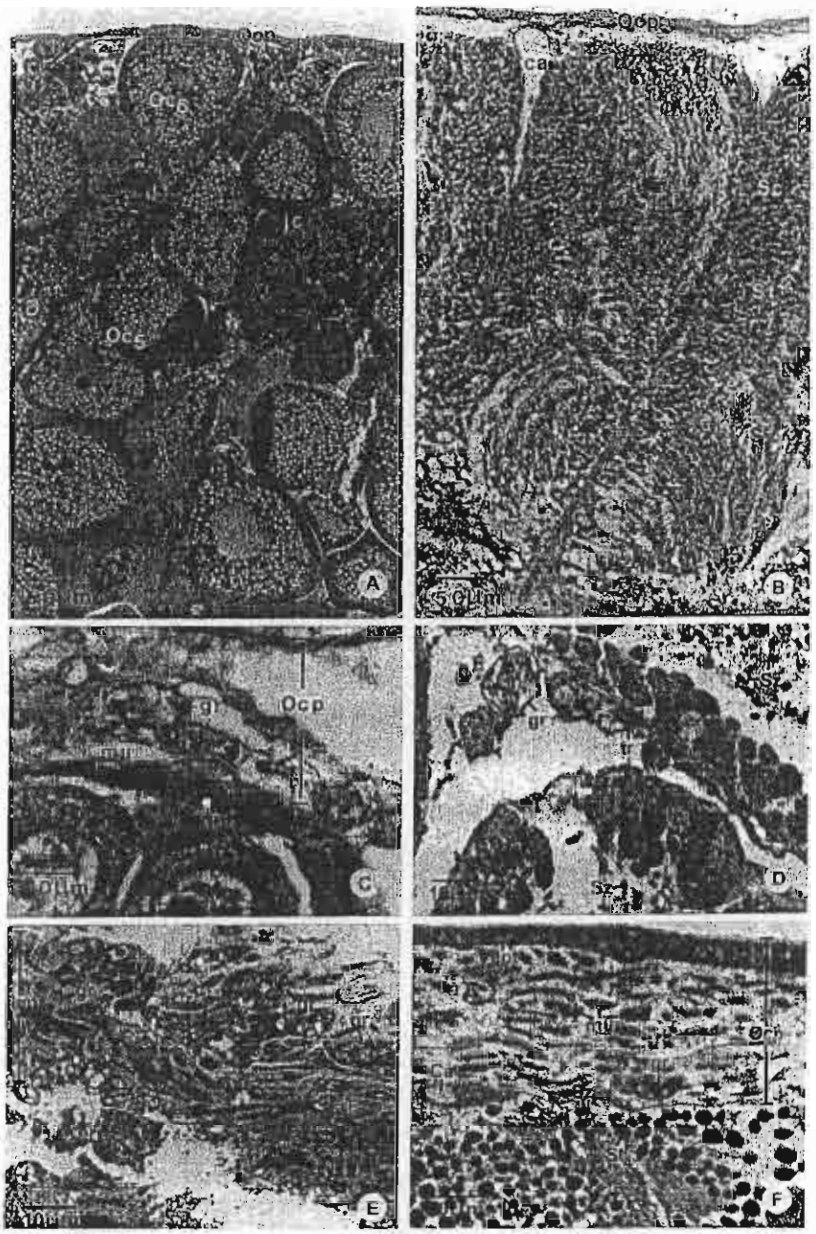

Figure 1. (A, B) Light micrographs of PAS-hematoxylin stained paraffin sections of *H. asinina* ovary (A) and testis (B) in mature (prespawning) phase, where there are abundant mature stage V oocytes (Oc_5) with fully form jelly coat (jc) in the ovary (in A), and numerous spermatozoa (S_z) with dense nuclei in the testis (in B). The connective tissue scaffolds of the gonads in both sexes consist of the outer capsule (Ocp), the trabeculae (tr) and the inner capsule (not shown). In the core of each trabecula, there is a small hemolymph capillary (Ca). Sc = spermatocytes, St = spermatids. (C, D) High magnification micrographs showing the granulated cells containing PAS positive granules (gr-in C) in the outer capsule of the ovary (Ocp) and in a trabecula (tr) of the testis (gr-in D). F = fibroblasts, LSc = leptotene spermatocyte, mu = muscle cells, Sz = spermatozoa. (E, F) The semi-thin plastic sections of the ovarian inner capsule (Icp- in E) and the testicular outer capsule (Ocp-in F) showing the granulated cells with their ellipsoid nuclei (gr-in E), and their attenuated processes containing dense granules (gr-in F). Ca = haemolymph capillary, ept = epithelium, F = fibroblast, mu = muscle cells, St_4 = spermatid stage 4.

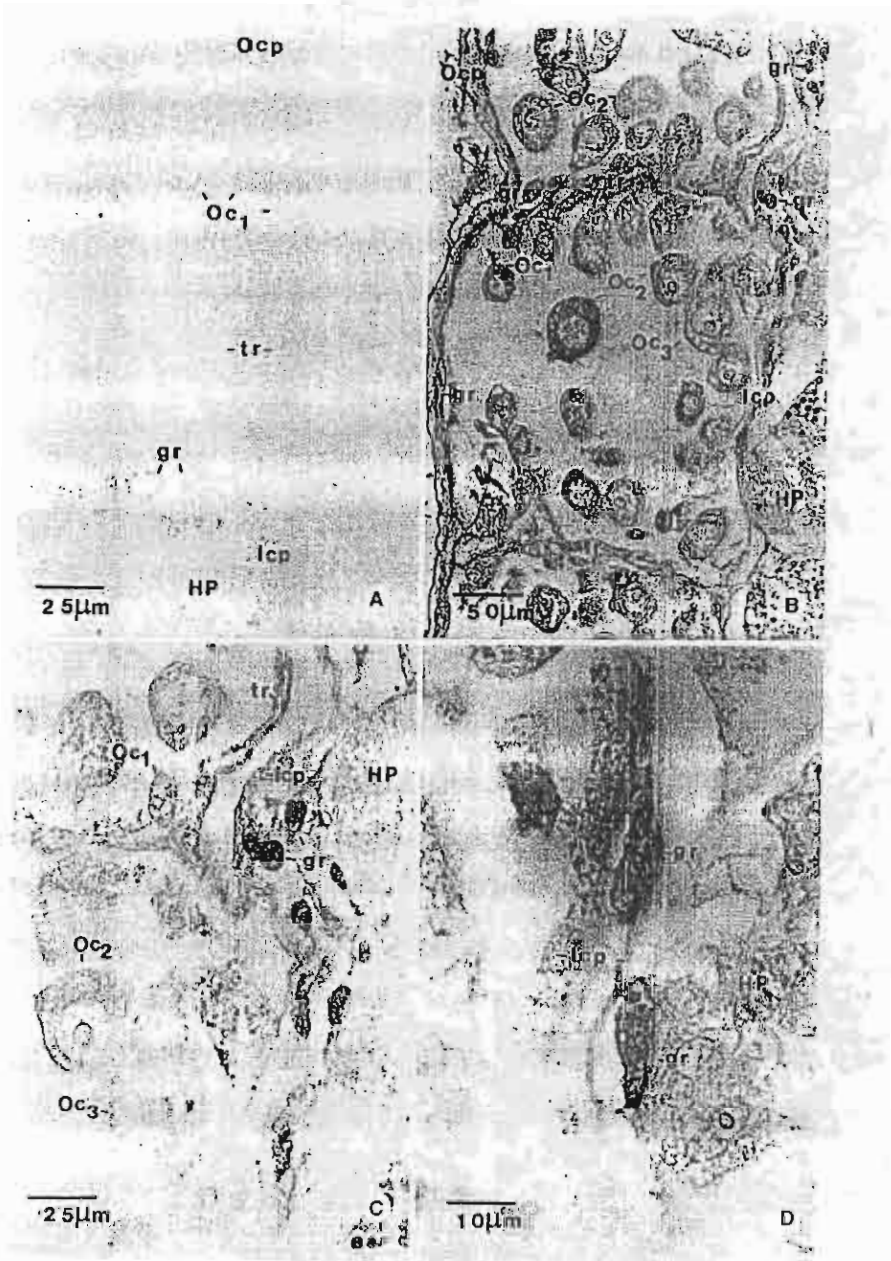

Figure 2. Light micrographs of the ovary in proliferate phase, stained with anti-aELH by immunoperoxidase method. (A) Control section shows no staining in the ovarian tissue. (B–D) Sections stained with anti-aELH, showing intense staining in granulated cells (gr) within the inner (Icp) and the outer capsules (Ocp). While moderate staining is seen in the connective tissue proper of trabecula (tr), both capsules (Ocp & Icp), and the cytoplasm of immature oocytes (Oc_1, Oc_2, Oc_3). HP = hepatopancreas.

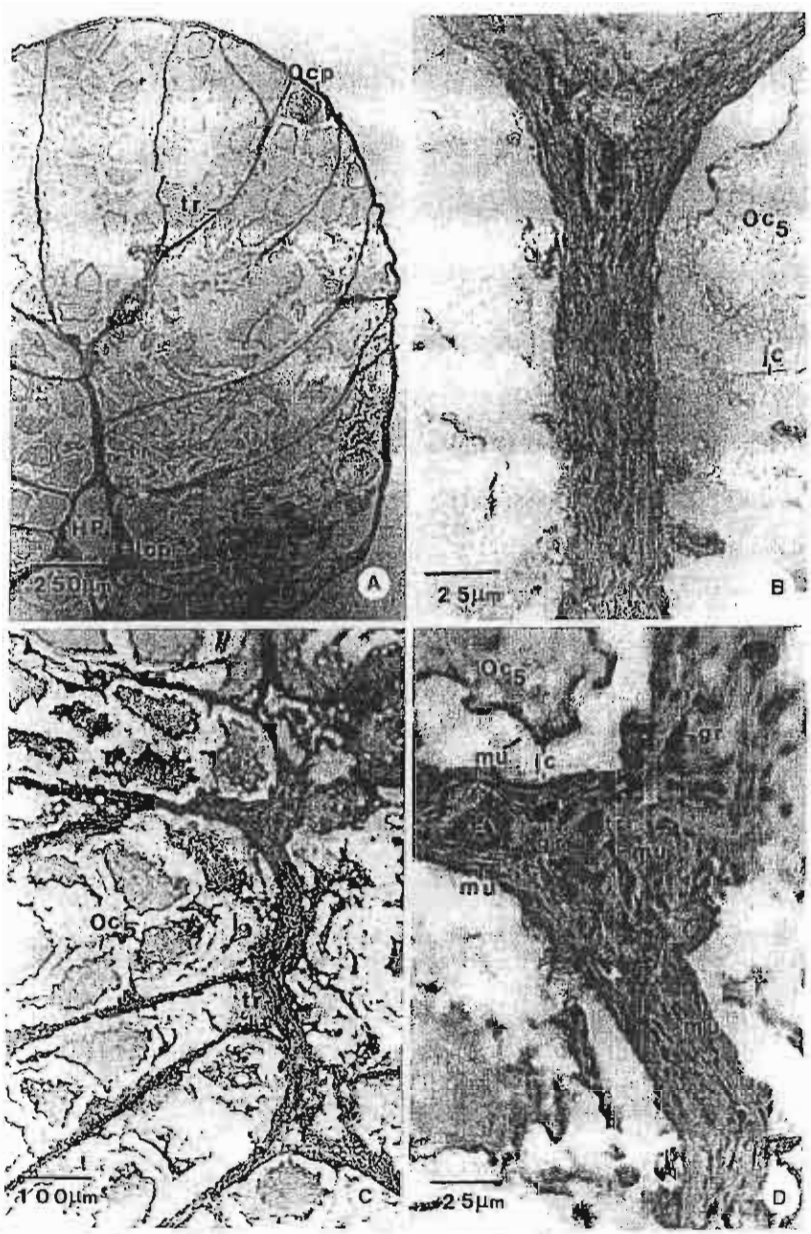

Figure 3. Light micrographs of the ovary in mature phase, stained with anti-aELH by immunoperoxidase method. (A, B) In A, anti-aELH exhibits staining in the trabeculae (tr) and both capsules (Ocp, Icp) of the gonad. In B, granulated cells (gr) in a trabecula are intensely stained. The cytoplasm of late stage oocytes (Oc_5) surrounded by thick jelly coat (jc) is not stained. (C, D) Sections stained with anti-aELH and counter-stained with hematoxylin. In C, the connective tissue of the trabeculae (tr) is positively stained in comparison to oocytes (Oc_5). In D, which is the high magnification of an area from the trabeculae in C, granulated cells (gr) and muscle cells (mu) are intensely stained.

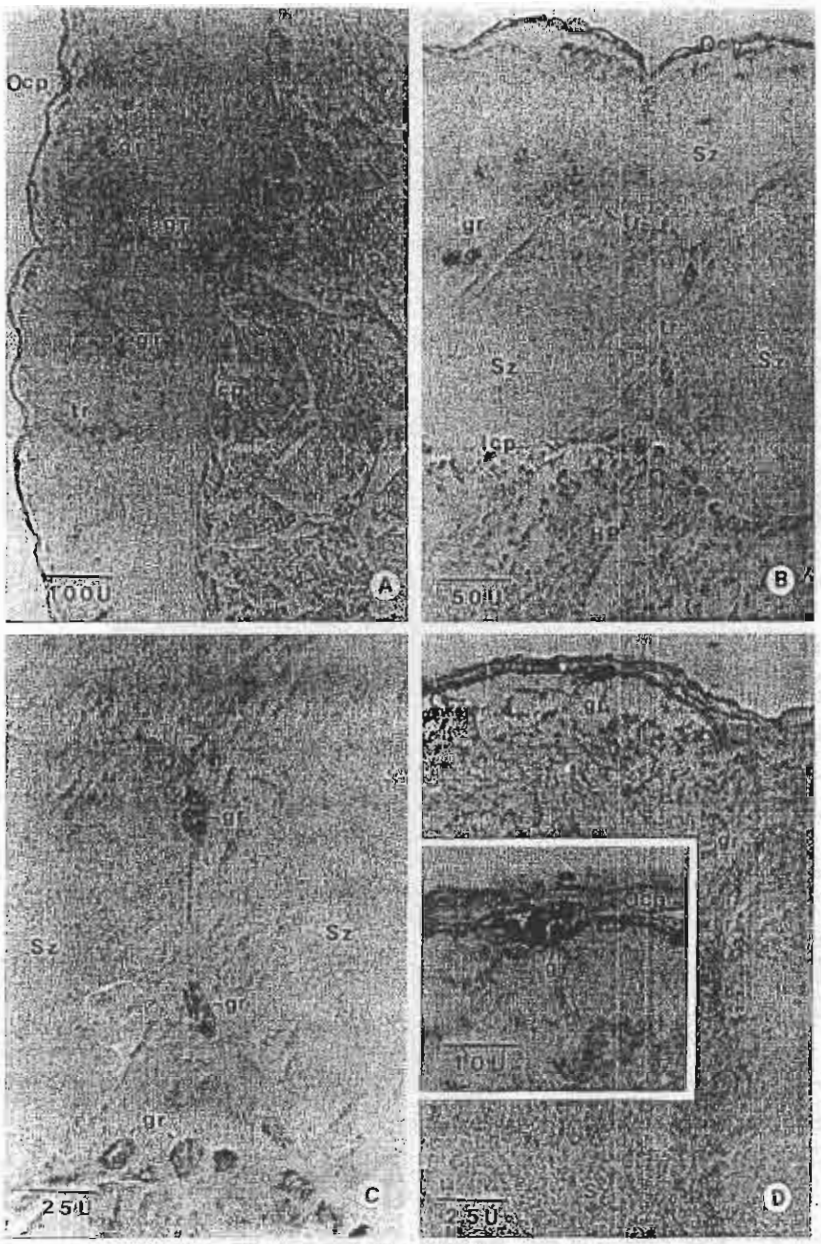

Figure 4. Light micrographs of the testis in mature phase, stained with anti-aELH by immunoperoxidase method. (A–D) Sections stained with anti-aELH, showing strong staining of the trabeculae (tr), both the outer and inner capsules (Ocp, Icp). In C, and D inset, which are high magnifications of a trabecula and the outer capsule, granulated cells (gr) with large granules in their cytoplasm are intensely stained, while spermatocytes and spermatozoa (Sz) are not stained.

munocytochemical data which implied that CDCH is transported through the axon and released by exocytosis to the hemolymph (Dirks et al. 1989, Dirks et al. 1993, Van Minnen et al. 1988). Expression of CDCH was not restricted to the CNS alone, but was also found in the reproductive tract, including oothecal gland, muciporous gland, and pars contorta, which are female accessory sex glands in *Lymnaea stagnalis*. In these glands the processes of positively labeled neurons terminated on the secretory cells, suggesting that they controlled the activities of these tissues (Van Minnen et al. 1988). CDCH immunoreactive material has also been found in secretory cells of the prostate gland and sperm duct (Van Minnen et al. 1989). In contrast to CDCH little is known about the origin of egg-laying hormone in abalone. Histological studies in the Japanese abalone, *Haliotis discus hannai*, showed that the number of neurosecretory cells, especially type 1 and 7, in pleural-pedal ganglia were correlated with the induction of spawning (Hahn 1992). Injections of pleural-pedal and visceral ganglion crude homogenates, or the combination of both, caused female EDS *H.discus hannai* to spawn (Yahata 1973). The quantity of eggs being spawned were significantly greater with the injections of homogenates from visceral ganglion or the combination of pleural-pedal and visceral ganglion, when compared with the injection of pleural-pedal ganglion alone (Yahata 1973). In our preliminary study of *H.asinina* visceral ganglia, neurosecretory cells type 1 were also positively stained with anti-aELH (unpublished observation). Hence, existing evidence imply that abalone egg-laying hormone is mostly produced by neurosecretory cells of the nerve ganglia, particularly pleuropedal and visceral ganglia

In the present study, we found that anti-aELH from *H. rubra* showed strong cross reaction with *H. asinina* gonadal connective tissues, and this implied that aELH may also be produced and stored in the granulated cells within the trabeculae and capsules of the gonad. Similarly, muscle cells in these connective tissue scaffolds were also stained with the anti-aELH, which suggested that this group of cells also bind aELH. Coggeshall (1972) suggested that, in *Aplysia*, ELH acted directly on muscle cells to induce their contraction, which caused the expulsion of ripe oocytes from the ovary. From the evidence gathered in the present study we, therefore, would like to suggest that the granulated cells in the trabeculae and the capsules of gonad in both sexes of abalone can synthesize aELH. After being released from the granulated cells, this hormone could bind to muscle cells in trabeculae and capsules and cause them to contract, which results in the expelling of ripe oocytes or spermatozoa from the gonads. The significance of the binding of anti-aELH to early stage oocytes is not known, but this hormone may also participate in the developmental process of germ cells. In contrast aELH did not bind to male germ cells thus its role in the male abalone may be limited to controlling the release of spermatozoa as has recently been demonstrated by our group (unpublished observation).

ACKNOWLEDGMENTS

We sincerely thank Associate Professor Peter J. Hanna, School of Biological & Chemical Sciences, Deakin University, Geelong, Australia, who kindly supplied mouse polyclonal antibody against aELH of *H.rubra*. This work was supported by the Thailand Research Fund (Senior Research Scholar Fellowship to P. Sobhon).

LITERATURE CITED

Arch, S. 1976. Neuroendocrine regulation of egg-laying in *Aplysia californica*. *Am. Zool.* 16:167–175.

Chiu, A. Y., M. W. Hunkapiller, E. Heller, D. K. Stuart, L. E. Hood & F. Strumwasser. 1979. Purification and primary structure of the neuropeptide egg-laying hormone of *Aplysia californica*. *Proc. Natl. Acad. Sci. USA* 76:6656–6660.

Choate, J. V. A., T. E. Kruger, M.-A. Micci & J. E. Blankenship. 1993. Isolation of an egg-laying hormone-binding protein from the gonad of *Aplysia californica* and its localization in oocytes. *J. Comp. Physiol. A.* 173:475–483.

Coggeshall, R. E. 1972. The muscle cells of the follicle of the ovotestis in *Aplysia* as the probable target organ for bag cell extracts. *Am. Zool* 12:521–523.

Dirks, R. W., A. K. Raap, J. Van Minnen, E. Vreugdenhil, A. B. Smit & M Van der Ploeg. 1989. Detection of mRNA molecular coding for neuropeptide hormones of the pond snail *Lymnaea stagnalis* by radioactive and non-radioactive *in situ* hybridization: a model study for mRNA detection. *J. Histochem. Cytochem.* 37:7–14.

Dirks, R. W., A. G. M. Van Dorp, J. Van Minnen, J. A. M. Fransen, M. Van der Ploeg & A. K. Raap. 1993. Ultrastructural evidence for the axonal localization of caudodorsal cell hormone mRNA in the central nervous system of the mollusc *Lymnaea stagnalis*. *Micros. Res* 25:12–18.

Ebberink, R. H. M., H. Van Loenhout, W. P. M. Geraerts & J. Joosse. 1985. Purification and amino acid sequence of the ovulation neurohormone of *Lymnaea stagnalis*. *Proc. Nat. Acad. Sci. USA* 82:7767–7771.

Geraerts, W. P. M. & S. Bohlken. 1976. The control of ovulation in the hermaphrodite freshwater snail *Lymnaea stagnalis* by the neurohormone of the caudodorsal cells. *Gen. Comp. Endocrinol.* 28:350–357.

Hahn, K. O. 1992. Review of endocrine regulation of reproduction in abalone *Haliotis* spp. In: Abalone of the World. Fishing News Books. pp. 49–56.

Kupfermann, I. 1967. Stimulation of egg-laying: possible neuroendocrine functions of bag cells of abdominal ganglion of *Aplysia californica*. *Nature* 216:814–815.

McAllister, L. B., R. H. Scheller, E. R. Kandel & R. Axel. 1983. *In situ* hybridization to study the origin and fate of identified neurons. *Science* 222:800–808.

Scheller, R. H., J. F. Jackson, L. B. McAllister, B. S. Rothman, B. Mayeri & R. Axel. 1983. A single gene encodes multiple neuropeptides mediating a stereotyped behaviour. *Cell* 32:7–22.

Singhagraiwan, T. & M. Doi. 1993. Seed production and culture of a tropical abalone, *Haliotis asinina* Linnaeus. The Research Project of Fishery Resource Development in the Kingdom of Thailand. Thailand: Department of Fisheries, Ministry of Argriculture and Cooperatives. 32 pp.

Van Minnen, J., C. Van der Haar, A. K. Raap & E. Vreugdenhil. 1988. Localization of ovulation hormone-like neuropeptide in the central nervous system of the snail, *Lymnaea stagnalis* by means of immunocytochemistry and *in situ* hybridization. *Cell. Tiss. Res.* 251:477–484.

Van Minnen, J., R. W. Dirks, E. Vreugdenhil & J. Van Diepen. 1989. Expression of the egg-laying hormone genes in peripheral neurons and exocrine cells in the reproductive tract of the mollusc, *Lymnaea stagnalis*. *Neuroscience* 33:35–46.

Vreugdenhil, E., J. F. Jackson, T. Bouwmeester, A. B. Smit, J. Van Minnen, H. Van Heerikhuizen, J. Kloetwijk & J. Joosse. 1988. Isolation, characterization and evolutionary aspects of a cDNA clone encoding multiple neuropeptides involved in the stereotyped egg-laying behavior of the freshwater snail *Lymnaea stagnalis*. *J. Neurosci.* 8:4184–4191.

Wang, L. & P. J. Hanna. 1998. Isolation, cloning and expression of a DNA sequence encoding an egg-laying hormone of the blacklip abalone (*Haliotis Rubra* Leach). *J. Shellfish Res* 17:789–793.

Yahata, T. 1973. Induced spawning of abalone (*Nordotis discus* Reeve) injected with ganglional suspensions. *Bull. Jap. Soc. Sci. Fish* 39: 1117–1122.

Journal of Shellfish Research, Vol. 20, No. 2, 000–000, 2001.

MORPHOFUNCTIONAL STUDY OF THE HEMOCYTES OF *HALIOTIS ASININA*

[AQ1] S. SAHAPHONG,[1,*] V. LINTHONG,[2] C. WANICHANON,[2] S. RIENGROJPITAK,[1] N. KANGWANRANGSAN,[1] V. VIYANANT,[3] E. S. UPATHAM,[3,4] T. PUMTHONG,[5] N. CHANSUE,[6] AND P. SOBHON[2]

[1]*Department of Pathobiology, Mahidol University, Bangkok, 10400, Thailand;* [2]*Department of Anatomy, Mahidol University, Bangkok 10400, Thailand;* [3]*Department of Biology, Mahidol University, Bangkok 10400, Thailand;* [4]*Department of Biology, Burapha University, Chonburi, Thailand;* [5]*Coastal Aquaculture Development Center, Department of Fishery, Ministry of Agriculture and Cooperatives, Prachuapkhirikhun 77000, Thailand;* [6]*Veterinary Medical Aquatic Animal Research Center, Department of Veterinary Medicine, Faculty of Veterinary Science, Chulalongkorn University, Bangkok 10400, Thailand*

ABSTRACT The hemocytes of abalone (*Haliotis asinina*) were studied by light and electron microscopy in order to describe their main morphological features and to relate these to their role in immune defense. The cells are comprised of two differentiated types: agranulocyte or hyalinocyte and granulocyte. The hyalinocyte is characterized by the presence of several filopodia, large nucleus with dense chromatin, moderate amount of cytoplasm, microfilaments, oval and round-shaped mitochondria with rather dense matrix, considerable amount of rough endoplasmic reticulum, few cytoplasmic granules, coated pits and vesicles, phagocytic vacuoles, and numerous large and small vacuoles. Like hyalinocyte, the granulocyte possesses similar cytoplasmic organelles but in fewer number, and a peripheral organelle-free zone containing numerous dense granules of various types. The shape of the granules varies from round, oval to elongated forms. Several dense granules exhibit crystalloid substructure that show close relationship to the plasma membrane. The average size of granulocyte is 9.68 ± 1.12 μm and hyalinocyte is 8.65 ± 0.77 μm.

KEY WORDS: *Haliotis asinina*, hemocytes

INTRODUCTION

Approximately 75 species of abalone have been reported in the world. Thailand harbors 3 species, namely, *Haliotis asinina*, *H. ovina*, and *H. varia* (Nateewatana and Hylleberge 1986, Tookvinart et al. 1986, Nateewatana and Bussarawit 1988). Among the three species, *H. asinina* is the biggest and has the most economic potential because of its large proportion of flesh [AQ3] and its good taste (Singhakriwan & Doi 1993). Due to the economic potential of this abalone species, a thorough understanding of the biology including its immune response of *H. asinina* is needed. In molluscs, hemocytes are involved in a variety of physiological and pathological functions including nutrient transport and digestion, wound and shell repair, internal defense, and exogenous and endogenous material excretion (Cheng 1981, Bayne 1983, Fisher 1986). In the literature, most of the morphological studies of molluscan hemocytes reported are of bivalve molluscs; only a few exist on abalone. There has been no study on the hemocytes of *H. asinina*. In this report, we studied the morphology of *H. asinina* hemocytes by using light and electron microscopy.

MATERIALS AND METHODS

Hemolymph was withdrawn from the cephalic arterial sinus of individual abalone and pooled. Pooled hemolymph was immediately poured into cold 2% glutaraldehyde in 0.1 M sodium cacodylate buffer pH 7.4, at 4°C, for overnight. The hemocytes were centrifuged at 800× *g* for 10 minutes at 25°C. The hemocyte pellets were post-fixed in 1% osmium tetroxide in 0.1 M sodium

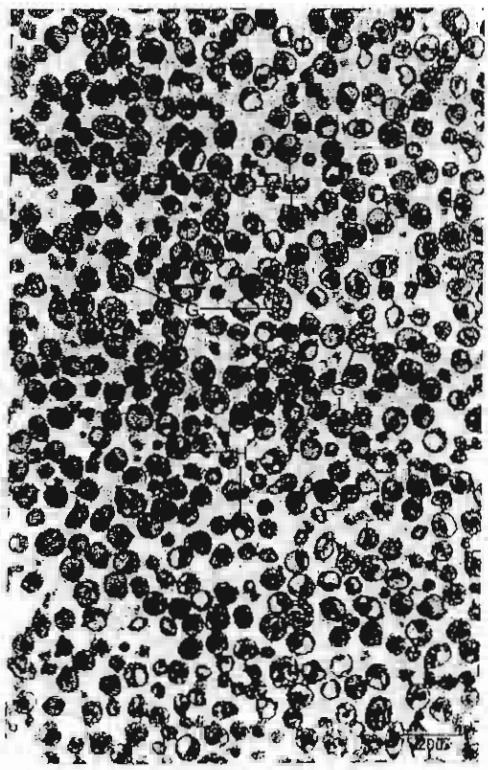

Figure 1. Semithin section of hemocytes of *H. asinina*, Methylene blue stain. At this magnification, granulocytes (G) and hyalinocytes (H) are clearly differentiated.

[AQ2] *Corresponding author. E-mail address:

cacodylate buffer, at 4°C, for an additional two hours. They were then washed with sodium cacodylate buffer, dehydrated in graded series of alcohol, cleared in propylene oxide and embedded in Araldite 502 resin. Blocks were sectioned at one-micron thickness by an ultramicrotome and stained with Methylene blue for light microscopic observation. Ultrathin sections were cut and stained with uranyl acetate and lead citrate and viewed by Hitachi TEM H-300 at 75 kV.

RESULTS

Light Microscopy

Micrographs of the semithin sections of the *H. asinina* hemocytes are shown in Figures 1 and 2. Two populations of hemocytes, granulocytes and agranulocytes or hyalinocytes, were observed based on the presence and the absence of cytoplasmic granules. The proportions of granulocytes and hyalinocytes are 11.43% and 88.57% in this present study, respectively.

Granulocytes are characterized by the presence of numerous cytoplasmic granules. The granules tend to be arranged at the periphery of the cell, thus leaving the clear zone around the nucleus. Most of the cells are spherical or slightly oval, the largest measured 13.15 μm (9.68 ± 1.12 μm in diameter on average) with some filopodia extending from the plasma membrane. The nucleus is round to oval shape and centric with rather small nucleus/cytoplasmic ratio. The maximum nuclear size is 4.70 μm with the average of 3.70 ± 0.59 μm. Some nuclei are bilobed, elongated and indented.

The agranulocytes or hyalinocytes are spherical or oval. They are characterized by large nuclei and contain one or two prominent clear cytoplasmic zones. The cells are only slightly smaller than the granulocytes. The largest cell measured 11.22 μm in diameter and the average size is 8.65 ± 0.77 μm. Similar to the granulocytes, the nuclear profiles were round or oval, with some bilobed and indented. Nuclei were both eccentrically and centrically placed. The maximum nuclear size of the hyalinocyte is 5.98 μm with the average of 4.70 ± 0.60 μm. The nucleus/cytoplasmic ratio was relatively larger than that of the granulocyte. Filopodia were clearly visible extending from the cell.

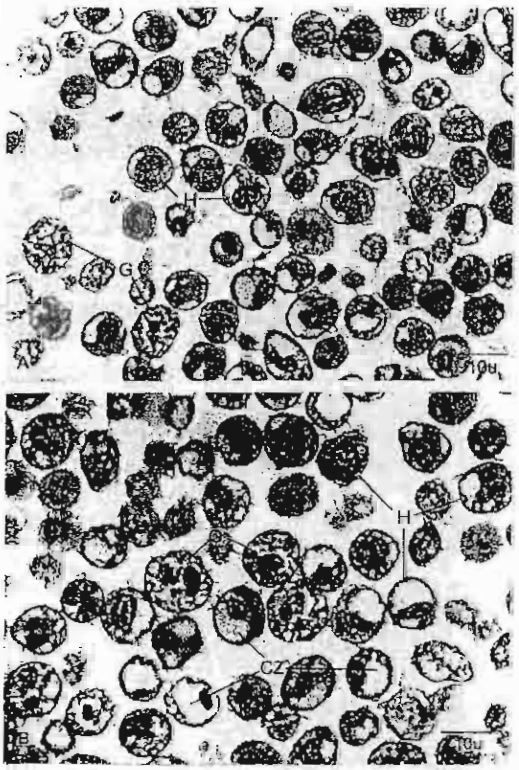

Figure 2. A-B. At higher magnification, more details are seen. Note the peripheral distribution of the granules and perinuclear clear area in the granulocytes, while large cytoplasmic clear zones (CZ) are seen in the hylinocytes. Different shape, size and location of the nucleus in both granulocytes and hyalinocytes can be observed. Note also the filopodia (arrow) in both cell types.

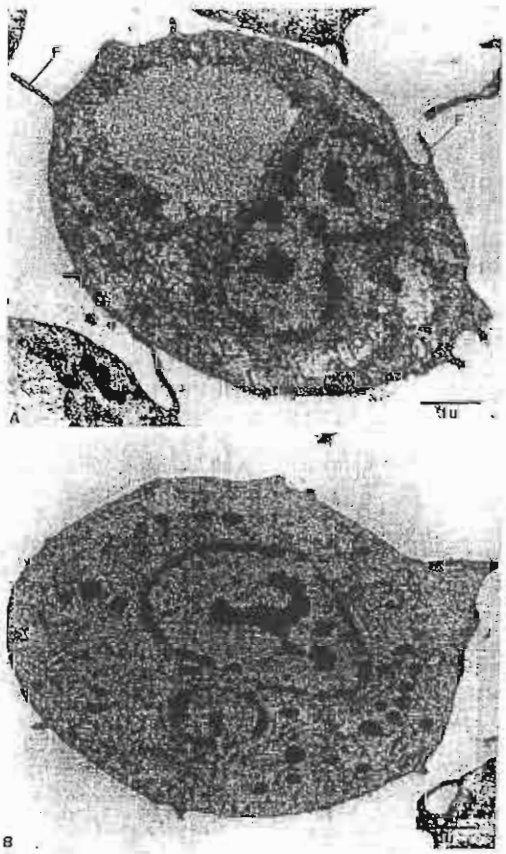

Figure 3. Electron micrographs of hyalinocyte. A. Hyalinocyte showing bilobed nucleus (N) with moderate amount of heterochromatin. A lake of glycogen (Gly) is prominent. Few mitochondria (M) are seen. F, filopodia. B. In contrast to figure A, this hyalinocyte does not contain as prominent a glycogen area. There are few small round electron dense granules (G), rough endoplasmic reticulum (RER) and mitochondria (M). Note the presence of small vesicular bodies (arrow).

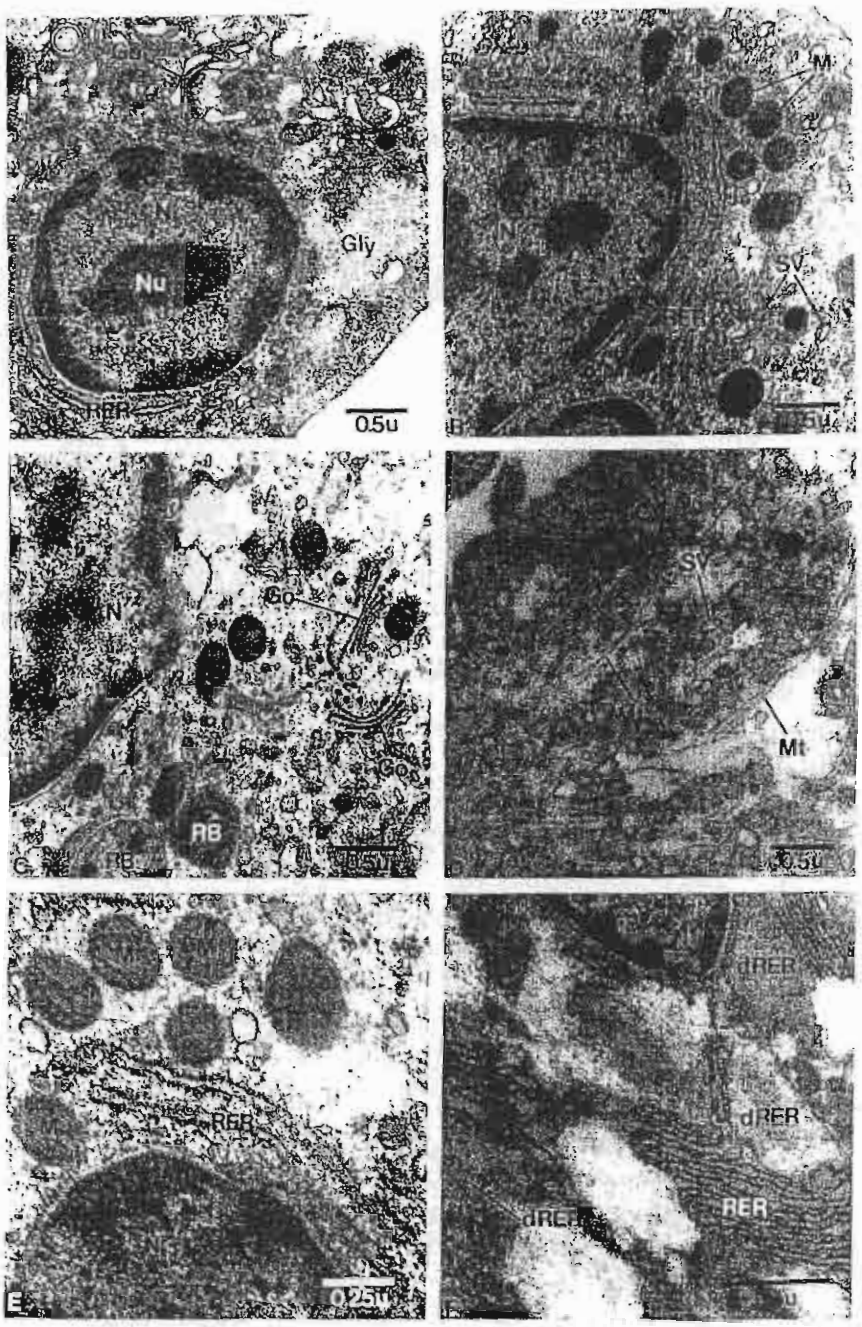

AQ6 Figure 4. A series of electron micrographs showing details of some of hyalinocyte organelles. A. Hyalinocyte with spherical nucleus (N) containing moderate amount of chromatin and a prominent nucleolus (Nu). Note the presence of glycogen area (Gly), Golgi apparatus (Go), and rough endoplasmic reticulum (RER). PM, plasma membrane. B. Hyalinocyte shows profiles of oval shape mitochondria (M) with rather dense matrix. Several small vesicles (SV) are also seen. M, mitochondria. N, nucleus. RER, rough endoplasmic reticulum. C. Well developed Golgi apparatus (Go) and residual bodies (RB) are seen here in this electron micrograph. Go, Golgi apparatus. N, nucleus. RB, residual body. D. Microtubules (Mt) and small vesicles (SV) are seen in the cytoplasm of the hyalinocyte. Mt, microtubule. SV, small vesicle. E. Mitochondria (M) with rather dense matrix are shown here with rough endoplasmic reticulum (RER). N, Nucleus. F. Hyalinocyte showing stack of rough endoplasmic reticulum (RER) and a few dilated endoplasmic reticulum (dRER) with light density amorphous material within cisternae. N, nucleus, RER, rough endoplasmic reticulum.

Electron Microscopy

The hyalinocyte is characterized by the presence of several filopodia, large nucleus with dense chromatin and moderate amount of cytoplasm. The mitochondria are round or oval in shape with rather dense matrix. A considerable amount of rough endoplasmic reticulum, Golgi apparatus, few cytoplasmic granules mostly of round shape, coated pits and vesicles, phagocytotic vacuoles, numerous large and small vacuoles including microfilaments were observed. When viewed by electron microscopy, the clear cytoplasmic zones observed by light microscopy corresponded to the areas composed mostly of unstained glycogen with some visible glycogen particles within. In some cells the pools of glycogen are quite large and seem to push the nuclei to the periphery.

Like hyalinocytes, the granulocyte possesses similar cytoplasmic organelles but in fewer numbers and peripheral organelle free zone containing are cytoplasmic granules of various shape and size and various densities. The shapes of the granules vary from round, oval to polyhedral elongated forms. The maximum size of the granule is 0.78 μm and the average size is 0.34 ± 0.11 μm. However, most of them are polyhedral elongated and only a few are spherical or oval. The close relationship of the granules and plasma membrane is noted. Some of the granules protruded from the plasma membrane, while others coalesced or fused with the cell membrane. The nucleus is relatively small size and round and located either eccentrically or centrically.

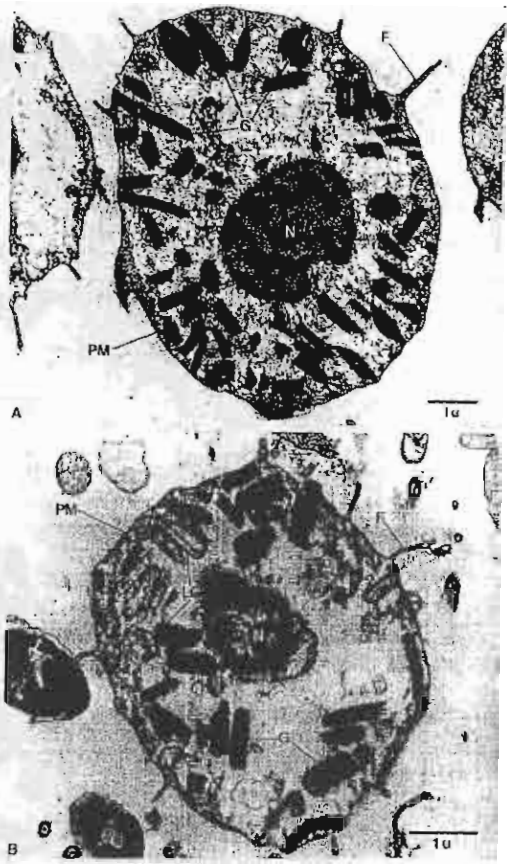

Figure 5. Electron micrographs of granulocyte. A. Granulocyte showing different shapes and sizes of its granules. Note the peripheral distribution of the granules (G), several of them in the close relationship with the plasma membrane (PM). As in hyalinocytes, the oval shaped nucleus contains moderate amount of heterochromatin. This cell is almost devoid of recognizable organelles. F, filopodia, N, nucleus. B. Variation of intragranular densities are illustrated in this micrograph from marked to light electron dense. The light granules (LG) contain intragranular inclusion bodies. F, filopodia, N, nucleus, PM, plasma membrane. AQ7

DISCUSSION

In this preliminary study on the hemocytes of the *H. asinina*, were composed of two differentiated cell types, the granular and the agranular or hyalinocytes. Cheng (1981) suggested that hemocytes should be designated as granulocytes and hyalinocytes. By using different techniques such as phase contrast microscopy, several fixatives and stains including electron microscopy, Foley and Cheng (1972), Foley and Cheng (1974), Cheng and Foley (1975), identified another cell type in the hemolymph of the bivalve mollusc, the fibrocyte. Fibrocyte was also described in the black abalone, *Haliotis cracherodii* (Shields et al. AQ8 1977).

In this study, we have shown that hyalinocyte contained very prominent area or aggregates of glycogen. Cheng and Cali (1974) however reported that the granulocytes not the hyalinocytes contained a large aggregate of glycogen in the cytoplasm. This is in contrast to our findings in which we found glycogen primarily in the hyalinocytes.

Of interest, is the observation of the close relationship of the granules of the granulocyte to the plasma membrane. Several granules protruded from the membrane and some fused with the membrane. This represents the process of releasing the content of the granules or most likely the lysosomes into the serum. The migration of the lysosome to the cell membrane and the extrusion from the granulocytes in *Mercenaria mercenaria* as evidenced by scanning and transmission electron microscopy were reported by Mohandas et al. (1985) and Mohandas and Cheng (1985). Fewer organelles observed in granulocytes is that when a cell becomes fully differentiated, reduction in organelles accompanies this process.

This present study shows for the first time, the presence of two main types of hemocytes in *H. asinina*: hyalinocytes and granulocytes. We believe that the granules are the lysosomes based on the marked morphological resemblance to the lysosomal granules observed in the eosinophil. Particular function of each population in defense mechanism in this species of abalone will be further studied.

ACKNOWLEDGMENT

This work was supported by the Thailand Research Fund (Senior Research Scholar Fellowship to P. Sobhon and grant No. BRG4080004).

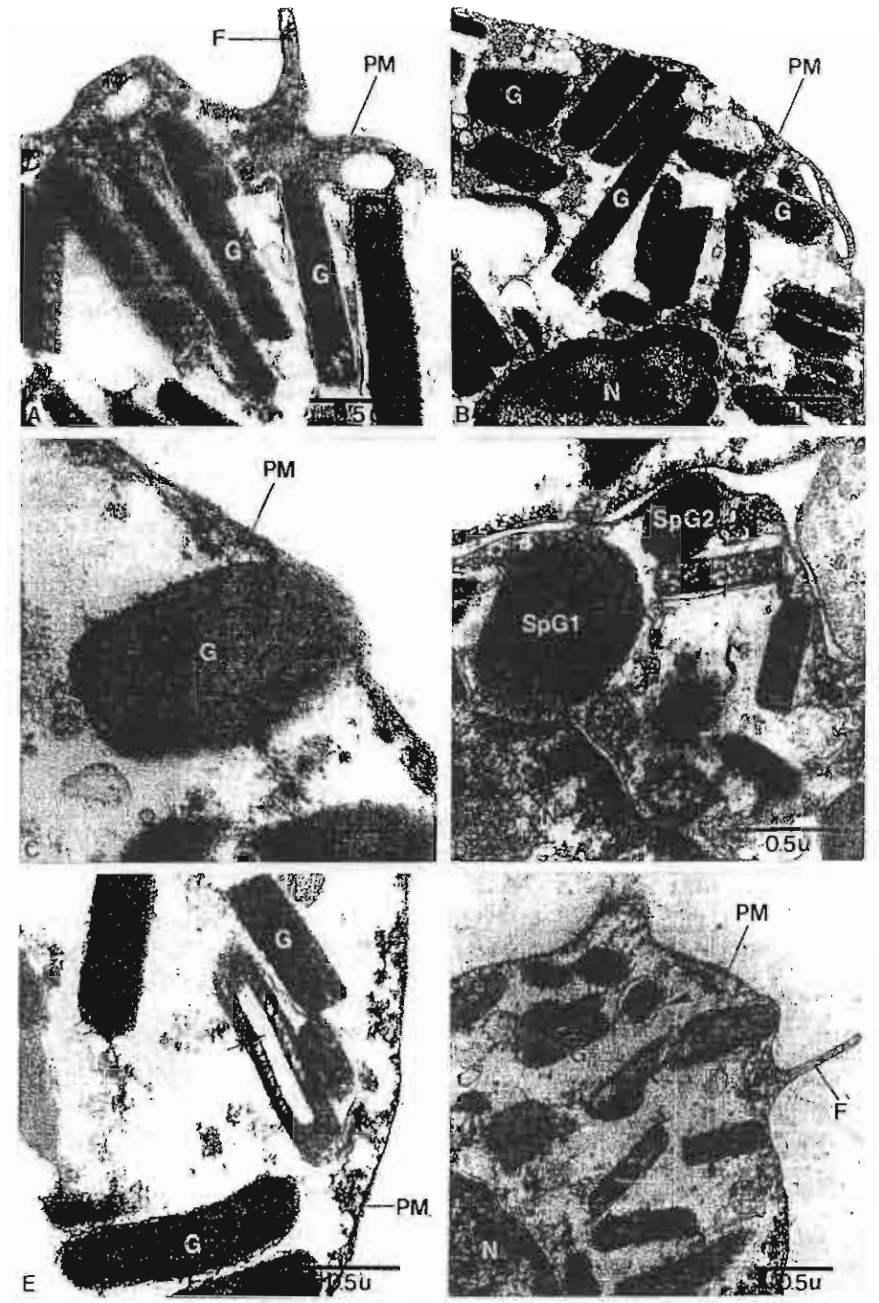

[A08] **Figure 6.** Variations in shapes, size, density and the relationship to the plasma membrane of the cytoplasmic granules in the granulocyte of *H. asinina* are illustrated in details in this series of electron micrographs (A-F). A. Elongated polyhedral forms. F, filopodia. G, granule. PM, plasma membrane. B. Another view of the cytoplasmic granule of the granulocyte. G, granule. N, nucleus. PM, plasma membrane. C. Fusion of one of the granule (G) with plasma membrane (PM). D. One large and one small spherical granules (SpG1 and SpG2) are seen. Note the heterogenicity of the elongated form granules, some of which contain intragranular inclusions. F. Picture frame like granule with hollow core is seen here (arrow). G, granule, PM, plasma membrane. F. Protrusion of one of the granule is evident here. Note the limiting membrane (arrow) around the small round shape granule (G). N, nucleus. PM, plasma membrane.

LITERATURE CITED

Bayne, C. J. 1983. Molluscan immunobiology. In: Saleuddin A. S. M. & K. M. Wilbur, editors. The Mollusca, 5, Physiology, Part 2. London: Academic Press. pp. 407–486.

Cheng, T. C. 1981. Bivalves. In: Ratcliffe N. A. & A. F. Rowley, editors. Invertebrate blood cells. London, New York: Academic Press. pp. 231–300.

Cheng, T. C. & A. Cali. 1974. An electron microscope study of the fate of bacteria phagocytized by granulocytes of *Crassostrea virginica*. *Contemp. Topics Immunobiol.* 4:25–35.

Cheng, T. C. & D. A. Foley. 1975. Hemolymph cells of the bivalve mollusc. *Mercenaria mercenaria*: an electron microscopical study. *J. Invertbr. Pathol* 26:341–351.

Fisher, W. S. 1986. Structure and function of oyster hemocytes. In: M. Brehelin, editor. Immunity in invertebrates. Berlin, Heidelberg: Springer-Verlag. pp. 25–35.

Foley, D. A. & T. C. Cheng. 1972. Interaction of molluscs and foreign substances: the morphology and behavior of hemolymph cells of the American oyster, *Crassostrea virginica, in vitro*. *J. Invertbr. Pathol* 19:282–394.

Foley, D. A. & T. C. Cheng. 1974. Morphology, hematologic parameters, and behavior of hemolymph cells of the quohaug clam *Mercenaria mercenaria*. *Biol. Bull.* 146:343–356.

Mohandas, A. & T. C. Cheng. 1985. An electron microscope study of the structure of lysosome released from *Mercenaria mercenaria* granulocytes. *J. Invertbr. Pathol.* 46:332–334.

Mohandas, A., T. C. Cheng & J. B. Cheng. 1985. Mechanism of lysosomal enzyme release from *Mercenaria mercenaria* Granolocytes: a scanning electron microscope study. *J. Invertbr. Pathol* 46:189–197.

Nateewatana, A. & S. Bussarawit. 1988. Abundance and distribution of abalones along the Andaman Sea Coast of Thailand. *Kasetsart J. (Nat. Sci.)* 22:8–15.

Nateewatana, A. & J. Hylleberge. 1986. A survey on Thai abalone around Phuket Island and feasibility study of abalone culture in Thailand. *Thai Fish. Gazette.* 39:177–190.

Shields, J., F. O. Perkins, W. Biggs, P. L. Haaker & C. S. Friendman. 1977. Hematology of black abalone afflicted with withering syndrome. For the 3rd International Abalone Symposium, Monterey, CA, Oct 26–31,1997

Singhakriwan, T. & M. Doi. 1993. Seed production and culture of tropical abalone, *Haliotis asinina* Linne. Thailand: The Eastern Marine Fisheries Development Center, Department of Fisheries, Ministry of Agriculture and Cooperatives, 33pp.

Tookvinart, S., W. Leknim, Y. Donyadul, Y. Preeda-Lampabutra & P. Perngmak. 1986. Survey on species and distribution of abalone (*Haliotis* spp.) in Surajthani, Nakornsrithammaraj and Songkhla provinces. Technical Paper No. 1/1986, Thailand: National Institute of Coastal Aquaculture, Department of Fisheries, Ministry of Agriculture and Cooperatives. 16 pp.

Journal of Shellfish Research, Vol. 20, No. 2, 000–000, 2001.

ULTRASTRUCTURE OF NEUROSECRETORY CELLS IN THE CEREBRAL AND PLEUROPEDAL GANGLIA OF *HALIOTIS ASININA* LINNAEUS

A. THONGKUKIATKUL,[1,*] P. SOBHON,[2] E. S. UPATHAM,[3,4] M. KRUATRACHUE,[4] C. WANICHANON,[2] Y. P. CHITRAMVONG[3] AND T. PUMTHONG[5]

[1]*Department of Biology, Faculty of Science, Burapha University, Chonburi 20131, Thailand;* [2]*Department of Anatomy, Faculty of Science, Mahidol University, Bangkok 10400, Thailand;* [3]*Department of Biology, Faculty of Science, Mahidol University, Bangkok 10400, Thailand;* [4]*Faculty of Science, Burapha University, Chonburi 20131, Thailand;* [5]*Coastal Aquaculture Development Center, Prachuap Khiri Khan 77000, Thailand*

ABSTRACT The ultrastructure of all three types of neurosecretory cells (NS_1, NS_2 and NS_3) in the cerebral and pleuropedal ganglia of *Haliotis asinina* was studied. NS_1 cells contained a euchromatic nucleus, and the cytoplasm contained RER, Golgi complexes, mitochondria and ribosomes. There were two types of neurosecretory granules in the NS_1 of cerebral ganglia: type 1 were large osmiophilic membrane-bound granules and type 2 were small electron-dense spherical granules. The NS_1 cells of pleuropedal ganglia only had one type of round cytoplasmic granule with moderate to strong electron-dense matrix. NS_2 cells contained blocks of heterochromatin in the nucleus. The cytoplasm of the NS_2 of cerebral ganglia contained the usual organelles similar to those of NS_1 cells and large membrane-bound granules containing crystalline structures embedded in a moderately dense osmiophilic matrices. The NS_2 cells of pleuropedal ganglia contained one type of granule that had a dense matrix. NS_3 cells were smaller than NS_1 and NS_2. The nucleus contained thick heterochromatin strands. The organelles in the cytoplasm appeared to be fewer than those of NS_1 and NS_2. The secretory granules of NS_3 of both cerebral and pleuropedal ganglia were composed of aggregates of dense osmiophilic globules of various sizes.

KEY WORDS: *Haliotis asinina*, neurosecretory cells, cerebral ganglia, pleuropedal ganglia, ultrastructure

INTRODUCTION

Neurosecretory cells present in the cerebral ganglia of prosobranchs have not been extensively studied, and consequently little is known about them. The neurosecretory cells in the cerebral ganglia of *Bithynia tentaculata* Linnaeus stained with phloxine (Andrews 1968). They were found to be unipolar and their nuclei were usually concave on one side. Neurosecretory material accumulated in the periphery of the cytoplasm and the axon hillock (Andrews 1968). In *Haliotis discus hannai* Ino and *Nordotis discus* Reeve, two cell types in the cerebral ganglia were identified as neurosecretory cells. They were large and medium sized cells with euchromatic nuclei and contained neurosecretory granules in the cytoplasm (Yahata 1971, Hahn 1994).

More recently, in the cerebral ganglia of *Haliotis asinina* Linnaeus, two types of neurosecretory cells were found (Upatham et al. 1997). These cells are either large or medium in size and stained positively with chrome-hematoxylin-phloxine and paraldehyde-fuchsin. The large sized cells contain a round nucleus with euchromatin and a distinct nucleolus. The medium sized cells also contain a round nucleus with patches of heterochromatin. Neurosecretory granules are present in both cell types (Upatham et al. 1997).

Most studies on the ultrastructure of neurosecretory cells in gastropods have concentrated on pulmonates and opisthobranchs with only a few on prosobranchs. In the cerebral ganglia of *Lymnaea stagnalis* (Linnaeus), two groups of neurosecretory cells have been described (Joosse 1964, Boer 1965, Boer et al. 1968). The cytoplasm of these cells contain electron-dense granules, which had a mean diameter of 20 nm, extremely elongated mitochondria, rough endoplasmic reticulum, free ribosomes, polyribosomes, Golgi complexes, multivesicular bodies, neurotubules and cytosomes. Bonga (1970), using the alcian blue-alcian yellow staining technique, reported that there was only one type of neurosecretory cells *i.e.* dark green cells in the pleuropedal ganglia of *L. stagnalis*. At the electron microscopic level, the dark green cells appear to contain a large quantity of elementary granules with a mean diameter of 20 nm. Numerous Golgi complexes were found to be evenly distributed in the cytoplasm, and there was extensive rough endoplasmic reticulum. A low number of cytosomes were present. In *Achatina fulica* (Bowdich), neurosecretory cells in the cerebral ganglia contain a round shaped nucleus with patches of heterochromatin and a conspicuous single large vacuole in the cytoplasm. In addition, electron-dense granules with a mean diameter of 16nm are associated with extensive Golgi complexes and rough endoplasmic reticulum (Kruatrachue et al. 1994).

In the prosobranchs, the ultrastructure of neurosecretory cells and neurons have been described in *B. tentaculata* (Andrews 1971) and *Haliotis rufescens* Swainson (Miller et al. 1973). In *B. tentaculata*, there are three types of neurosecretory cells, viz., S1, S2 and S3. In the cytoplasm of these cells, there are well-developed rough endoplasmic reticulum and Golgi complexes, mitochondria, lysosomes, glycogen granules, neurofibrils, and neurosecretory granules (Andrews 1971). Miller et al. (1973) describe that most of the neurons of *H. rufescens* contain the usual cytoplasmic organelles along with large membrane-bound inclusions. A few neurons contain small dense granules, which are similar in appearance to typical neurosecretory granules.

It was, therefore, apparent that an extensive investigation of the ultrastructure of neurosecretory cells in *Haliotis* was needed. Hence, the aim of the present study was to describe the ultrastructure of different types of neurosecretory cells in the cerebral and pleuropedal ganglia of *H. asinina*.

MATERIALS AND METHODS

Cerebral and pleuropedal ganglia from mature *H. asinina* were fixed in a mixture of 4% v/v glutaraldehyde and 2% v/v paraform-

*Corresponding author. E-mail address: .

aldehyde in 0.1M Millonig buffer (pH 7.8) at 4°C for 24 hours, washed several times with the same buffer, and postfixed in 1% OsO_4 in 0.1M Millonig buffer. The specimens were dehydrated in a graded series of ethanol, infiltrated in acetone and embedded in Araldite 502-epoxy resin. Sections were cut on a Sorvall MT2 ultramicrotome, stained with saturated uranyl acetate and lead citrate, and viewed with a Hitachi H-300 TEM, operating at 75KV.

RESULTS

Based on ultrastructural characteristics, there are three types of neurosecretory cells in the cerebral and pleuropedal ganglia of *H. asinina*. These are: type 1 neurosecretory cell (NS_1), type 2 neurosecretory cell (NS_2), and type 3 neurosecretory cell (NS_3).

NS_1 cells are round to oval (15–20 μm in dimension) and contain round nuclei (6–8 μm in diameter) (Fig. 1, Fig. 2). The [illegible]

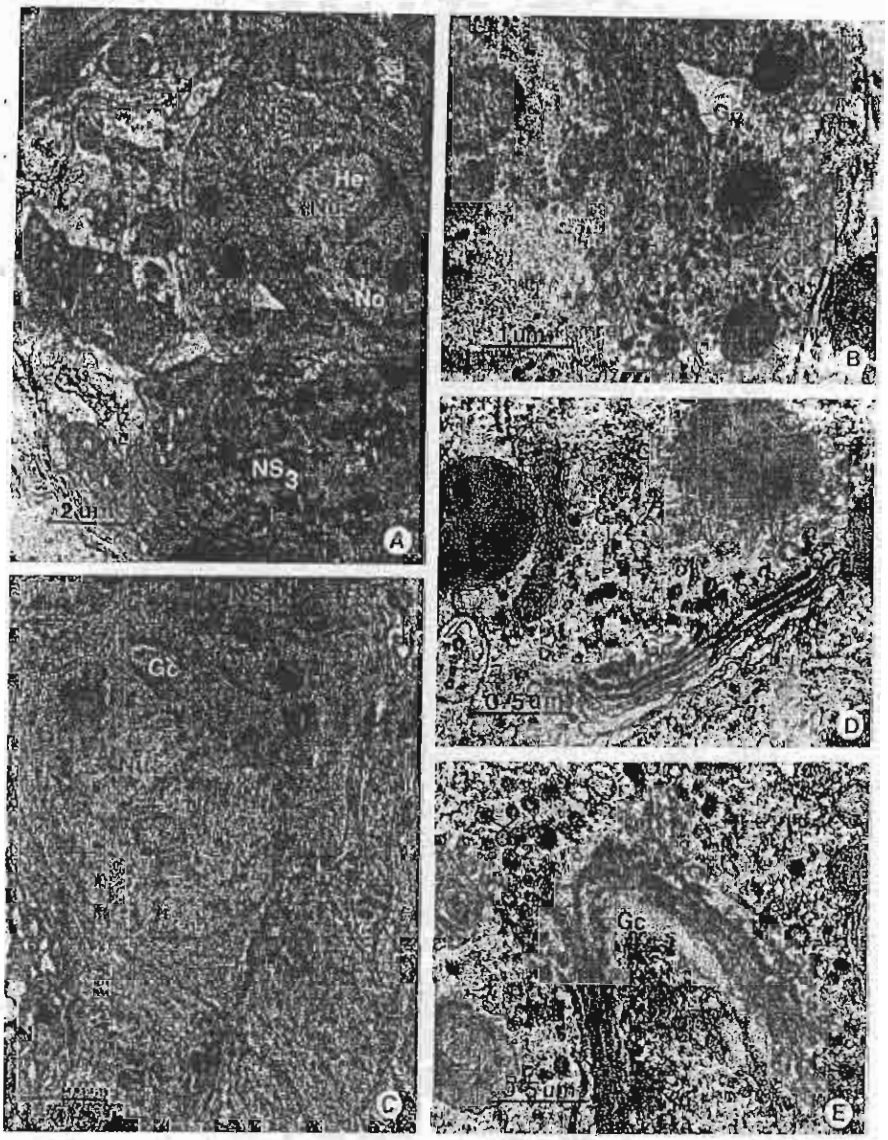

Figure 1. Figure 1. TEM micrographs of NS_1 cells of cerebral ganglia. (A, C) Medium power micrographs of the NS_1 showing round nucleus (Nu) which contains thin rim of heterochromatin (He) near the nuclear envelope. Nucleolus (No) is round, large and very distinct. There are abundant secretory granules in the cytoplasm. NS_1, type 1 neurosecretory cell; NS_3, type 3 neurosecretory cell; Gc, Golgi complex; Gr_1, type 1 granule. (B, D, E) High magnifications of the cytoplasm of the NS_1 demonstrating abundant rough endoplasmic reticulum (rer), Golgi complexes (Gc) and secretory granules. Type 1 granules (Gr_1) are large spherical membrane bound granules whereas type 2 granules (Gr_2) are small and round, containing electron-dense cores.

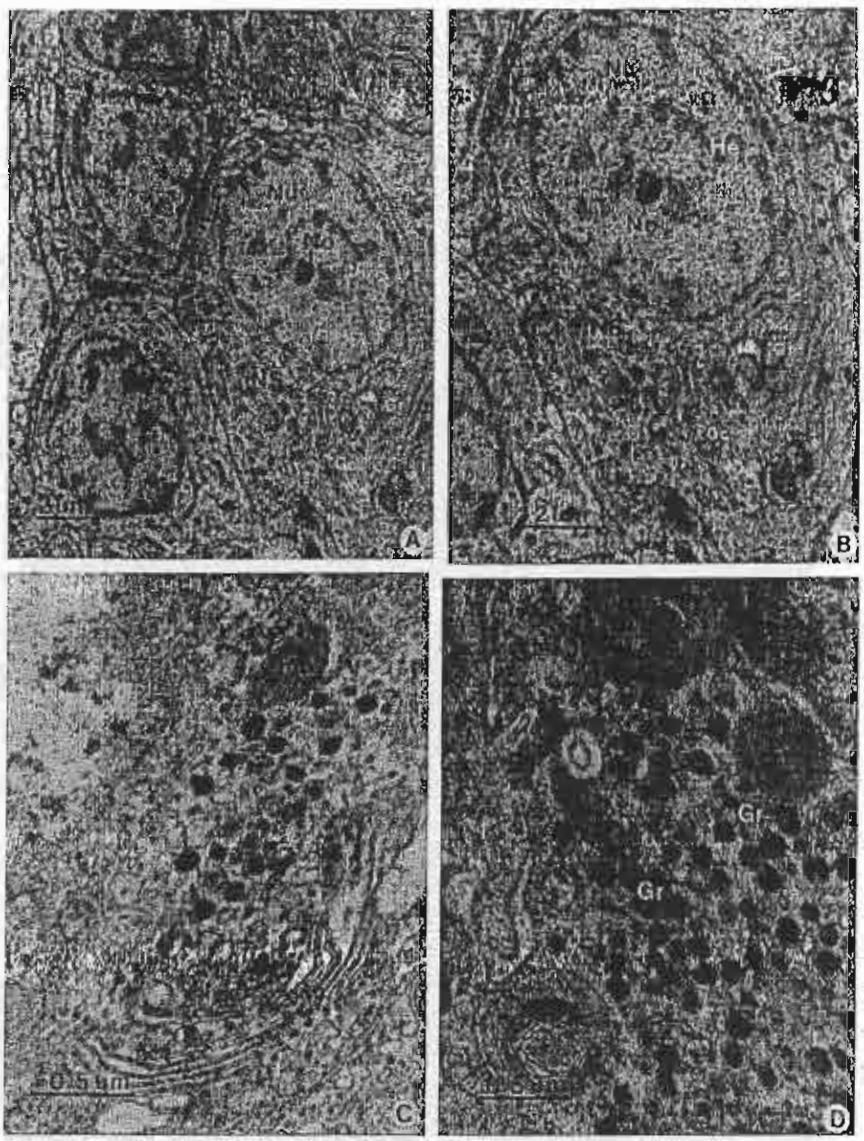

Figure 2. TEM micrographs of NS_1 cells of pleuropedal ganglia. (A, B) Low and medium power micrographs of NS_1 showing a round nucleus (Nu) which contains a thin rim of heterochromatin (He) near the nuclear envelope. The nucleolus (No) is round and very distinct. The cytoplasm contains rough endoplasmic reticulum (rer), mitochondria (Mt), Golgi complexes (Gc) and secretory granules (Gr). (C, D) Enlarged view of A & B exhibiting the cytoplasm of NS_1 containing mitochondria (Mt), extensive Golgi complexes (Gc) and electron-dense granules (Gr) near the maturing face of the Golgi complexes.

nucleus contains a thin rim of heterochromatin near the nuclear envelope. Small patches of heterochromatin are scattered in the central region of the nucleus, while the rest of nucleoplasm contains finely dispersed euchromatin. The nucleolus is large, round and very prominent (Figs. 1A, C, Figs. 2A, B). The cytoplasm shows abundant rough endoplasmic reticulum consisting of many large stacks of membrane in straight arrays (Fig. 1D, Fig. 2C). Golgi complexes are extensively developed and each consists of four to five elongated and slightly bent cisternae and saccules, which are often surrounded by dense vesicles (Fig. 1D, Fig. 2C). There are mitochondria and abundant polyribosomes in the cytoplasm. Two types of secretory granules are present in the NS_1 of cerebral ganglia. Type 1 are large, membrane-bound, spherical granules (Figs. 1B, C). Their diameter is about 500–800 nm and contain moderately osmiophilic material. There are few granules present, and these are usually dispersed around the maturing face of the Golgi complexes (Fig. 1D). Type 2 are small membrane-bound spherical secretory granules, containing electron-dense matrices. Their diameter is about 60 nm, and they are scattered throughout the cytoplasm (Figs. 1B, D). The newly synthesized

granules indicated by their light matrices are concentrated mainly in the maturing face of the Golgi complexes (Figs. 1D, E). In the NS_1 of pleuropedal ganglia, only one type of secretory granule is present. These granules are round and have a mean diameter of 120 nm. They contain moderate to strong electron-dense matrices (Figs. 2C, D).

NS_2 cells are round or oval (10–12 μm in dimension) (Fig. 3, Fig. 4). Their nucleus is round (6–8 μm in diameter) with a thin rim of heterochromatin near the nuclear envelope, and large blocks of heterochromatin are scattered in the central region(Fig. 3A, Fig. 4A). The cytoplasm of the NS_2 cells in the cerebral ganglia possesses extensively developed rough endoplasmic reticulum, and has numerous mitochondria (Fig. 3D). There could be more than one Golgi complex per cell. Each Golgi complex usually consists of four to six elongated cisternae and saccules, which are often surrounded by dense vesicles (Fig. 3B). The most prominent gran-

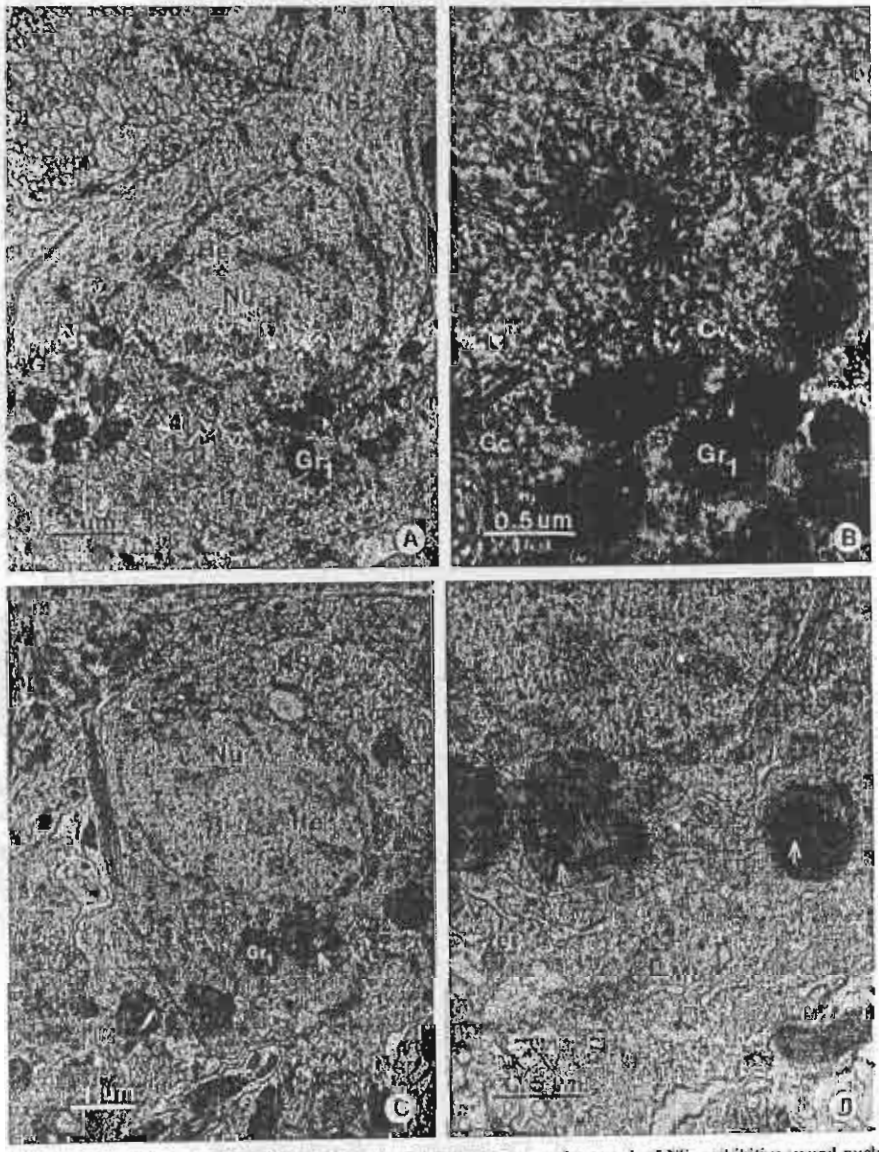

Figure 3. TEM micrographs of NS_2 cells of cerebral ganglia. (A, C) Medium power micrograph of NS_2, exhibiting round nucleus (Nu) with a thin rim of heterochromatin (He) attached to the nuclear envelope and large block of heterochromatin scattered in the central area of the nucleus. The cytoplasm possesses rough endoplasmic reticulum, mitochondria, Golgi complexes (Gc), and type I granules (Gr_1) containing a crystalline structure (arrow). (B, D) Enlarged view of C exhibiting the cytoplasm of the NS_2 containing Golgi complexes (Gc), rough endoplasmic reticulum (rer), mitochondria (Mt), condensing vesicles (Cv) and secretory granules. Type I granules (Gr_1) contain a crystalline structure (arrow) embedded in a moderately osmiophilic matrix. Nu, nucleus.

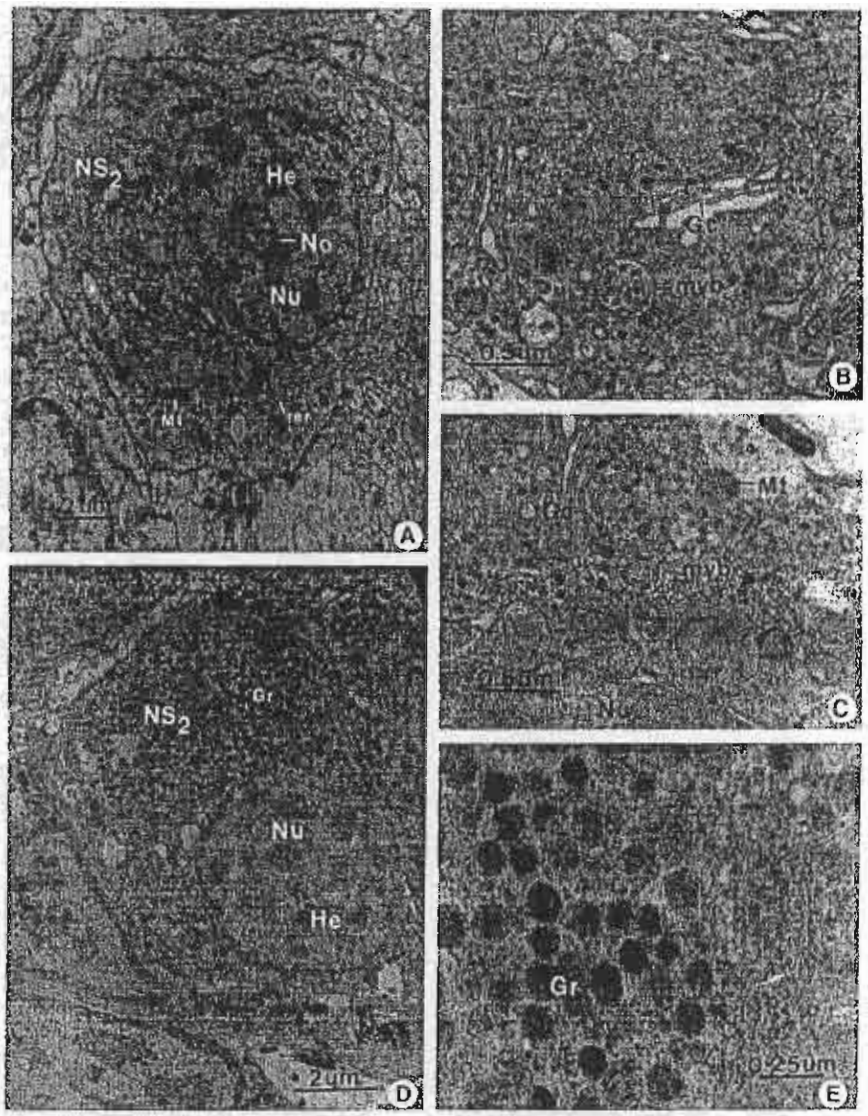

Figure 4. TEM micrographs of NS_2 cells of pleuropedal ganglia. (A) An electron micrograph of subtype a of NS_2 showing round nucleus (Nu) with a thin rim of heterochromatin (He) along the periphery and in the central region of the nucleus. The nucleolus (No) is very prominent. Mt, mitochondria; rer, rough endoplasmic reticulum. (B, C) Enlarged view of A, exhibiting the cytoplasm of NS_2 containing Golgi complexes (Gc), mitochondria (Mt), multivesicular body (mvb) and secretory granules (Gr). Nu, nucleus. (D) An electron micrograph of subtype b of NS_2, exhibiting a cytoplasm filled with a large number of spherical secretory granules (Gr). Nu, nucleus; He, heterochromatin. (E) An enlarged view of spherical secretory granules (Gr) with dense matrices.

ules appear large and round, membrane-bound, and about 500 to 800 nm in diameter. Each granule contains crystalline structures of various sizes, embedded in moderately dense osmiophilic matrices (Figs. 3B, D). These granules are concentrated at the maturing face of Golgi complexes (Fig. 3D).

The NS_2 cells of the pleuropedal ganglia contain abundant cell organelles, i.e., mitochondria, rough endoplasmic reticulum, Golgi complexes, multivesicular bodies (Figs. 4B, C), and small spherical secretory granules with dense matrices about 240 nm in diameter (Figs. 4D, E). NS_2 cells can be divided into two subtypes, viz. subtypes A and B. Subtype A contains only few neurosecretory granules, which are mostly concentrated at the Golgi complexes, and there is a large amount of rough endoplasmic reticulum, numerous mitochondria and extensively-developed Golgi complexes. Hence, they show evidence for high secretory activity (Figs. 4A, B). In contrast, cytoplasm of subtype B is filled mostly with neurosecretory granules and has few additional organelles (Fig. 4D). These cells appear to be in a storage phase where granules are ready to be discharged.

NS_3 cells are smaller (8–10 µm in size) than NS_1 and NS_2 (Fig.

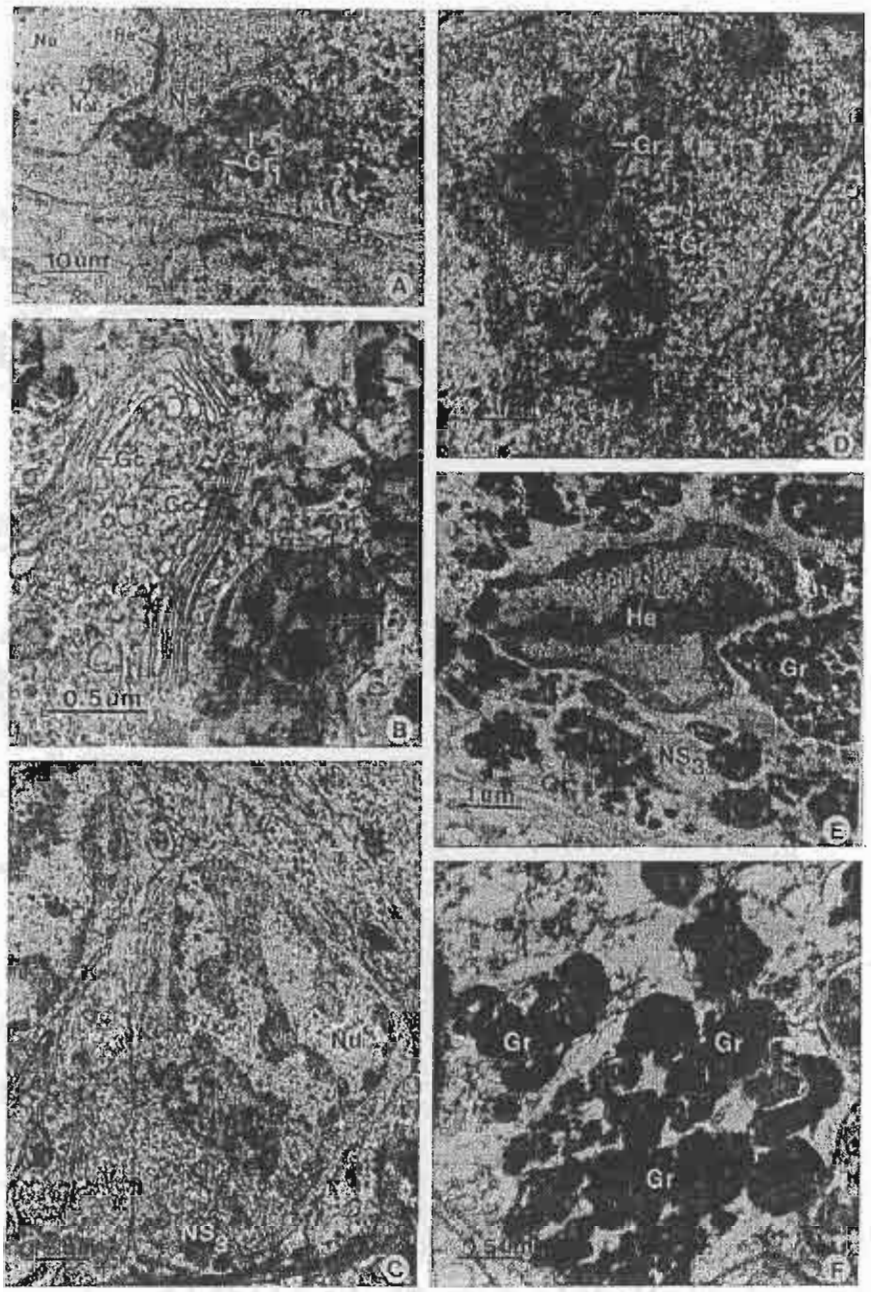

Figure 5. TEM micrographs of NS_3 cells of cerebral ganglia. (A) Medium power micrograph of NS_3 showing an oval nucleus (Nu) which contains thick strands of heterochromatin (He) near the nuclear envelope. The nucleolus (No) is very distinct. The cytoplasm contains rough endoplasmic reticulum, mitochondria, Golgi complexes (Gc) and secretory granules. Type 1 granules (Gr_1) are composed of strong osmiophilic material. Type 2 granules (Gr_2) are composed of highly condensed osmiophilic globules. (B) A high magnification of the cytoplasm of NS_3 showing extensive Golgi complexes (Gc) and type 1 granules (Gr_1). (C) Medium power micrograph of NS_3 showing oval nucleus (Nu) containing thick strands of heterochromatin (He) near the nuclear envelope and blocks of heterochromatin passing through the center of the nucleus. (D) A high magnification of the cytoplasm of NS_3 containing type 1 granules (Gr_1) and type 2 granules (Gr_2). (E) Medium power micrograph of NS_3 showing indented nucleus (Nu) which contains thick strands of heterochromatin (He) near the nuclear envelope and blocks of heterochromatin passing through the center of the nucleus. The cytoplasm contains aggregated granules (Gr). (F) An enlarged view of E exhibiting aggregated granules (Gr).

5, Fig. 6). The nuclei are oval (about 5–6 μm in dimension) and some are indented (Figs. 5C, E, Figs. 6A, C, D). They contain a thick rim of heterochromatin near the nuclear envelope, and a thick strand of heterochromatin in the center (Figs. 5C, E, Fig. 6D). In the NS_3 cells of the cerebral ganglia, the cytoplasm contains rough endoplasmic reticulum, mitochondria, and Golgi complexes, but these organelles are present less abundant, and of smaller sizes, than those in NS_1 and NS_2 cells. Much cytoplasm is filled with secretory granules (Figs. 5A, D). These granules are large (2000–7000 nm in diameter), membrane-bound, and contains dense, osmiophilic globules of various sizes that are aggregated together. When examined in detail, these granules are divided into two subtypes. Type 1 secretory granules are composed of strongly osmiophilic crystalline material in a clear ground substance (Figs. 5A, B), and type 2 secretory granules are composed of highly condensed osmiophilic globules aggregated together (Figs. 5D, E, F). It is possible that type 2 secretory granules are developed from type 1 secretory granules.

In the NS_3 cells of pleuropedal ganglia, the cytoplasm contains less rough endoplasmic reticulum, fewer mitochondria, and less Golgi complexes, than those of NS_1 and NS_2. NS_3 cells are divided into two subtypes. Subtype 1 cytoplasm contains few, but large

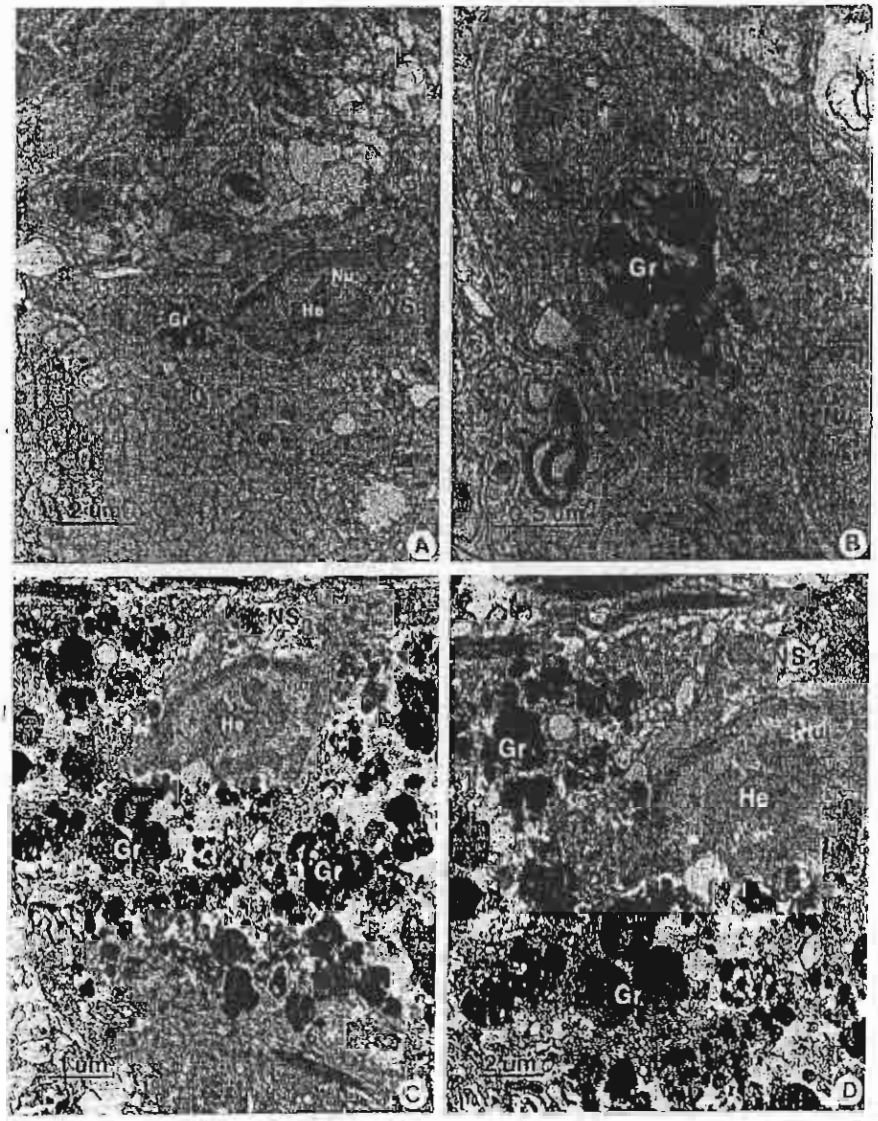

Figure 6. TEM micrographs of NS_3 cells of the pleuropedal ganglia. (A, B) Low and high power micrographs of NS_3 subtype 1 showing oval nuclei (Nu) which contain thick strands of heterochromatin (He) at the nuclear envelope and in the central region. The cytoplasm contains few large secretory granules (Gr). (C, D) Low and high power micrographs of NS_3 subtype 2, showing oval nucleus (Nu) which contains thick strands of heterochromatin (He) near the nuclear envelope and in the central region. The cytoplasm contains aggregated granules (Gr).

Figure 7. Comparison of the ultrastructures of three types of neurosecretory cells in the cerebral and pleuropedal ganglia of *H. asinina*.

secretory granules, with a strong osmiophilic substance within a clear ground matrix (Figs. 6A, B), and subtype 2 cytoplasm contains numerous large secretory granules, each composed of strong osmiophilic globules aggregated together in a homogeneous ground substance (Figs. 6C, D). It is possible that neurosecretory cells of subtype 1 develop from subtype 2 through the condensation and dehydration of the osmiophilic substance.

DISCUSSION

The ultrastructural study of the neurosecretory cells in the cerebral ganglia of *H. asinina* revealed that there are three types of neurosecretory cells (i.e. NS_1, NS_2, NS_3). This is in contrast to only two types reported by Upatham et al. (1997) using light microscopy. The pleuropedal ganglia also contain three types of neurosecretory cells. The details of the heterochromatin and euchromatin in the nuclei of cerebral and pleuropedal ganglia neurosecretory cells were revealed by light microscopy and confirmed by the extra resolution of TEM. The NS_1 nucleus contains mostly euchromatin, while large amounts of heterochromatin was present in NS_2 and NS_3 cells. In general, the cytoplasm of these cells resembles that of neurosecretory cells described in other gastropods, such as *B. tentaculata* (Andrews 1971), *H. rufescens* (Miller et al. 1973), *A. fulica* (Kruatrachue et al. 1994) and *L. stagnalis* (Boer et al. 1968).

The main differences between the neurosecretory cells of the cerebral ganglion and those of the pleuropedal ganglion are the type and size of neurosecretory granules. In the cerebral ganglia, the NS_1 cell contains 2 types of secretory granules (large and small) while the NS_1 cell of the pleuropedal ganglion contains only one type (small granules). In addition, the NS_2 cells of the cerebral and pleuropedal ganglia both contain one type of secretory granules. However, they are different both in size and content. The NS_3 of both ganglia appear to contain one type of secretory granule that contains aggregates of dense globules.

In the cerebral ganglia, the NS_1 cytoplasm is composed of cell organelles, including numerous mitochondria, rough endoplasmic reticulum, Golgi complexes and secretory granules, which reflects a highly active secretory functions. Golgi complexes are extremely large and there may be several present in a cell. Small electron-dense secretory granules are associated with the maturing face of Golgi complexes. These granules were later formed widely distributed throughout the cytoplasm. Hence, this indicates that the Golgi complexes in the neurosecretory cells of *H. asinina* have a similar role in packing of electron-dense material, similar to those of neurosecretory cells reported in other gastropods (Boer et al. 1968, Kai-Kai & Kerkut 1979).

The ultrastructural characteristics of the NS_1 of the cerebral ganglia indicate that it is a highly active synthetic cell. In comparison, the cytoplasm of NS_2 and NS_3 contains only one type of granules, which are large round in NS_2 and polymorphic in NS_3. These granules bear crystalline structures in NS_2 and in NS_3 and are composed of aggregates of dense osmiophilic substances. The similarity between granules in NS_2 and NS_3 tends to indicate that the two cells could be of the same group. While the NS_2 appears to be in a more active secretory phase, the NS_3 has reached the fully differentiated state, in which hormonal product is already produced in abundance, stored, and ready for release.

In the present study, the cytoplasms of NS_1 and NS_2 cells in the pleuropedal ganglia of *H. asinina* exhibit characteristics which imply that they have actively synthetic features. These are the numerous mitochondria, rough endoplasmic reticulum, Golgi complexes, multivesicular bodies and secretory granules, and numerous small clear vesicles that may be transport vesicles in the cytoplasm. Rough endoplasmic reticulum and Golgi complexes are well developed. The electron-dense secretory granules are probably formed from the Golgi complex. This process is similar to that described in neurosecretory cells in the pleural ganglia of *L. stagnalis* (Bonga 1970).

ACKNOWLEDGMENT

This study received financial support from the Thailand Research Fund

LITERATURE CITED

Andrews, E. 1968. An anatomical and histological study of the nervous system of *Bithynia tentaculata* (Prosobranchia) with special reference to the possible neurosecretory activity. *Proc. Malac. Soc. Lond* 38:213–232.

Andrews, E. 1971. The fine structure of the nervous system of *Bithynia tentaculata* (Prosobranchia) in relation to possible neurosecretory activity. *Veliger* 14:13–28.

Boer, H. H. 1965. A cytological and cytochemical study of neurosecretory cells in Basommatophora, with particular reference to *Lymnaea stagnalis* (L.). *Arch. Neerl. Zool* 16:313–356.

Boer, H. H., E. Douma & J. M. A. Koksma. 1968. Electron microscope study of neurosecretory cell and neurohaemal organs in the pond snail *Lymnaea stagnalis*. *Symp. Zool. Soc. Lond* 22:237–256.

Hahn, K. O. 1994. The neurosecretory staining in the cerebral ganglia of the Japanese abalone (ezoawabi), *Haliotis discus hannai*, and its relationship to reproduction. *Gen. Comp. Endocrinol* 93:295–303.

Joosse, J. 1964. Dorsal bodies and dorsal neurosecretory cells of the cerebral ganglia of *Lymnaea stagnalis* (L.). *Arch. Neerl. Zool* 16:1–103.

Kai-Kai, M. A. & G. A.Kerkut. 1979. Mapping and ultrastructure of neurosecretory cells in the brain of *Helix aspersa*. *Comp. Biochem. Physiol.* 64A:97–107.

Kruatrachue, M., V. Sretabunt, J. Chavadej, P. Sretarugsa, E. S. Upatham & P. Sobhon. 1994. Development and histological characteristics of

neurosecretory cells in the cerebral ganglia of *Achatina fulica* (Bowdich). *Moll. Res* 15:29–37.

Miller, W., R. S. Nishioka & H. A. Bern. 1973. The "juxtaganglionic" tissue and the brain of the abalone, *Haliotis rufescens* Swainson. *Veliger* 16:125–129.

Upatham, E. S., A. Thongkukiatkul, M. Kruatrachue, C. Wanichanon, Y. P. Chitramvong, S. Sahavacharin & P. Sobhon. 1997. Classification of neurosecretory cells, neurons, and neuroglia in the cerebral ganglia of *Haliotis asinina* Linnaeus by light microscopy. *J. Shellfish Res* 17:737–742.

Wendelaar Bonga, S. E. 1970. Ultrastructure and histochemistry of neurosecretory cells and neurohaemal areas in the pond snail *Lymnaea stagnalis*. *Z. Zellforsch. Mikrosk. Anat* 108:190–224.

Yahata, T. 1971. Demonstration of neurosecretory cells in the cerebral ganglion of the abalone, *Nordotis discus* Reeve. *Bull. Fac. Fish. Hokkaido Univ* 22:207–214.

Science Asia
Journal of the Science Society of Thailand
http://scienceasia.tiac.or.th ISSN 1513-1874

July 9, 2001

Dr. Chaitip Wanichanon,
Department of Anatomy,
Faculty of Science,
Mahidol University, Rama VI Road,
Bangkok 10400.

Dear Dr. Chaitip

Thank you very much for submitting the manuscript entitled Chromatin Condensation During Spermiogenesis in Rats (Code 0101-157, received 10 January 2001) for consideration for publication in *ScienceAsia*.

The manuscript has been read by two independent referees, who have recommended acceptance of the manuscript for publication in *ScienceAsia*. Would you please ensure that your final manuscript follows the style of the journal, especially references, and send to us together with a diskette of the final manuscript. Your paper is expected to be published in ScienceAsia Vol. 27 No. 4. You will receive further information later.

Thank you for your interest in contributing to our journal.

Yours sincerely,

Prof. Dr. MR. Jisnuson Svasti
Editor
ScienceAsia

EDITORIAL OFFICE: c/o Department of Biochemistry, Faculty of Science, Mahidol University
Rama VI Road, Bangkok 10400
Tel:+66-2-2461360-69 ext.6619 Fax:2480375 E-mail: scjss@mahidol.ac.th

Title: Chromatin Condensation During Spermiogenesis in Rats

Authors: *C. Wanichanon, W. Weerachatyanukul, W. Suphamungmee, A. Meepool, S. Apisawetakan, V. Linthong, P. Sretarugsa, J. Chavadej, P. Sobhon*

Afflilitation: Department of Anatomy, Faculty of Science, Mahidol University, Rama VI Road, Bangkok 10400, Thailand

Running title: Chromatin in rat spermatids

Correspondences and reprint request to: Dr. Chaitip Wanichanon Ph.D.
Department of Anatomy,
Faculty of Science, Mahidol University
Rama VI Rd., Bangkok 10400, Thailand
E-mail: sccwn@mahidol.ac.th
Fax. 662-247-9880
Tel. 662-245-5198

Key Words: Chromatin, Condensation, Rat, Spermatids

Abstract

The process of chromatin condensation during the transformation from spermatids to spermatozoa in rat was observed by transmission electron microscopy. In Golgi and cap phase spermatids (stages 1-7) chromatin fibers consist of 2 sizes, i.e., 10 nm and 30 nm thick (level 1 and 2). The latter are uniform fibers that appear as dense dots in cross section, while the former are thin zigzag fibers that link between 30 nm fibers. Both of these chromatin fibers are evenly distributed in the nuclei of these spermatids. In earlier stages, level 1 fibers tend to predominate, while in later stages level 2 fibers are the majority. In early acrosome phase spermatids (stages 8-9) the nuclei transform from round to pear shape with partially formed acrosomes covering the anterior ends; and the chromatin fibers, which are mostly at level 2, are packed closely and evenly together. There are increasing number of larger fibers about 40 nm in diameter (level 3) in the subacrosomal region of the nuclei, particularly in stage 9. In mid acrosome phase spermatids (stages 10-12) the 40 nm fibers appear to grow in width to 50 nm (level 4) which transform into long straight fibers that are interlaced together in several directions, and become distributed evenly throughout the nuclei. In late acrosomal phase spermatids (stages 13-14) the chromatin appears as 60 and 70 nm thick knobs and branching cords (levels 5 & 6) in the anterior part of the nucleus which becomes highly tapered, while the posterior part still contains mainly 50 nm straight fibers. The wave of transformation to thick chromatin cords continues from the anterior to posterior regions, until in maturation phase spermatids (stages 15-17) when chromatin in the anterior halves of some nuclei is completely condensed and the rest of chromatin appears as 90-100 nm thick (level 7) branching cords with intervening light narrow spaces. In immature spermatozoa (stages 18-19) the chromatin becomes completely condensed with only few pale spots scattered widely throughout each nucleus.

Introduction

During the process of spermiogenesis of most mammals, DNA in the haploid male germ cells are progresssively condensed by the gradual replacement of histones with transitional proteins. These proteins are replaced in turn by protamines which are the most basic nuclear proteins (Balhorn et al., 1984; Grime and Smart, 1985). Concurrent with the histones' replacement, the original nucleosomal-based chromatin fibers transform into different organization and become condensed into various patterns which finally form completely electron-opaque mass as seen in the nuclei of the fully mature spermatozoa (Dooher et al., 1973). The degree of chromatin compactness in mature sperm of various species depend on the amount of histones being replaced by protamines. Rat spermatozoa exhibit denser chromatin than human spermatozoa, which is probably due to the lower percentage of histones remaining in their chromatin (Subirana, 1975). Whereas nucleohistone chromatin fibers in spermatids of all mammals examined so far appear to have nucleosomal organization which may be arranged in form of 30 nm solenoid fibers, nucleoprotamine chromatin fibers may vary in forms; and in rat spermatozoa they may exist in the form of large fibers or cords with thickness about 80-100 nm that are aligned in parallel (Sobhon et al., 1981). In this study we have identified in rat spermatids, the different levels of higher-ordered of chromatin fibers and the pattern of their condensation.

Materials and Methods

Adult Wistar rats age 10-12 weeks were obtained from National Center for Experimental Animals, Salaya Campus, Mahidol University, Bangkok, Thailand. They were anesthetized by ether inhalation, and the testes were removed, sliced into small pieces and fixed in 2.5 % glutaraldehyde in 0.1 M phosphate buffer, pH 7.4, at 4^0C overnight, and postfixed in 1 % OsO_4 in the same buffer for 2 hours. Subsequently, the

tissue blocks were dehydrated by ethanol and embedded in Araldite 502 resin. Ultrathin sections were cut and stained with lead citrate-uranyl acetate and examined under a Hitachi TEM H-300 at 75 kV. Catalase crystal (Agar Aids) were photographed at various magnifications and used for the measurement of chromatin fiber sizes.

Results

The organizational levels of chromatin fibers in various stages of spermatids were examined by TEM and their thickness measured.

Round spermatids These cells belong to the Golgi and cap-phase which, according to the classification proposed by Leblond and Clermont (1952), correspond to stages 1 to 7 (Fig.1A; 6). The nuclei of these cells, which are round, have two levels of chromatin fibers (Table 1): level 1 are fine zig-zag fibers that are dispersed throughout the nucleus, each with the thickness about 10 nm. Level 2 are thicker fibers having about 30 nm in diameter, which usually appear as dense dots in cross section; and these fibers correspond to fundamental chromatin fibers that are present in the nuclei of various stages of spermatocytes as well as in somatic cells. Level 2 fibers may aggregate tightly together to form small blocks or narrow strips of heterochromatin close to the nuclear envelope (Fig.1B). Only small amount of heterochromatin blocks were observed in the nuclei of round spermatids, as the majority appear in the form of 10 nm and 30 nm fibers which constitute the main mass of euchromatin.

Early acrosome phase spermatids These cells correspond to stage 8 and 9 (Leblond and Clermont, 1952, also see Fig.6). The nuclei of these cells are transformed into oval or pear shape, and the acrosome becomes definitive structure covering the anterior part of the nucleus. The nuclear membrane under the acrosome is thickened and the nuclear ring together with manchette consisting of 4-5 layers of longitudinally oriented microtubules are formed (Fig.1C, D). The main mass of cytoplasm moves to the posterior end (Fig.1C). Within the nucleus, in addition to the two levels of